THE UNIVERSITY *of* EDINBURGH

Refraction of Nonlinear Light Beams in Nematic Liquid Crystals

Wenjun Xia

Doctor of Philosophy
University of Edinburgh
2012

Declaration

I declare that this thesis was composed by myself and that the work contained therein is my own, except where explicitly stated otherwise in the text.

(*Wenjun Xia*)

To my lovely parents

Abstract

Optical spatial solitons in nematic liquid crystals, termed nematicons, have become an excellent test bed for nonlinear optics, ranging from fundamental effects to potential uses, such as designing and demonstrating all-optical switching and routing circuits in reconfigurable settings and guided-wave formats. Following their demonstration in planar voltage-assisted nematic liquid crystal cells, the spatial routing of nematicons and associated waveguides have been successfully pursued by exploiting birefringent walkoff, interactions between solitons, electro-optic controlling, lensing effects, boundary effects, solitons in twisted arrangements, refraction and total internal reflection and dark solitons. Refraction and total internal reflection, relying on an interface between two dielectric regions in nematic liquid crystals, provides the most striking results in terms of angular steering. In this thesis, the refraction and total internal reflection of self-trapped optical beams in nematic liquid crystals in the case of a planar cell with two separate regions defined by independently applied bias voltages have been investigated with the aim of achieving a broader understanding of the nematicons and their control. The study of the refraction of nematicons is then extended to the equivalent refraction of optical vortices.

The equations governing nonlinear optical beam propagation in nematic liquid crystals are a system consisting of a nonlinear Schrödinger-type equation for the optical beam and an elliptic Poisson equation for the medium response. This system of equations has no exact solitary wave solution or any other exact solutions. Although numerical solutions of the governing equations can be found, it has been found that modulation theories give insight into the mechanisms behind nonlinear optical beam evolution, while giving approximate solutions in good to excellent agreement with full numerical solutions and experimental results. The modulation theory reduces the infinite-dimensional partial differential equation problem to a finite dynamical system of comparatively simple ordinary differential equations which are, then easily solved numerically. The modulation theory results on the refraction and total internal reflection of nematicons are in excellent agreement with experimental data and numerical simulations, even when accounting for the birefringent walkoff. The modulation theory also gives excellent results for the refraction of optical vortices of +1 topological charge. The modulation theory predicts that the vortices can become unstable on interaction with the nematic interface, which is verified in quantitative detail by full numerical solutions. This prediction of their azimuthal instability and their break-up into bright beams still awaits an experimental demonstration, but the previously obtained agreement of modulation theory models with the behaviour of actual nematicons leads us to expect the forthcoming observation of the predicted effects with vortices as well.

Contents

List of Abbreviations:

PDE - Partial Differential Equation

KdV - Korteweg-de Vries

IST - Inverse Scattering Transform

NLS - Nonlinear Schrödinger Equation

LCs - Liquid Crystals

NLC - Nematic Liquid Crystal

ITO - Indium-tin-oxide

HNS - Highly Nonlocal Solitons

ODE - Ordinary Differential Equations

FFT - Fast Fourier Transform

CNLS - Coupled Nonlinear Schrödinger Equations

List of Commonly-Used Symbols:

u - wave function

κ - wave number

ω - angular frequency

C - group velocity

E - electric field (with complex envelope)

θ - orientation angle (director)

λ - wavelength

w - waist

K - Single elastic constant

G - Green function

L - Lagrangian

$\mathcal{L}$ - Averaged Lagrangian

a - amplitude

σ - phase

V - propagation constant

ξ - beam axis

Λ - the area of the shelf of low wavenumber radiation under the beam

Chapter 1

Introduction

1.1 Nonlinear Waves

Waves are ubiquitous in nature. There are a lot of wave phenomena with which we are familiar from everyday experience, such as water waves, sound waves and light waves. Other phenomena, such as sonic booms or moving bottlenecks in traffic can also be studied as wave motion. Though well-known as one of the broadest ranging scientific subjects, it seems to be not easy to give a precise definition of a wave, other than waves involve energy propagation at a finite speed. At an intuitive level, a wave is any recognizable feature of a disturbance, such as a maximum or an abrupt change in some quantity, that travels through space and time at a finite speed[1]. As a simple instance, a wave travelling along the direction of x axis with speed c can be described by the function

$$u(x,t) = f(x - ct), \tag{1.1}$$

where the speed c can be positive or negative and f is an arbitrary function.. As shown in Figure 1.1, the function $f(x - d)$ is identical to $f(x)$ except displaced by a distance d. Each and every wave has its own function f, depending on the shape and speed of the wave [2]. For example, for sinusoidal waves, $u(x,t) = \sin(x - ct)$.

Different features are important for different types of waves. The two main classes of wave motion can be distinguished— hyperbolic and dispersive. Basically, hyperbolic waves can be described from the form of their governing equations, while dispersive waves can be discriminated from the form of solutions of their governing equations. The classes are not exclusive [1]. Some wave motions shows both types of behaviour, and some exceptions fit neither.

1.1.1 Hyperbolic waves

Hyperbolic waves are governed mathematically by the equations in terms of hyperbolic PDEs. In mathematics the general second-order PDE (partial differential equation) in two independent variables has the form

$$Au_{xx} + 2Bu_{xy} + Cu_{yy} + (\text{lower order derivatives}) = 0, \tag{1.2}$$

where the coefficients A, B, C etc. may depend on x and y. The discriminant of the PDE is given by $B^2 - AC$. When $B^2 - AC < 0$, the PDE is classified as an elliptic PDE. For example, the motion of a fluid at subsonic speeds can be approximated with elliptic PDEs.

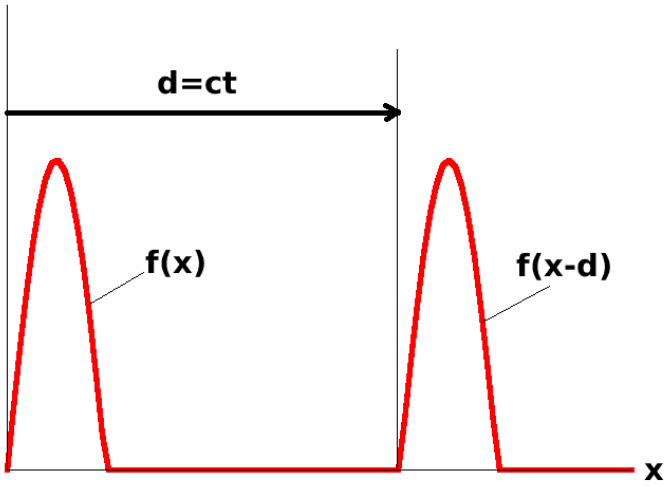

Figure 1.1: The graph of $f(x-d)$ looks the same as the graph of $f(x)$ except that it is shifted distance d to the right.

When $B^2 - AC = 0$, the PDE is classified as a parabolic PDE, such as the heat equation. Specifically, when $B^2 - AC > 0$, the PDE is classified as a hyperbolic PDE, which is what we want to highlight here. Many wave equations belong to this class. The wave equation

$$u_{tt} = c_0^2 \nabla^2 u, \tag{1.3}$$

is the classic example of a hyperbolic PDE, although the simplest of all is

$$u_t + c_0 u_x = 0, \tag{1.4}$$

which is first-order and one dimensional and its general solution is

$$u = f(x - c_0 t). \tag{1.5}$$

The equation (1.4) can describe many wave motions, such as waves in traffic flow, flood waves, waves in glaciers, and certain wave phenomena in chemical reactions [1].

The one dimensional and second-order equation

$$u_{tt} - c_0^2 u_{xx} = 0 \tag{1.6}$$

which describes plane waves can be rewritten in terms of new characteristic variables

$$\alpha = x - c_0 t, \qquad \beta = x + c_0 t. \tag{1.7}$$

By the chain rule,

$$
\begin{aligned}
u_t &= \frac{\partial u}{\partial \alpha}\frac{\partial \alpha}{\partial t} + \frac{\partial u}{\partial \beta}\frac{\partial \beta}{\partial t} = -c_0 u_\alpha + c_0 u_\beta, \\
u_{tt} &= \frac{\partial u_t}{\partial \alpha}\frac{\partial \alpha}{\partial t} + \frac{\partial u_t}{\partial \beta}\frac{\partial \beta}{\partial t} = c_0^2 u_{\alpha\alpha} - 2c_0^2 u_{\alpha\beta} + c_0^2 u_{\beta\beta}; \\
u_x &= \frac{\partial u}{\partial \alpha}\frac{\partial \alpha}{\partial x} + \frac{\partial u}{\partial \beta}\frac{\partial \beta}{\partial x} = u_\alpha + u_\beta, \\
u_{xx} &= \frac{\partial u_x}{\partial \alpha}\frac{\partial \alpha}{\partial x} + \frac{\partial u_x}{\partial \beta}\frac{\partial \beta}{\partial x} = u_{\alpha\alpha} + 2u_{\alpha\beta} + u_{\beta\beta}.
\end{aligned}
\tag{1.8}
$$

Substituting u_{tt} and u_{xx} into equation (1.6) and simplifying terms yields

$$u_{\alpha\beta} = 0. \tag{1.9}$$

The general solution for equation (1.9) is obviously

$$u = f(\alpha) + g(\beta) = f(x - c_0 t) + g(x + c_0 t), \tag{1.10}$$

where f and g are arbitrary functions. The solution (1.10) can also be obtained by factoring (1.6) as

$$(\frac{\partial}{\partial t} - c_0\frac{\partial}{\partial x})(\frac{\partial}{\partial t} + c_0\frac{\partial}{\partial x})u = 0. \tag{1.11}$$

Developed from equation (1.4), the prototype for hyperbolic waves is then the wave equation

$$u_t + c(u)u_x = 0. \tag{1.12}$$

when the propagation speed $c(u)$ is a constant c_0, it is linear, but when $c(u)$ is a function of the local disturbance u, it leads to a nonlinear equation.

Interestingly, hyperbolic waves of different orders can be present simultaneously, such as

$$\eta(u_{tt} - c_0^2 u_{xx}) + u_t + a_0 u_x = 0. \tag{1.13}$$

This equation is hyperbolic with characteristic velocities $\pm c_0$ determined from the second order wave operator, but if η is small, the lower order terms $u_t + a_0 u_x$ start to dominate the equation so that $u_t + a_0 u_x = 0$ becomes a good approximation which predicts waves with speed a_0. In some sense both kinds of waves can play important roles with their interaction.

The wave equation (1.3) arises in some areas of classical physics, such as acoustics, elasticity, and electromagnetism [1]. The equations for a compressible fluid are nonlinear, even when viscosity and heat conduction are ignored. Linearising the supersonic gas equations about an ambient constant state leads to the wave equation (1.3), for acoustic waves with c_0 the speed of sound. However, if the disturbances are not weak, as in explosions or in the disturbances caused by high speed supersonic aircraft and missiles, other mathematical theories developed from gas dynamics need to be used. In elasticity, the classical wave theory is also obtained after linearisation [1] as in acoustic waves. S-wave and P-wave exist simultaneously in elastic media. The S-wave moves as a shear or transverse wave, so the motion is perpendicular to the direction of wave propagation. While P-waves are like waves moving through a slinky, as opposed to waves in a rope, the S-waves. Therefore, this time a system of two wave equations

of the form (1.3) dominates, not only just a single equation. So the situation becomes more complicated than in acoustics. The complication can be even further for the free surface of an elastic body for which Rayleigh waves [3] exist, which are dispersive. In electromagnetism, (1.3) can describe different components of the electric and magnetic fields. But in general the electric and magnetic fields are coupled with their boundary conditions. While classical electromagnetic theory is linear, nowadays much attention is given to "nonlinear optics", where devices such as lasers produce intense waves and various media respond nonlinearly [1, 4].

1.1.2 Dispersive waves

In contrast to hyperbolic waves, the prototype for dispersive waves is based on a type of solution rather than a type of equation [1]. Linear dispersive waves admit solutions of the form

$$u = a\cos(\kappa x - \omega t), \tag{1.14}$$

where the angular frequency ω is a function of the wavenumber κ and the function $\omega(\kappa)$ is determined by the specific system. The wavenumber is the spatial frequency of a wave. In general, the wavenumber κ is given by

$$\kappa = \frac{2\pi}{\lambda} = \frac{2\pi\nu}{c} = \frac{\omega}{c}, \tag{1.15}$$

where ν is the frequency of the wave, λ is the wavelength, $\omega = 2\pi\nu$ is the angular frequency, and c is the phase speed of the wave. The phase speed is then

$$c = \frac{\omega}{\kappa}. \tag{1.16}$$

The waves are called "dispersive" if this phase speed is not a constant but depends on κ. Solutions of the form (1.14) stem from a variety of partial differential equations and also certain integral equations. Obviously, the dispersion relation

$$\omega = \omega(\kappa) \tag{1.17}$$

characterizes the problem. For example, equations appear in approximate theories of small amplitude long water waves, such as the linearised Korteweg-deVries equation [1]

$$u_t + c_0 u_x + \nu u_{xxx} = 0, \qquad \omega = c_0\kappa - \nu\kappa^3, \tag{1.18}$$

and the linearised Boussinesq equation [1]

$$u_{tt} - \alpha^2 u_{xx} = \beta^2 u_{xxtt}, \qquad \omega = \pm\alpha\kappa(1+\beta^2\kappa^2)^{-\frac{1}{2}}. \tag{1.19}$$

Another example is for which electromagnetic pulse propagation in dispersive planar dielectrics [1],

$$(\omega^2 - \nu_0^2)(\omega^2 - c_0^2\kappa^2) = \omega^2\nu_p^2. \tag{1.20}$$

For linear equation, a Fourier integral which consist of the superposition of modes of the

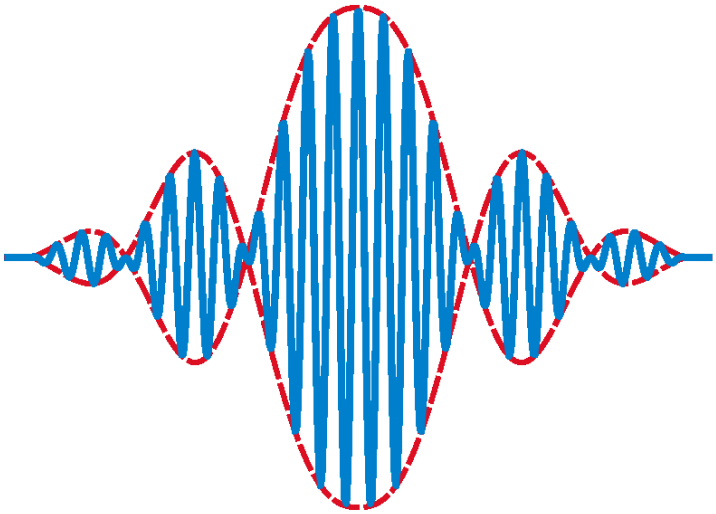

Figure 1.2: Solid line: A wave packet. Dashed line: The envelope of the wave packet. The envelope moves at the group velocity. (Quoted from Wikipedia, the free encyclopaedia; Graph by Oleg Alexandrov; Released into the public domain by the author.)

form (1.14) with different wave numbers is the most general solution [1]

$$u = \int_0^\infty F(\kappa)\cos(\kappa x - \omega t)d\kappa, \tag{1.21}$$

where $\omega(\kappa)$ is the dispersion relation (1.17) appropriate to the system. The Fourier inversion theorem $F(\kappa)$ is used to fit the boundary/initial conditions. Every wavetrain in (1.21) has its own phase speed

$$c(\kappa) = \frac{\omega(\kappa)}{\kappa}. \tag{1.22}$$

The case $\omega \propto \kappa$ is excluded so that the waves are genuinely dispersive. So the different component modes form a single concentrated hump at the beginning of propagation, as time evolves it will disperse and broaden due to the various phase speeds of each mode. The group velocity of the dispersive waves is defined as

$$C(\kappa) = \frac{d\omega}{d\kappa}. \tag{1.23}$$

The formula (1.23) for group velocity can be derived as follows. By the superposition principle, consider a wave packet as a function of position x and time t

$$u(x,t) = \int_{-\infty}^\infty F(\kappa)e^{i(\kappa x - \omega t)}\, d\kappa. \tag{1.24}$$

At time 0,

$$u(x,0) = \int_{-\infty}^\infty F(\kappa)e^{i\kappa x}\, d\kappa. \tag{1.25}$$

Assume that the wave packet u is almost monochromatic, so that $F(\kappa)$ is nonzero only in the vicinity of a central wavenumber κ_0. Linearising the dispersion relation gives

$$\omega(\kappa) \approx \omega_0 + (\kappa - \kappa_0)\omega_0', \tag{1.26}$$

where $\omega_0 = \omega(\kappa_0)$ and ω_0' is the derivative of $\omega(\kappa)$ at $\kappa = \kappa_0$. Then, after some algebra,

$$u(x,t) = e^{it(\omega_0'\kappa_0 - \omega_0)} \int_{-\infty}^{\infty} F(\kappa) e^{i\kappa(x-\omega_0' t)}\, d\kappa. \tag{1.27}$$

The factor in front of the integral has absolute value 1. Hence,

$$|u(x,t)| = |u(x - \omega_0' t, 0)|, \tag{1.28}$$

which means that the envelope of the wavepacket travels at velocity

$$\omega_0' = \left(\frac{d\omega}{d\kappa}\right)_{\kappa=\kappa_0}. \tag{1.29}$$

This explains the group velocity formula (1.23).

The overall shape of a wave packet, the modulation or envelope of the wave, propagates through space at the group velocity, for example see Figure (1.2). It is found that energy propagates with the group velocity as well. Thus group velocity plays the dominate role in dispersive waves [1]. For some cases for which exact solutions are unobtainable, such as in nonuniform media or more dimensions, the use of group velocity is vital. Using group velocity arguments leads to a surprisingly simple, but powerful, method which can deduce the main features of any linear dispersive system.

From the phase function

$$\theta(x,t) = \kappa x - \omega t, \tag{1.30}$$

a local wave number $\kappa(x,t)$ and a local angular frequency $\omega(x,t)$ can be defined by

$$\kappa(x,t) = \frac{\partial \theta}{\partial x}, \qquad \omega(x,t) = -\frac{\partial \theta}{\partial t}. \tag{1.31}$$

Eliminating θ from (1.31) yields

$$\frac{\partial \kappa}{\partial t} + \frac{\partial \omega}{\partial x} = 0. \tag{1.32}$$

Using the dispersive relation gives

$$\frac{\partial \omega}{\partial x} = \frac{\partial \omega}{\partial \kappa}\frac{\partial \kappa}{\partial x} = C(\kappa)\frac{\partial \kappa}{\partial x}, \tag{1.33}$$

so that

$$\frac{\partial \kappa}{\partial t} + C(\kappa)\frac{\partial \kappa}{\partial x} = 0. \tag{1.34}$$

Here $C(\kappa)$ is the group velocity defined in (1.23). Surprisingly, this equation for κ is just the simplest nonlinear hyperbolic equation given in (1.12) [1]. In such a subtle way, hyperbolic phenomena are hidden in dispersive waves. This may be exploited to bring the methods used in hyperbolic waves to bear on dispersive waves [1].

With the same role that gas dynamics has played for hyperbolic waves, water waves provides the impetus and background for the development of dispersive wave theory, and particularly the original ideas for nonlinear dispersive waves. For a plane wavetrain on deep water, the surface elevation u can be expanded in powers of the amplitude a as [5]

$$u = a\cos(\kappa x - \omega t) + \frac{1}{2}\kappa a^2 \cos 2(\kappa x - \omega t) + \frac{3}{8}\kappa^2 a^3 \cos 3(\kappa x - \omega t) + \cdots, \tag{1.35}$$

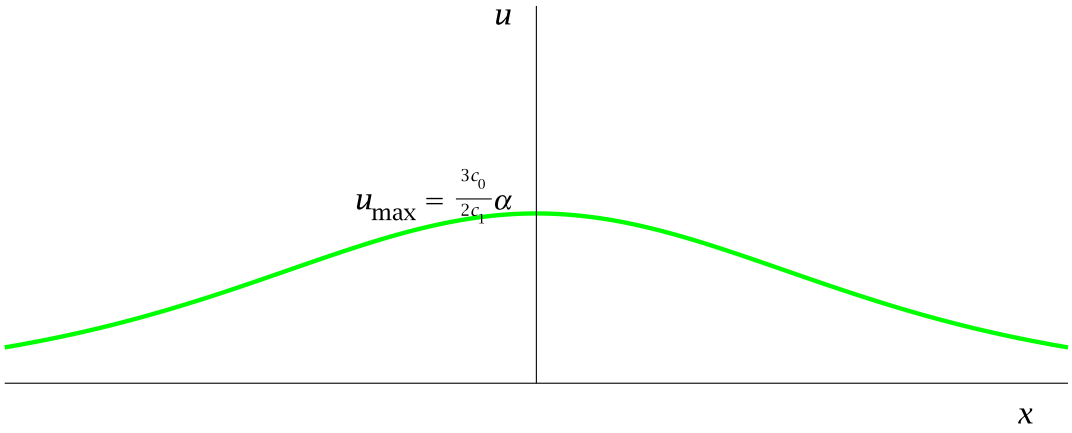

Figure 1.3: Solitary wave.

where the dispersive relation is nonlinear

$$\omega^2 = g\kappa(1 + \kappa^2 a^2 + \cdots). \tag{1.36}$$

This nonlinear phenomenon is named after George Gabriel Stokes, who derived it in 1847. The first term in (1.35) is a linear dispersive wave (1.14), which has the linear dispersive relation

$$\omega^2 = g\kappa, \tag{1.37}$$

where g is the gravitational acceleration. Equation (1.35) reveals that a periodic wavetrain solution exists which can be expanded in Fourier series (1.35). Equation (1.36) shows that the nonlinear dispersive relation includes the amplitude. This brings a qualitatively new feature to nonlinear dispersive waves[1]. In the present work variational techniques will be used as the approximate analysis for nonlinear dispersive waves.

1.1.3 Overlap

The waves are said to be "dispersive" if the phase speed $\omega(\kappa)/\kappa$ is not a constant, but depends on κ. However, it should be noted that the hyperbolic wave equation (1.3) has the dispersion relation $\omega = \pm c_0\kappa$, or (1.4) has $\omega = c_0\kappa$. These wave equations are then not dispersive as their wave speeds c are constant. Nevertheless, there are also cases of genuine overlap in which equations are hyperbolic and yet have solutions (1.14) with non-trivial dispersion relations $\omega = \omega(\kappa)$. An example is the Klein-Gordon equation

$$u_{tt} - u_{xx} + u = 0. \tag{1.38}$$

Equation (1.38) is hyperbolic, but has the dispersion relation $\omega^2 = \kappa^2 + 1$. These relatively few cases should not be allowed to obscure the overall differences between the two main classes. Although plenty and various instances belong to the class of hyperbolic waves, the majority of wave motions fall into the dispersive class [1].

1.2 Solitons

The soliton phenomenon was first recorded by John Scott Russell who discovered a solitary wave in Edinburgh's Union Canal in 1834 [6]. Boussinesq [7] and Rayleigh [8] showed that "solitary waves" arise from the water wave equations in the limit of long waves of small amplitude. The system favoured by Boussinesq is

$$h_t + (\psi h)_x = 0, \tag{1.39}$$

$$\psi_t + \psi\psi_x + gh_x + \frac{1}{3}h_0 h_{xtt} = 0, \tag{1.40}$$

where the constant g is acceleration due to gravity and the constant h_0 is undisturbed water depth. This system of equations (1.39) and (1.40) can be linearised to

$$u_{tt} - c_0^2 u_{xx} - \frac{1}{3}h_0^2 u_{xxtt} = 0, \tag{1.41}$$

which has the dispersion relation

$$\omega^2 = \frac{c_0^2\kappa^2}{1 + \frac{1}{3}\kappa^2 h_0^2}. \tag{1.42}$$

In 1895 Korteweg and de Vries derived what is now known as the Korteweg-de Vries (KdV) equation

$$u_t + (c_0 + c_1 u)u_x + \nu u_{xxx} = 0, \tag{1.43}$$

which approximately describes long waves in water of relatively shallow depth [1, 9]. Here c_0, c_1 and ν are constants related to the water stratification. This nonlinear equation is a reduction of the equations (1.39) and (1.40) of Boussinesq when the wave motion is in one direction. The linearised KdV equation has the periodic wave solution

$$u = a\cos(\kappa x - \omega t), \tag{1.44}$$

with the dispersion relation

$$\omega = c_0\kappa - \nu\kappa^3. \tag{1.45}$$

But Korteweg and de Vries did better. They found explicit solutions in closed form of the nonlinear equation (1.43). Periodic solutions

$$u = f(\theta), \qquad \theta = \kappa x - \omega t, \tag{1.46}$$

exist with $f(\theta)$ in terms of the elliptic function $cn\theta$. This solution was named cnoidal waves by Korteweg and de Vries. This work agrees with the conclusions of Stokes' work introduced in section (1.1.2). Firstly, the existence of periodic wavetrains is demonstrated explicitly [1]. Secondly, the amplitude a is included in the dispersion relation. But even more was found, which is the main topic of this section. The solitary waves described by (1.43) are found as solutions of constant shape moving with constant velocity. As the modulus tends to 1, $cn\theta$ approaches the sech function. Then the solution for a solitary wave is

$$u = \frac{3c_0}{2c_1}\zeta(X), \qquad X = x - Ut, \tag{1.47}$$

where ζ is a periodic function.

This solution can also be found directly from (1.43), as follows

$$\frac{3c_0^2}{8c_1^2}\zeta''' + \frac{3}{2}\zeta\zeta' - (\frac{U}{c_0} - 1)\zeta' = 0. \tag{1.48}$$

This integrates immediately to

$$\frac{3c_0^2}{8c_1^2}\zeta'' + \frac{3}{4}\zeta^2 - (\frac{U}{c_0} - 1)\zeta + G = 0. \tag{1.49}$$

Then by multiplying ζ', further integration yields

$$\frac{3c_0^2}{4c_1^2}\zeta'^2 + \zeta^3 - 2(\frac{U}{c_0} - 1)\zeta^2 + 4G\zeta + H = 0, \tag{1.50}$$

where G and H are constants of integration. For the special case of solitary waves, ζ and its derivatives tend to zero at ∞, which yields $G = H = 0$. Then equation (1.50) can be written as

$$\frac{3c_0^2}{4c_1^2}(\frac{d\zeta}{dX})^2 = \zeta^2(\alpha - \zeta), \qquad \frac{U}{c_0} = 1 + \frac{\alpha}{2}, \tag{1.51}$$

The solution of (1.51) is

$$\zeta = \alpha\,\mathrm{sech}^2\{(\frac{c_1^2\alpha}{3c_0^2})^{\frac{1}{2}}X\}. \tag{1.52}$$

Hence the solitary wave solution is

$$u = a\,\mathrm{sech}^2\{(\frac{2c_1^3 a}{9c_0^3})^{\frac{1}{2}}(x - Ut)\}, \tag{1.53}$$

where $a = \frac{3c_0}{2c_1}\alpha$ is the amplitude of the solitary wave and

$$U = c_0 + \frac{1}{3}c_1 a \tag{1.54}$$

in terms of the amplitude is the velocity of propagation. As shown in Figure. 1.3, u increases from $u = 0$ at $X = \infty$, reaches a maximum $u = \frac{3c_0}{2c_1}\alpha$ at $X = 0$, and then returns symmetrically to $u = 0$ at $X = -\infty$. This is the solitary wave. When $G, H \neq 0$, periodic cnoidal wave solutions result equation (1.54).

In the mid-1960s the term "soliton" was coined for the solitary wave solution of the KdV equation as it was found to possess particle-like properties [10]. These particle-like properties were found to be the result of the KdV equation possessing an exact solution given by the inverse scattering transform (IST) [11]. As we know Fourier transform can be applied to solve many linear PDEs, while as a non-linear analogue of Fourier transform, IST is a method for solving some nonlinear PDEs. Some other nonlinear PDEs, such as the Sine-Gordon equation

$$u_{tt} - u_{xx} + \sin u = 0, \tag{1.55}$$

and the cubic Schrödinger equation or nonlinear Schrödinger equation

$$iu_t + u_{xx} + \nu|u|^2 u = 0, \tag{1.56}$$

share with the KdV equation in having solitary wave solutions. Solitary waves are of interest,

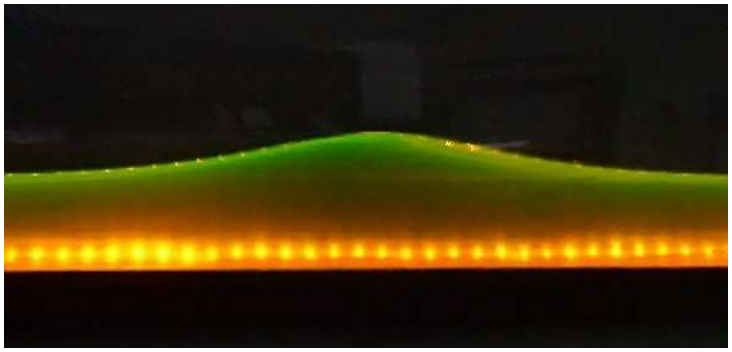

Figure 1.4: Solitary wave in a laboratory wave channel. (Quoted from Wikipedia, the free encyclopaedia; Photo by Christophe Finot et Kamal HAMMANI; Released into the public domain by the author.)

since they are strictly nonlinear phenomena with no counterparts in linear dispersive theory [1]. More surprisingly, it is found both from analytical solutions of some nonlinear PDEs, such as the Sine-Gordon equation by Perring and Skyrme (1962) and Lamb (1967, 1971), and computational results, such as the first demonstration of solution for the KdV equation in 1965 by Norman Zabusky and Martin Kruskal, that solitary waves retain their individuality under interaction and eventually emerge with their original shapes and speeds [10]. This resembles particle behaviour in Physics. In the context of quantum mechanics, microscopic particles show wave-particle duality. Incredibly, macroscopic solitary waves show this wave-particle duality as well. This may imply some unity between the microscopic world and the macroscopic world. Thus a solitary wave that maintains its shape while it travels at constant speed is also called a "soliton". As shown in Figure 1.4, the existence of a soliton was also demonstrated experimentally.

It is difficult to find a single, consensus definition of a soliton. Drazin and Johnson [12] summarise three properties of solitons

1. They are of permanent form;
2. They are localised within a region;
3. They can interact with other solitons, and emerge from the collision unchanged, except for a phase shift.

From the 1970's to the present day many experiments have been done using solitons as information carriers, or "bits", in fibre optics applications [12, 13, 14, 15]. Due to a soliton's inherent stability they are ideal carriers of information in long distance transmission. In optics, a soliton refers to any localised optical field that does not change during propagation and interacts with other solitons clearly.

A soliton is due to a balance between nonlinear and dispersive or diffractive effects in a medium. There are two main kinds of solitons

- temporal solitons: They are formed via a balance between nonlinear self-phase modulation and linear dispersion.
- spatial solitons: They rely on balancing nonlinear self-focusing and linear diffractive spreading. Solitary waves in nematic liquid crystals, are an example of a spatial soliton.

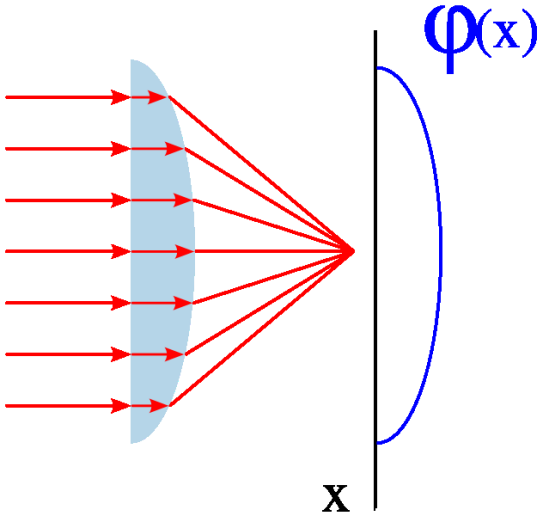

Figure 1.5: How spatial solitons behave like a normal electric field focused by a lens. (Quoted from Wikipedia, the free encyclopaedia; Released into the public domain by the author Alessio Damato.)

It should be noted that the term soliton refers to a solitary wave with the additional property that any number can interact clearly, so that the only effect of a collision is a phase shift. In particular, the amplitudes and velocities of the solitons do not change due to the collision. However, in the non-mathematical literature the terms soliton and solitary wave are used interchangeably.

Solitons are ubiquitous in nature, appearing in such different fields as fluid dynamics, plasma physics, acoustics, magnetohydrodynamics, quantum electrodynamics, Bose-Einstein condensates and even in proteins and DNA, [16, 17, 18, 19, 20, 21]. In optics, bright spatial solitons have been identified as nonlinear solutions of the propagation equation when light travels in materials whose dielectric constant increases with increasing field intensity [72]. After the invention of lasers in the early sixties and the discovery of light self-action [22, 23], spatial solitons in optics have been investigated in a large variety of nonlinear materials in both one and two transverse dimensions [24, 25, 26, 27, 28, 29, 30, 31, 32, 33, 34, 35, 36, 37, 38, 39, 42, 41].

To explain how a spatial soliton can exist, let us start from a simple convex lens. As shown in Figure 1.5, an optical field approaches the lens and then is focused. The focusing is caused by a non-uniform phase change introduced by the lens. The phase change is a function of space. Define this function as $\varphi(x)$, whose shape can be approximately represented in Figure 1.5. Let $L(x)$ be the width of the lens. Then the phase change can be expressed as

$$\varphi(x) = k_0 n L(x), \tag{1.57}$$

where k_0 is the phase constant and n is the refractive index. It can be seen that the key getting a focusing effect is to introduce a phase change of such a shape. But changing the width is not the only way to cause this. A completely different approach is changing the value of the refractive index $n(x)$ while leaving the width L fixed. Fortunately, graded-index fibres can work in this way where the change in the refractive index introduces a focusing effect that can balance the natural diffraction of the field. When the two effects balance each other perfectly, a confined field can propagate within the fibre. Based on the same principle, spatial solitons can be obtained due to a self-phase modulation introduced by the Kerr effect.

The Kerr effect, discovered in 1875 by John Kerr [40], a Scottish physicist, is a change in the refractive index of a material in response to an applied electric field. All materials can show a Kerr effect, but certain liquids display it more strongly than others. The Kerr effect is normally classified as two special cases: the Kerr electro-optic effect (also called DC Kerr effect), and the optical Kerr effect (also called AC Kerr effect). The DC Kerr effect, happens when a change slowly varying external electric field is applied by, for instance, a voltage on electrodes across the sample material. For a nonlinear media, the electric polarization field P depends on the electric field E as

$$\mathbf{P} = \varepsilon_0 \chi^{(1)} \cdot \mathbf{E} + \varepsilon_0 \chi^{(2)} \cdot \mathbf{EE} + \varepsilon_0 \chi^{(3)} \cdot \mathbf{EEE} + \cdots, \tag{1.58}$$

where ε_0 is the vacuum permittivity and $\chi(n)$ is the n-th order component of the electric susceptibility of the medium. The "$\cdot$" symbol represents the scalar product between matrices. In components, equation (1.58) can be also expressed as

$$P_i = \varepsilon_0 \sum_{j=1}^{3} \chi_{ij}^{(1)} E_j + \varepsilon_0 \sum_{j=1}^{3}\sum_{k=1}^{3} \chi_{ijk}^{(2)} E_j E_k + \varepsilon_0 \sum_{j=1}^{3}\sum_{k=1}^{3}\sum_{l=1}^{3} \chi_{ijkl}^{(3)} E_j E_k E_l + \cdots \tag{1.59}$$

where $i = 1, 2, 3$. For a linear medium, the first term of equation (1.58) dominates and the polarization varies linearly with the electric field. For materials exhibiting a non-negligible Kerr effect, the third term via a cubic (third-order) susceptibility $\chi^{(3)}$ is significant, with the even-order terms typically dropping out due to inversion symmetry of the Kerr medium. Consider the electric field $\mathbf{E}$ produced by a light wave of frequency ω travelling through an external electric field $\mathbf{E_0}$

$$\mathbf{E} = \mathbf{E}_0 + \mathbf{A}_\omega \cos(\omega t), \tag{1.60}$$

where $\mathbf{A}_\omega$ is the vector amplitude of the wave. Combining equation (1.58) and equation (1.59) yields a complex expression for $\mathbf{P}$. For the DC Kerr effect, all terms can be neglected except the linear terms and those with $\chi^{(3)}$

$$\mathbf{P} \simeq \varepsilon_0 \left(\chi^{(1)} + 3\chi^{(3)} |\mathbf{E}_0|^2\right) \mathbf{A}_\omega \cos(\omega t), \tag{1.61}$$

which is similar to the linear relationship between polarization and the electric field of a wave, with an additional non-linear susceptibility term proportional to the square of the amplitude of the external field. For non-symmetric media such as liquids, this induced change of susceptibility turns the sample material to be birefringent with different indices of refraction for light polarized parallel to or perpendicular to the applied field. The difference in index of refraction, Δn, is given by

$$\Delta n = \lambda K_e |\mathbf{E}_0|^2, \tag{1.62}$$

where λ is the wavelength of the light, K_e is the Kerr constant, and $\mathbf{E}_0$ is the strength of the electric field.

Compared with the DC Kerr effect, the AC Kerr effect is the case in which the electric field is due to the light itself, without the need for an external field to be applied. The effect causes a variation in index of refraction which is proportional to the local irradiance of the light and only becomes significant for very intense beams such as those from lasers. This refractive index variation leads to the nonlinear optical effects of self-focusing, self-phase modulation and

modulational instability. For the AC Kerr effect, the electric field is given by

$$\mathbf{E} = \mathbf{A}_\omega \cos(\omega t), \tag{1.63}$$

without the external field $\mathbf{E}_0$ term, c.f. equation (1.60) for the DC Kerr effect. Combining equation (1.63) with the equation for the polarization (1.58), and taking only linear terms and those with $\chi^{(3)}$, results in

$$\mathbf{P} \simeq \varepsilon_0 \left(\chi^{(1)} + \frac{3}{4}\chi^{(3)} |\mathbf{A}_\omega|^2 \right) \mathbf{A}_\omega \cos(\omega t), \tag{1.64}$$

This is of the form of a susceptibility with a linear susceptibility plus an additional nonlinear term

$$\chi = \chi_{\text{linear}} + \chi_{\text{nonlinear}} = \chi^{(1)} + \frac{3\chi^{(3)}}{4} |\mathbf{A}_\omega|^2. \tag{1.65}$$

We then have

$$n = (1+\chi)^{1/2} = (1 + \chi_{\text{linear}} + \chi_{\text{nonlinear}})^{1/2} \simeq n_0 \left(1 + \frac{1}{2{n_0}^2} \chi_{\text{nonlinear}} \right), \tag{1.66}$$

where $n_0 = (1+\chi_{\text{linear}})^{\frac{1}{2}}$ is the linear refractive index. Because $\chi_{\text{nonlinear}} \ll n_0^2$, a Taylor expansion in the intensity dependent refractive index gives

$$n = n_0 + \frac{3\chi^{(3)}}{8n_0} |\mathbf{A}_\omega|^2 = n_0 + n_2 I, \tag{1.67}$$

where n_2 is the second-order nonlinear refractive index (the Kerr coefficient), and I is the local intensity of the propagating optical wave. It can be seen that the refractive index change is thus proportional to the intensity of the light travelling through the medium.

Rather than changing the refractive index $n(x)$, the same effect can be obtained by introducing a phase change $\varphi(x)$, is as in equation (1.57). The change in the refractive index $n(x)$ is given by equation (1.67). Hence, this new approach yields a phase change

$$\varphi(x) = k_0 n(x) L = k_0 L [n_0 + n_2 I(x)]. \tag{1.68}$$

If $I(x)$ has a shape similar to the one shown in the figure 1.5, then the appropriate phase behaviour can be created to bring about a field which will show a self-focusing effect. In other words, there will be a fibre-like guiding structure, for which the focusing nonlinear and diffractive linear effects are perfectly balanced. As long as the medium does not change and if losses can be neglected, then the field will propagate forever without changing its shape. To have this self-focusing effect, n_2 has to be positive.

The basic equation governing optical spatial solitary waves will now be derived. From equation (1.67), in a medium showing the AC Kerr effect (optical Kerr effect), the refractive index is given by

$$n(I) = n_0 + n_2 I. \tag{1.69}$$

The relationship between intensity and electric field is

$$I = \frac{|E|^2}{2\eta}, \tag{1.70}$$

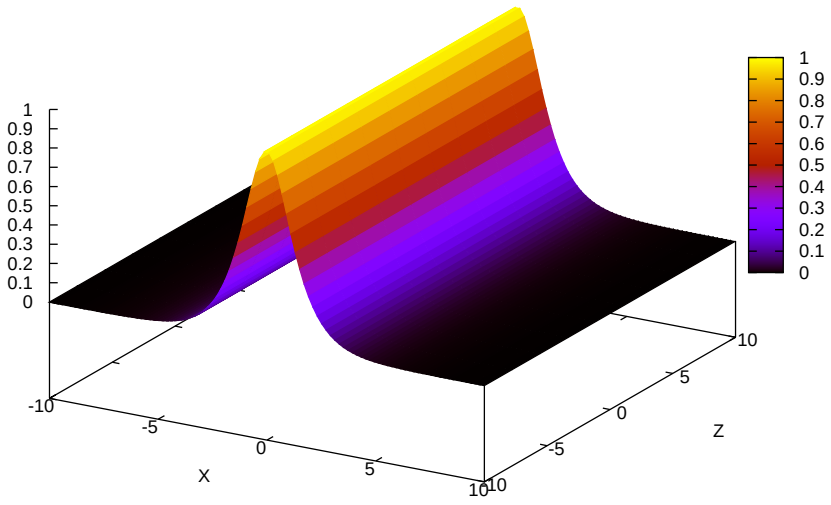

Figure 1.6: Fundamental spatial soliton by the solution from Kerr media.

where $\eta = \eta_0/n_0$ and η_0 is the impedance of free space.

Let us assume that the field is propagating in the z direction with a phase constant $k_0 n_0$. Now consider a $(1+1)D$ propagation by ignoring any dependence on y. The field can be expressed in the complex representation

$$E(x,z,t) = A_m u(x,z) e^{i(k_0 n_0 z - \omega t)}, \tag{1.71}$$

where A_m is the maximum amplitude of the field and $u(x,z)$ is a dimensionless normalized function (so that its maximum value is 1) that represents the shape of the electric field. The field E satisfies the Helmholtz equation

$$\nabla^2 E + k_0^2 [n(I)]^2 E = 0. \tag{1.72}$$

Assuming that the envelope $u(x,z)$ changes slowly in the propagation direction, i.e.

$$\left| \frac{\partial^2 u(x,z)}{\partial z^2} \right| \ll \left| k_0 \frac{\partial u(x,z)}{\partial z} \right|, \tag{1.73}$$

substituting equation (1.71) into equation (1.72) and then simplifying yields

$$\frac{\partial^2 u}{\partial x^2} + i2k_0 n_0 \frac{\partial u}{\partial z} + k_0^2 \{[n(I)]^2 - n_0^2\} u = 0. \tag{1.74}$$

Nonlinear effects are usually much smaller than linear ones, so that

$$[n(I)]^2 - n_0^2 = [n(I) - n_0][n(I) + n_0] = n_2 I(2n_0 + n_2 I) \approx 2n_0 n_2 I, \tag{1.75}$$

then expressing the intensity in terms of the electric field gives

$$[n(I)]^2 - n_0^2 \approx 2n_0 n_2 \frac{|A_m|^2|u(x,z)|^2}{2\eta_0/n_0} = n_0^2 n_2 \frac{|A_m|^2|u(x,z)|^2}{\eta_0}. \tag{1.76}$$

The governing equation thus becomes

$$2ik_0 n_0 \frac{\partial u}{\partial z} + \frac{\partial^2 u}{\partial x^2} + \frac{k_0^2 n_0^2 n_2 |A_m|^2}{\eta_0}|u|^2 u = 0. \tag{1.77}$$

This is a common equation known as the nonlinear Schrödinger equation (NLS). The analytical solution of equation (1.77) for the fundamental soliton is

$$u(x,z) = \sqrt{I_0}\,\mathrm{sech}(x/w_0)e^{iz/2L_d}, \tag{1.78}$$

where the peak intensity I_0 is related to the diffraction length $L_d = k_0 n_0 w_0^2$ through $I_0 = (k_0^2 n_0 n_2 w_0^2)^{-1} = (k_0 n_2 L_d)^{-1}$, and w_0 is the width of the light beam. This soliton solution is shown in Figure 1.6, where it can be seen that the shape of the field does not change during propagation. This stable field profile was proven by the inverse scattering method [43]: in such an integrable system, any N interacting solitons always remain individual entities. Bright spatial solitons in Kerr media give rise to a transverse refractive index profile or graded-index waveguide able to counteract their natural tendency to diffract [44]. Beams of any waist can be self-trapped as the effective size of the soliton scales with $I_0^{-\frac{1}{2}}$. In principle, only $(1+1)D$ (1-transverse + 1-propagation) stable Kerr solitons can be generated with the form (1.78). $(2+1)D$ Kerr solitons are unstable and when powers exceed the critical power P_c nonlinear self-focusing prevails over diffraction and causes what is usually called catastrophic collapse, unless the emergence of higher order dynamics counteracts the Kerr effect or until damage occurs [37, 45].

In 1974 the first experiment on spatial optical solitons was reported by Ashkin and Bjorkholm in a cell filled with sodium vapor, where what they found was $(2+1)D$ self-trapped filaments [24]. After more than ten years another experimental demonstration occurred at Limoge University in liquid carbon disulphide. Since then experiments on Kerr solitons were reported in glass, semiconductors and polymers [25, 46, 47, 58]. The lack of exact solutions for the $(2+1)D$ NLS-type model limited the immediate impact of these findings on nonlinear physics. But then it was predicted that a deviation from the pure Kerr response could balance and even arrest beam collapse in two spatial dimensions. There were corresponding demonstrations shown in several systems similar to sodium vapors, using stabilizing mechanisms such as self-steepening [37, 48], saturation [49, 50], multiphoton absorption [51, 52, 53, 54, 55, 56, 41] and higher order phenomena [57]. Meanwhile, nematic liquid crystals (NLC) show that their peculiar reorientational nonlinearity can provide for the stabilization of $(2+1)D$ optical solitons through nonlocality in the field-matter response. Here, nonlocality defines that the NLC reorientational response to electric fields or beams is highly nonlocal, i.e. the angular perturbation in director orientation diffuses from the excitation region on a finite area which could be much larger than the transverse beam size, as shown in Figure 1.7. During the last decade, several experiments have been reported on solitons in NLC, also referred to as nematicons [38, 42, 59], which will be the main topic of next section.

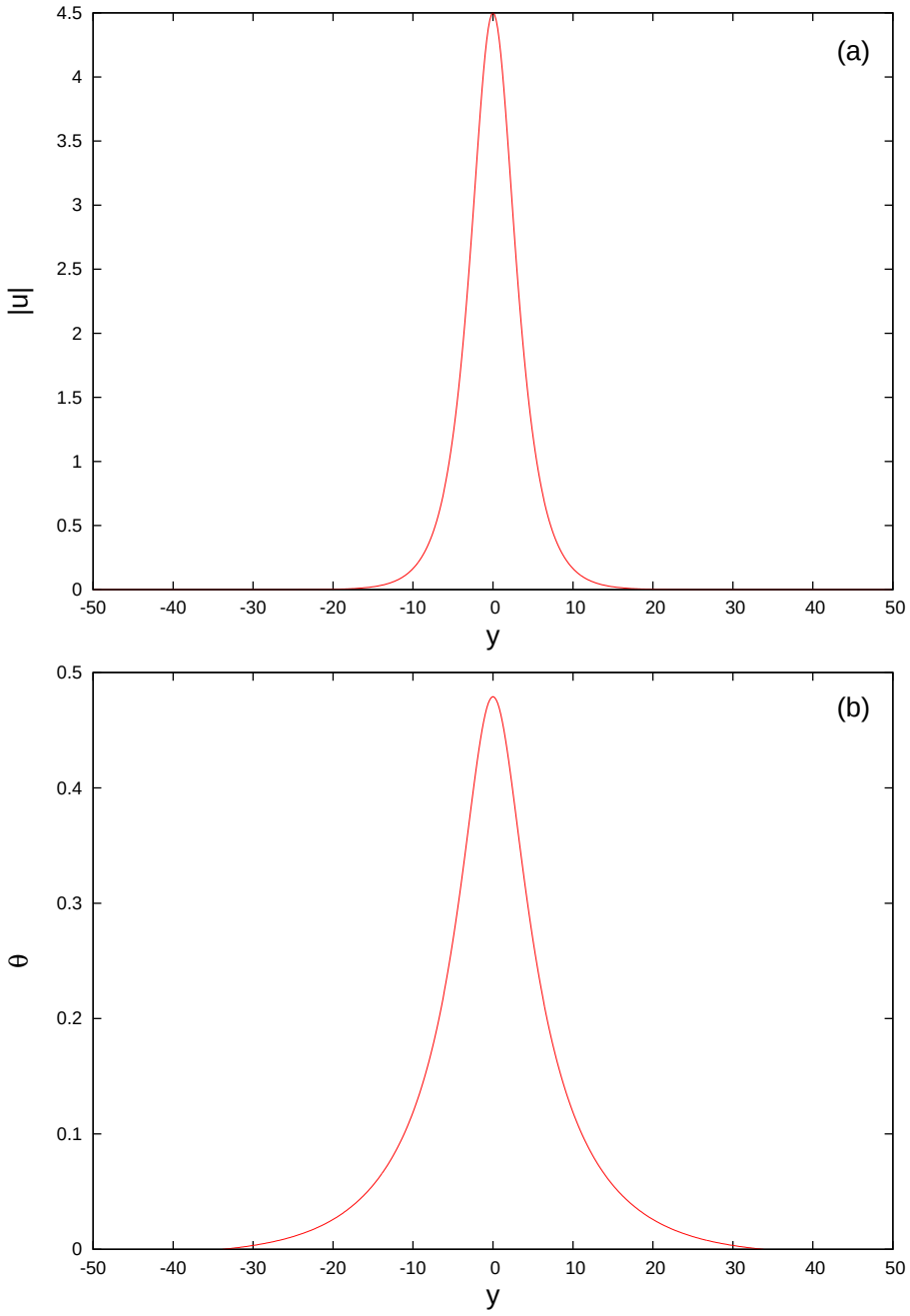

Figure 1.7: Numerically calculated steady nematicon. Cross-sections of **(a)** the nematicon beam profile and **(b)** the perturbation θ of the refractive index of the NLC caused by the beam and extending beyond it.

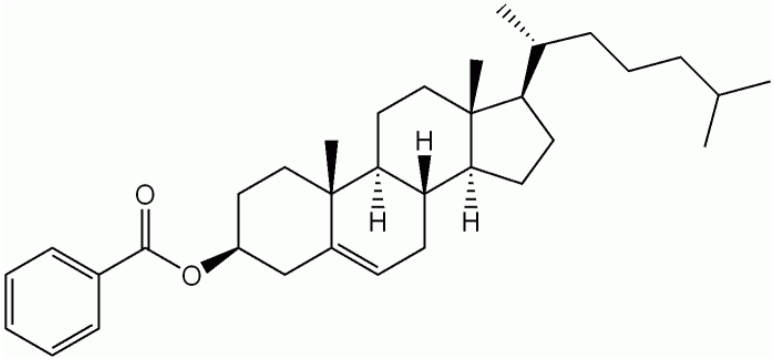

Figure 1.8: Chemical structure of Cholesteryl benzoate molecule. (Quoted from Wikipedia, the free encyclopaedia; Released into the public domain by the author Shaddack.)

1.3 Nematic Liquid Crystals and Nematicons

1.3.1 Nematic Liquid Crystals

Liquid crystals (LCs) are a state of matter which have properties between those of a conventional liquid and those of a solid crystal. An LC may flow like a liquid, but maintain some of the ordered structural characteristic of crystals. The first study of a liquid crystalline phase was in 1888 when an Austrian botanical physiologist, Friedrich Reinitzer, observed that a material known as cholesteryl benzoate (see Figure 1.8) had two distinct melting points [60]. In his experiments, Reinitzer increased the temperature of a solid sample and observed the crystal change into a hazy liquid. By increasing the temperature further, his material changed again into a clear, transparent liquid. LCs are unique in their properties and uses. As research into this field continues and as new applications are developed, LCs will play an important role in modern science and technology. Molecular order in LCs diffuses as in a liquid, while maintaining a certain degree of orientational and sometimes positional order. In other words, the molecules (mesogens) in LCs have the tendency to point along a common axis, called the director. This is in contrast to molecules in the liquid phase having no intrinsic order and molecules in the solid state having high order and little translational freedom. The degree of order of LCs can be expressed and measured in a number of ways [61]. The characteristic orientational order of the liquid crystal state is between the traditional solid and liquid phases and can be treated as a continuum of "mesogenic" states. Figure 1.9 shows the differences among the alignments of the molecules for each phase. The material in liquid crystalline phases possesses a specific macroscopic behaviour and specific molecular pattern organization [61, 62, 63]. The least organized liquid crystalline phase is usually referred to as "nematic" [62]. LCs can be divided into thermotropic, lyotropic and metallotropic phases [63]. As the name suggests, thermotropic LCs come into being as the temperature is changed. Thermotropic phases occur in a certain temperature range. Many thermotrpic LCs exhibit a variety of phases on changing the temperature, for example, nematic phase, smectic phase, chiral phase, blue phase and discotic phase. In the nematic phase the molecules have no positional order, but they self-align to have long-range directional order with their long axes roughly parallel. Thus, the molecules are free to flow and their centre of mass positions are randomly distributed as in a liquid, but still maintain their long-range directional order. So nematic liquid crystals (NLCs) exhibit a fluidity in motion, but with the optical properties of a crystal. Most NLCs are uniaxial, with

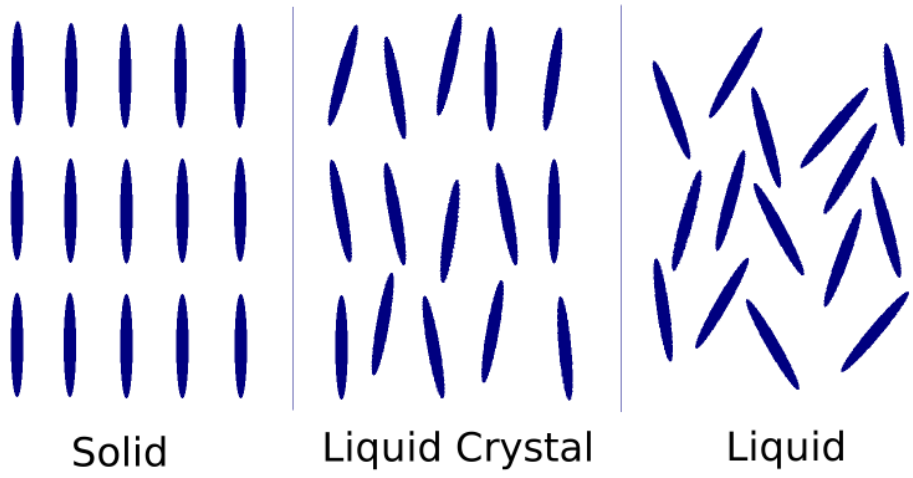

Figure 1.9: Arrangements of molecules in the solid, liquid crystal and liquid.

the optic axis corresponding to the molecular director or average orientation of the long axes [61].

By definition, an isotropic liquid has no orientational order, while the term "anisotropy" means that the properties of a material depend on the direction in which they are measured. To quantify just how much order is present in a material, an order parameter S_N is defined. Then the orientational order in NLCs can be described. A preferred average direction is denoted by a unit vector, the molecular director $\hat{n}$, see Figures 1.10 and 1.11. Consider a liquid crystalline system consisting of cylindrically shaped molecules with rotational symmetry around the major axis, as in NLC. Then [66]

$$S_N = \frac{1}{2}\langle 3\cos^2\alpha - 1\rangle, \tag{1.79}$$

where α is the angle between the long molecular axis and the director, and the average $\langle\ \rangle$ is taken over the total solid angle. Some extreme case, such as $\cos\alpha = \sqrt{1/3}$, cannot occur, because α is small, random and not uniform. In the most common class of NLCs, the order parameter depends on the temperature. In these materials S_N equals 1 in the solid state, decreases as the temperature increases, reaches $S_N = 0$ at a critical temperature corresponding to the transition to the isotropic phase, as shown in Figure 1.12. Typical values for the order parameter of a liquid crystal range between 0.3 and 0.9 as a result of the kinetic molecular motion.

Functions of the order parameter can describe the electromagnetic properties of NLCs. The dielectric tensor of NLCs in the director frame of reference can be represented as [66]

$$\bar{\bar{\varepsilon}} = \begin{pmatrix} \varepsilon_\perp & 0 & 0 \\ 0 & \varepsilon_\perp & 0 \\ 0 & 0 & \varepsilon_\parallel \end{pmatrix},$$

which means the medium exhibits a macroscopic birefringence, with distinct refractive indices $n_\parallel = \sqrt{\varepsilon_\parallel/\varepsilon_0}$ and $n_\perp = \sqrt{\varepsilon_\perp/\varepsilon_0}$ associated with electric fields parallel and normal to $\hat{n}$,

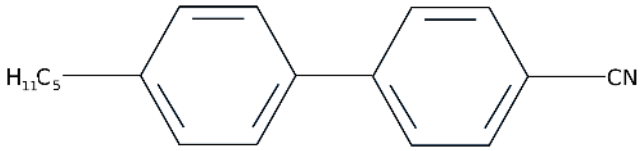

Figure 1.10: Organic molecule in the NLC known as 5CB.

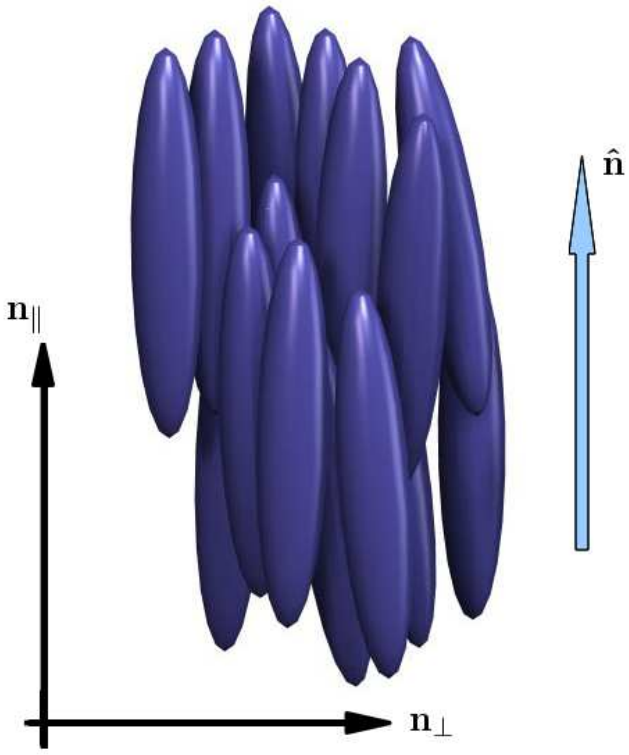

Figure 1.11: Schematic of mesogen alignment in a liquid crystal nematic phase. (Part quoted from Wikipedia, the free encyclopaedia; Released into the public domain by the author Kebes.)

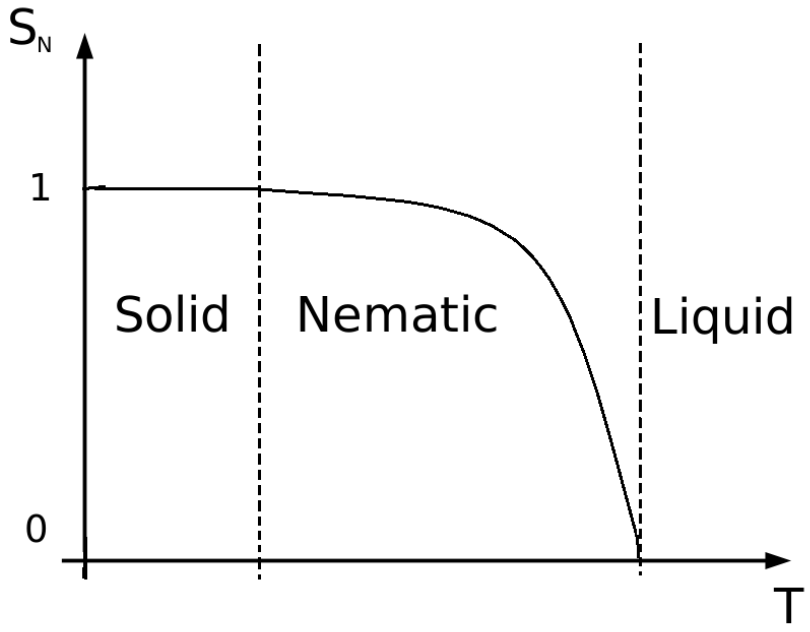

Figure 1.12: Order parameter S_N versus temperature in thermotropic liquid crystals.

respectively. ε_0 is the vacuum dielectric permeability and $\Delta\varepsilon = \varepsilon_{\parallel} - \varepsilon_{\perp}$. The refractive indices generally depend on the order parameter. Ideally, the molecules are along a common direction, but this organisation becomes deformed in the presence of interactions with the confining boundaries and/or applied electric or magnetic fields, so that the order parameter changes. There are three kinds of typical deformations, as shown in Figure 1.13, splay $\nabla \cdot \hat{n} \neq 0$, bend $\nabla \times \hat{n} \perp \hat{n}$, and twist $\nabla \times \hat{n} \parallel \hat{n}$. If the director alignment is homogeneous and $\hat{n}$ is perpendicular to the applied field, the reorientation of the molecules occurs above an intensity threshold, which is known as the Freédericks threshold. In nonlinear optics [63], if the intensity is strong enough the optical field propagating in the medium produces a nonlinear self-focusing response due to an increase in the extraordinary refractive index produced by the reorientation [63, 64, 65]. Considering a generic Cartesian reference system xyz, for a director $\hat{n}$ with a distribution described by the angles ξ and ρ in spherical polar coordinates

$$\hat{n} = \hat{n}(\sin(\xi), \cos(\xi)\cos(\rho), \cos(\xi)\sin(\rho)). \tag{1.80}$$

Then the steady state volume distribution of the director in the presence of arbitrary boundary/anchoring conditions and applied fields can be cast in the form

$$\begin{cases} \dfrac{\partial F}{\partial \xi} - \displaystyle\sum_{j\in\{x,y,z\}} \frac{\partial}{\partial j}\frac{\partial F}{\partial \frac{\partial \xi}{\partial j}} = 0, \\ \dfrac{\partial F}{\partial \rho} - \displaystyle\sum_{j\in\{x,y,z\}} \frac{\partial}{\partial j}\frac{\partial F}{\partial \frac{\partial \rho}{\partial j}} = 0, \end{cases} \tag{1.81}$$

where F is the total free energy for a stationary alignment of the NLC director.

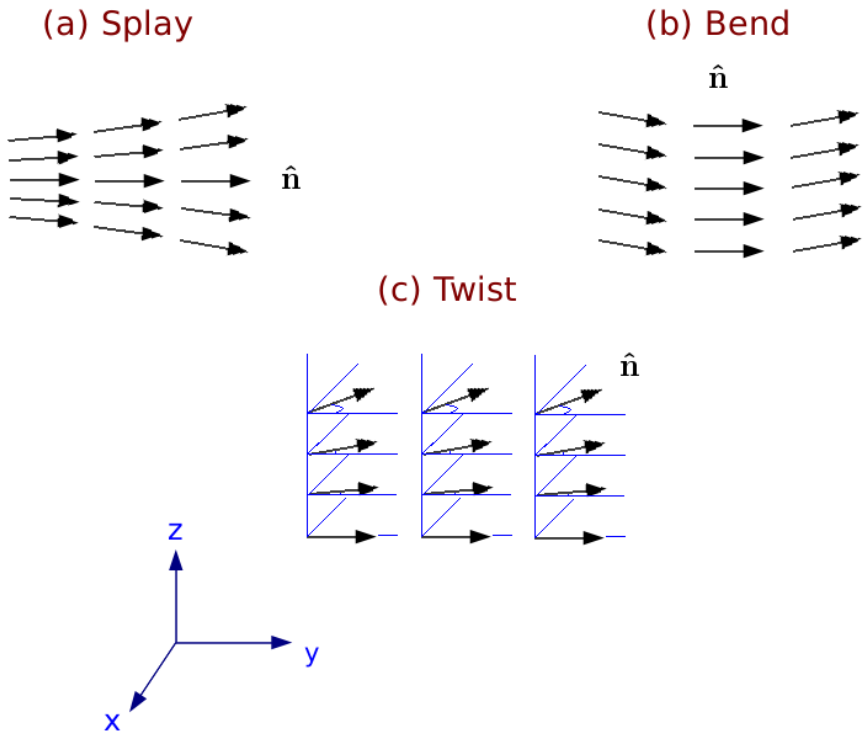

Figure 1.13: Macroscopic deformations in NLCs: (a) splay; (b) bend; (c) twist. Reproduced from [66].

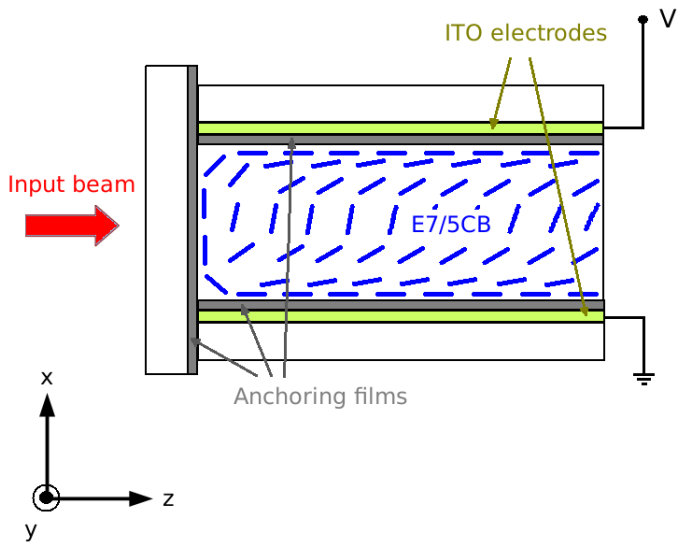

Figure 1.14: Sketch of the side view of a typical NLC cell and propagation geometry. Reproduced from [66].

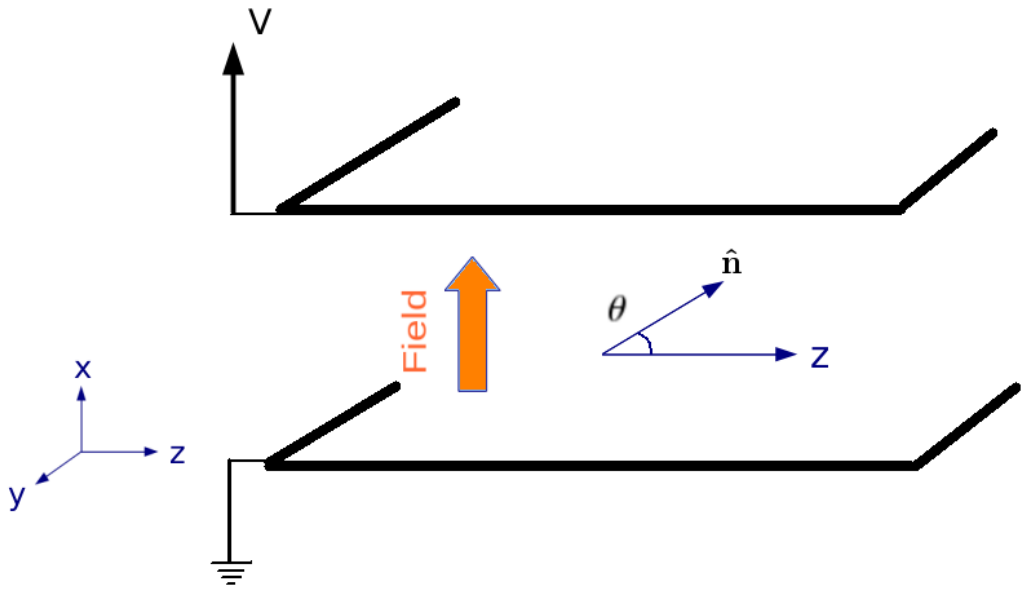

Figure 1.15: A planar cell of thickness d with a planarly aligned NLC and biased by a low-frequency voltage V.

Figure 1.14 shows a sketch of a typical planar glass cell used for the observation of nematicons [66]. There are two glass slides parallel to each other with a layer of NLCs, e.g. the commercial mixtures E7 or 5CB, filled in between them. Indium-tin-oxide (ITO) film electrodes on the internal surfaces of the slides apply a low-frequency (KHz) voltage across the NLC thickness [66]. Rubbed polymer films are deposited on the inner interfaces to induce planar anchoring of the molecules at the boundaries [63]. A third glass slide seals the cell entrance to avoid the formation of an undesired meniscus at the air-NLC interface because a meniscus might alter the polarization and phase distribution of the input beam [68]. The director is assumed to lie in the yz plane. Nevertheless a small pretilt of the order of one degree is usually impressed by the anchoring films and prevents the formation of disclinations in the bulk NLC [69, 70]. A light beam with electric field extraordinarily polarized in the xz plane is launched in the cell using a microscopic objective [68]. Due to scattering losses, its evolution in the plane yz can be imaged by collecting the photons scattered through the top slide using an optical microscope and a high-resolution CCD camera [68].

As shown in Figure 1.15, in a planar cell of thickness d with an applied low-frequency voltage V, the nematic molecular director is forced to reorientate by the action of a quasi-static field E across the cell thickness (x). Let $\theta(x, z)$ be the orientation angle. To overcome the Freédericks threshold the molecules are pre-titled by the static electric field so that $\theta \approx \frac{\pi}{4}$, the Freédericks threshold being 0 for $\theta = \frac{\pi}{4}$. Since the cell midplane $x = 0$ is an extraordinary plane, in this geometry where $\theta = \rho, \xi = 0$, and the system (1.81) can be shown to become [66]

$$K\nabla^2\theta + \frac{1}{4}\varepsilon_0\varepsilon_a E^2 \sin(2\theta) = 0, \tag{1.82}$$

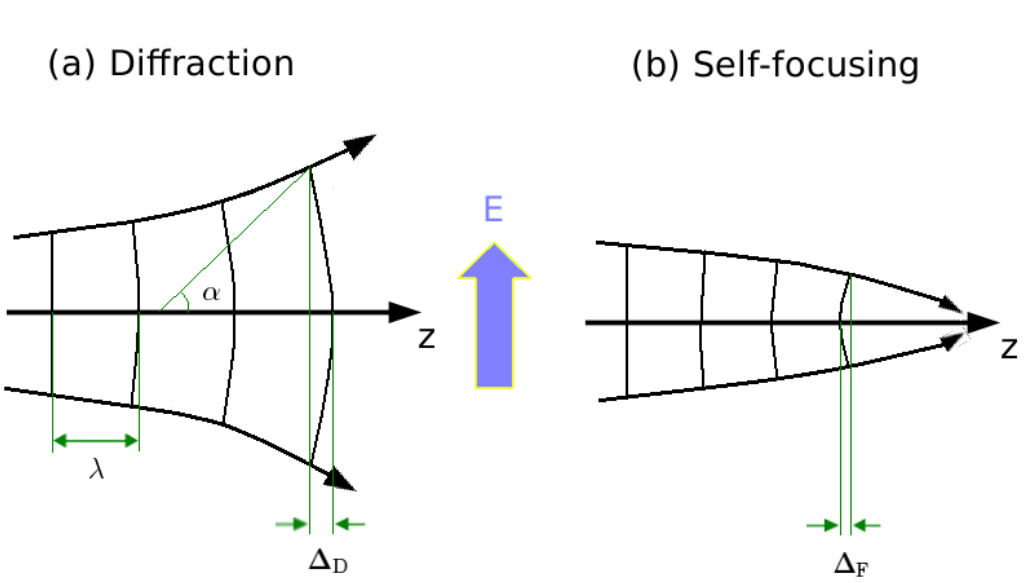

Figure 1.16: Wavefront bending due to (a) purely linear diffraction (b) pure self-focusing. Reproduced from [66].

where K is the elastic constant in the single constant approximation so that splay, bend and twist have the same elastic constant and $\varepsilon_a = n_{\parallel}^2 - n_{\perp}^2$ is the dielectric anisotropy at optical frequencies. Equation (1.82) is elliptic, so that the NLC reorientational response to electric fields or beams is highly nonlocal [63, 65, 67].

NLCs are chemically stable and have easily tunable nonlinearities because their refractive index is easily changed by electric fields, magnetic fields and boundary conditions. These properties mean that NLCs have become relatively common media for optical experimentation and applications.

1.3.2 Nematicons

In optics, nematicons are spatial optical solitary waves (self-trapped light beams) in nematic liquid crystalline systems. Due to their optically nonlinear, saturable, nonlocal and nonresonant response, such systems enable light to self-confine and to guide additional optical signals, which makes them an ideal testbed for applications in all-optical information processing [71].

Light induced reorientation results in the generation of a spatial solitary wave due to an appropriate balance between linear diffraction and nonlinear self-focusing. Let a Gaussian beam propagate with an extraordinarily polarized electric field in a principal plane of a positive uniaxial NLC. Figures 1.16 shows the curved phase-front of the beam in the cases of purely linear diffraction and pure self-focusing, where Δ_D and Δ_F are the wavefront phase delays acquired on-axis during propagation in the two cases, respectively. When only diffraction occurs, the far-field divergence is $\alpha \approx \lambda/(\pi w_0 n_0)$ in the paraxial approximation, with λ the wavelength, w_0 the waist and n_0 the linear refractive index. Simple geometric considerations give [66]

$$\Delta_D = z(1 - \cos\alpha) \approx \frac{z\lambda^2}{8\pi^2 w_0^2 n_0^2}. \tag{1.83}$$

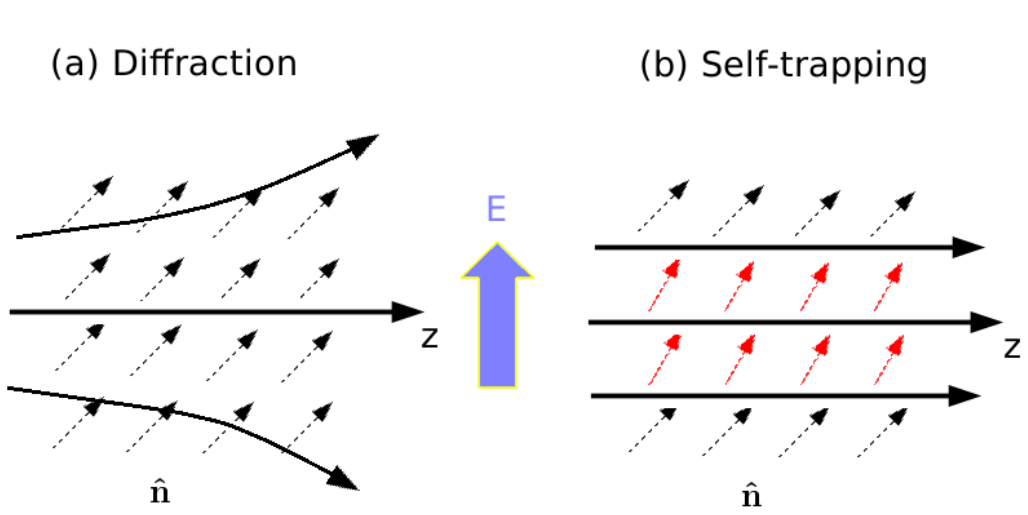

Figure 1.17: Self-confinement through reorientation and its physics in NLC. (a) A beam launched along z axis in homogeneously aligned NLC diffracts. (b) By inducing reorientation the extraordinary index increases and mediates beam self-focusing. Reproduced from [66].

For the simple Kerr dependence, Δ_F is linear with the index perturbation [66]

$$\Delta_F = -n_2 I_0 z, \tag{1.84}$$

with $I_0 = \lambda^2/(8\pi^2 w_0^2 n_0^2 n_2^2)$ the beam intensity. A balance between diffraction and self-focusing, i.e. $\Delta_D + \Delta_F = 0$, yields the critical beam power [66]

$$P_c = \frac{\pi}{2}\omega_0^2 I_0 = \frac{\lambda^2}{16\pi n_0^2 n_2^2}, \tag{1.85}$$

which means for an arbitrary input waist and power above P_c, self-focusing as shown in Figure 1.16(b) prevails, resulting in catastrophic collapse.

However, in the nonlocal regime, the index perturbation is much wider than the beam, so that the index change depends on power and position. Then accordingly [66]

$$\Delta_F = -n_{NL} P z, \tag{1.86}$$

with n_{NL} a constant independent on waist and P the beam power. Imposing nonlinear compensation of diffraction gives the critical power [66]

$$P_c = \frac{\lambda^2}{8\pi^2 w_0^2 n_0^2 n_{NL}^2}. \tag{1.87}$$

Equation (1.87) shows P_c varies with the waist w_0. That is to say, in the nonlinear regime, due to the nonlocal response, self-focusing weakens (the critical beam power increases) as the spot-size reduces, therefore preventing collapse and stabilising the self-trapped wavepacket. Figure 1.17 shows this, that when the input beam power goes up above the linear level, reorientation induces a focusing lens-like distribution of the extraordinary index. When the diffraction, as in Figure 1.17(a), is compensated, a spatial soliton is established and propagates as in Figure 1.17(b). A generated nematicon from Peccianti *et al.*'s experiments can be clearly seen in their

paper [68].

A spatial soliton is connected to an optically induced index perturbation, except notably in quadratic media [73, 74]. Hence, nematicon waveguides were found to be able to trap and transmit co-polarized signals of any modulation format, spectral content and temporal sequence, including high bit-rate data streams for optical communications [66]. This was confirmed by the confinement of a weak collinear He-Ne probe ($\lambda = 632.8nm$) which was colaunched with an Ar^+ beam [68]. Further, it was shown that the probe could be steered by changing the direction of propagation of the nematicon [75]. Furthermore, due to nonlocality nematicon waveguides can be multimoded and confine several extraordinarily polarized guided modes [76], as recently experimentally demonstrated [77].

As in Figure 1.14, let us consider a spatial soliton propagating in a planarly aligned liquid crystal cell, with the director lying in the plane xz. Neglecting walk-off, take the electric field with complex envelope $\mathbf{E}$ and polarisation along x (i.e. $\mathbf{E} = E\hat{x}$) to propagate in the midplane $x = 0$ with wavevector $\mathbf{k} = k\hat{z}$. And let a quasi-static field $\mathbf{E}' = E'\hat{x}$ pre-tilt the nematic at angle $\Theta(x)$ in xz and so avoid the Fréedericks threshold. We consider the structure to be invariant along both z and y, and the bias E' to be unaffected by the optical perturbation of the director. System (1.81) can be shown to reduce to an equation governing the total reorientation ϕ, i.e. $\xi = \phi$ and $\rho = 0$ in the single angle approximation [66]

$$K\frac{\partial^2\phi}{\partial z^2} + K\nabla_\perp^2\phi + \frac{\Delta\varepsilon_{RF}E'^2}{2}\sin(2\phi) + \frac{\varepsilon_0\varepsilon_a|E|^2}{4}\sin(2\phi) = 0, \tag{1.88}$$

where K is a single elastic constant which describes the mechanic response for splay, bend and twist deformations [61, 62], $\Delta\varepsilon_{RF}$ is the dielectric anisotropy at radio frequencies (1kHz) normally used for biasing NLC cells. The propagation of a light beam in the NLC is then governed by the NLC-type equation [68]

$$2ik\frac{\partial E}{\partial z} + \Delta_\perp^2 E + k_0^2(n_\parallel^2 - n_\perp^2)(\sin^2\phi - \sin^2\hat{\theta})E = 0, \tag{1.89}$$

with $\hat{\theta} = \Theta(0)$ the peak-tilt of the NLC director in the absence of light, ϕ the overall tilt due to the combined action of light and voltage and $k = k_0 n(\hat{\theta}) = 2n(\hat{\theta})\pi/\lambda$ the wavenumber in bulk. As shown in Figure 1.14, the planar interfaces and anchoring give the boundary conditions $\Theta(d/2) = \Theta(-d/2) = 0$. Combining voltage- and light-induced reorientation gives

$$\phi(x, y, z) = \Theta(x) + \frac{\Theta(x)}{\hat{\theta}}\theta(x, y, z), \tag{1.90}$$

where θ defines the all-optical (nonlinear) perturbation. Using equation (1.90), taking $|\theta| \ll \Theta$ which is the case for the usual milliwatt beam powers, and assuming that the cell is much thicker than the beam waist, so that $\Theta(x) = \hat{\theta}$, it can be shown that equations (1.88) and (1.89) reduce to [66]

$$2ik\frac{\partial E}{\partial z} + \nabla_\perp^2 E + k_0^2(n_\parallel^2 - n_\perp^2)\theta E = 0, \tag{1.91}$$

$$K\nabla_{xyz}^2\theta - \Delta\varepsilon_{RF}\theta E^2\frac{\sin 2\phi}{2\hat{\theta}}(1 - \gamma_0) + \frac{\varepsilon_0(n_\parallel^2 - n_\perp^2)|E|^2}{4}\sin 2\hat{\theta} = 0, \tag{1.92}$$

where $\gamma_0 = 2\hat{\theta}\cos 2\phi/\sin 2\phi$. Introducing a free parameter ν and normalising variables, the

system (1.91) and (1.92) can be reduced to

$$i\frac{\partial E}{\partial z} + \nabla^2 E - E + E\theta = 0, \tag{1.93}$$

$$\epsilon\nu\frac{\partial^2\theta}{\partial z^2} + \nabla^2\theta - \frac{1}{\nu}(1-\gamma_0)\theta + \frac{1}{2}|E|^2 = 0, \tag{1.94}$$

with $\epsilon = \sin 2\hat{\theta}\Delta\varepsilon_{RF}E^2/2\hat{\theta}k^2K$ being a material parameter.

Well away from the Fréedericks transition ($\hat{\theta} \approx \pi/4$ and $\gamma_0 \approx 0$), considering the limit $\epsilon\nu\frac{\partial^2\theta}{\partial z^2} = 0$, i.e. for small ϵ or in the case of slowly varying envelope along z, as in solitons, for small ν the field envelope E is governed by [78]

$$i\frac{\partial E}{\partial z} + \nabla^2 E + \frac{1}{2}\big(1+\nu\nabla^4\big)|E|^2 = 0, \tag{1.95}$$

which encompasses a nonlocal correction to the stardard Kerr model, sustaining stable and collapse-free soliton propagation in weakly-nonlocal bulk media. Therefore, the parameter ν quantifies the nonlocality in the response, ranging from highly nonlocal solitons (HNS) when $\nu \to \infty$ to local Kerr solitons for $\nu \to 0$. The HNS is Gaussian and depends on beam power rather than local intensity, as expected for a highly nonlocal nonlinearity [44].

NLC is a slowly responding medium, which is responsible for the inherent time-independence. A speckled or spatially incoherent beam with fast point-to-point phase and amplitude fluctuations can form incoherent solitons [80, 81]. This class of spatial soliton, excited by a beam with a low degree of spatial coherence, can be described by an infinite set of coupled nonlinear Schrödinger-like equations to account for the broadened angular spectrum [82, 83]. The features of these solitons rely on the degree of nonlocality [84, 85], including their mutual interactions [86]. Partially coherent solitons in NLC were experimentally demonstrated by placing a rotating random diffuser in the path of an Ar^+ laser beam. Then the rotation induces rapid variations in the speckle pattern with respect to the NLC time response, while randomness gives rise to beam profiles with significant angular spreading [87, 88].

As introduced in Section 1.3.1, the anisotropy of NLCs leads to the reorientational response. NLC with higher birefringence are expected to exhibit stronger self-focusing, even though mitigated by the modified elastic properties [66]. As in any uniaxial crystal, an electromagnetic plane wave propagating with wave normal in NLCs can be described as the superposition of ordinarily (o-) and extraordinarily (e-) polarized wave components, eigensolution of Maxwell equations [89]. Importantly, NLC displays birefringent walk-off, i.e. an e-wave energy flux (e-Poynting vector) noncollinear with the wavevector related to the group velocity. For the high birefringence of NLC, the walk-off can assume large values (e.g., up to 7-9 degrees in E7), thereby affecting the nematicon dynamics. Since birefringent walk-off is a large effect in uniaxial NLC, the reorientational response induced by extraordinarily polarized light waves and leading to beam self-focusing and self-trapping is expected to modify walk-off. Hence, nonlinear corrections to walk-off could affect the nematicon direction of propagation, i.e. its Poynting vector, when the power excitation is large enough to go beyond the first order perturbation [90], as shown in Figure 1.18. Let $\mathbf{S}$ denote the e-Poynting vector. Then three different regimes can be identified for beam propagation in NLC versus excitation: in the linear regime at low powers, the reorientation is negligible and the beam diffracts, with its Poynting vector at angle δ_0 with respect to the wavevector parallel to z; in the first-order nonlinear regime, all-optical reorientation promotes self-trapping and the resulting nematicon travels at the linear walk-off; in

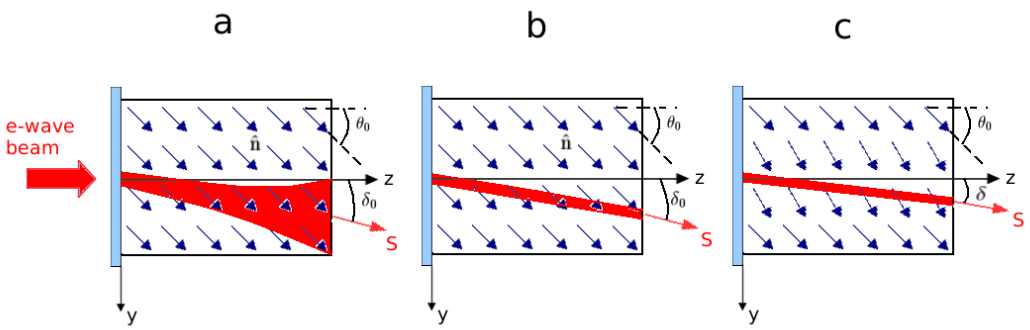

Figure 1.18: (**a**) Linear beam propagation in the plane yz (top view) with diffraction and walk-off (**b**) Nonlinear propagation in the first-order regime with self-confinement and walk-off (**c**) Highly nonlinear propagation with self-confinement and reduced walk-off. Reproduced from [66].

the highly nonlinear regime, the total orientation becomes comparable to the initial orientation θ_0 so that it alters the walk-off [66].

A remarkable soliton self-steering was reported in a guest-host system, using E7 doped with the dye 1-amino-anthraquinone to exploit the Janossy effect, a resonant enhancement of the reorientational nonlinearity [91, 92]. This steering, over $\approx 39°$ from negative to positive angles with respect to the input wavevector along z, cannot be explained by nonlinear walk-off as outlined above, but can be ascribed to nonparaxial nematicon propagation in conjunction with the excited-state microscopic response of the particular guest-host system [93, 94, 95].

Many standard mathematical techniques for solitons analysis cannot be applied due to a lack of exact solitary wave solutions for the governing equations of nematicon propagation. Due to this, variational techniques using reasonable approximations offer a powerful approach towards both qualitative and quantitative predictions. One of them, better known as 'modulation theory' [1] and based on the Lagrangian of the governing equations, was first extended to include the shed radiation which 'sits' under the soliton by [96] and found to be effective in describing nematicons in a wide range of experimental conditions [96, 97, 98, 99, 100, 101, 102, 103, 104, 111, 113, 115, 116, 118, 125]. In a remarkable set of experiments, Assanto and collaborators [179] demonstrated the possibility of producing stable spatial solitons in NLCs. Modulation theory was applied to study these solitons and good agreement with the experimental results and numerical simulations has been obtained [96, 97, 98, 99, 100, 101, 102, 103, 104, 111, 113, 115, 116, 118, 125]. Self-confined beams can interact, depending on the geometry, the nature of the nonlinear response and, ultimately, on the integrability of the model [105, 106]. Experiments on nematicon interactions were carried out with equally powered Ar^+-laser beams polarized along x and launched with a $20X$ microscope objective in a $75\mu m$ thick E7-NLC cell, with the molecular director lying in the plane xz and pretilted by an external bias to $\theta_0 \cong= \pi/4$ [88]. Potential applications of nematicons and their interactions have been demonstrated in the framework of all-signal processing and readdressing [107, 188]. Their nonlocal character allows these bright solitons not only to propagate in a stable fashion but also to encompass long-range interactions, which are attractive and phase-independent [66]. A number of optical logic operations can be designed exploiting this mechanism [66].

Besides collisional interactions, two spatial solitons initially carrying angular momentum, i.e., launched with propagation directions belonging to distinct planes, can spiral around one another and compensate refraction due to the centrifugal force with attraction due to nonlocality [108]. The spiralling of two incoherent nematicons, as well as the interaction of three nematicons of different wavelengths, have also been studied using modulation theory [116, 126]. Nematicon steering based on the voltage-tuned walk-off modulation was realized using a NLC cell $100\mu m$ thick and $P = 5mW$-solitons excited at $\lambda = 1064nm$, demonstrating not only angular deviations as large as 7 degrees, but also the intrinsic robustness of nematicons with respect to changes in the direction of propagation [168]. An external bias has been used in several configurations to avoid the optical Freédericks transition by pre-tilting the director [68, 87, 88, 147]. A layer of NLC confined between two transparent glass slides enables the investigation of nematicons interacting with beams propagating through the cell thickness [109, 110]. Nematicon propagation and steering through light-induced refractive potentials were studied by using modulation theory, with excellent agreement with numerical simulations obtained [111]. The nematicons discussed so far are described by a propagation equation for a scalar optical field coupled with a model of the light-matter interaction, the latter yielding the nonlinear refractive index distribution [66]. In some cases, however, the propagation of multiple components of different wavelengths, polarisation or wavevectors is described by a series of coupled nonlinear equations [66]. Self-confined solutions with a multi-component nature are called vector solitons, a term often extended to include self-trapped wavepackets with a periodic evolution [37]. For instance, parametric spatial solitons or simultons belong to the class of vector solitons as they result from the interaction of optical waves at distinct frequencies [28, 36, 38, 39, 73, 112]. Modulation theory was employed to study the stabilization of vortex solitons in optical media with a nonlocal, nonlinear response and excellent agreement with the previous numerical simulation was obtained [113]. Recently, two-colour nematicons were investigated with emphasis on the significant dispersion of both birefringence and walk-off in NLC [38, 114]. Excellent agreement with numerical solutions was also found on studying two colour nematicons using modulation theories [115, 116]. The propagation of a nematicon on crossing an interface between different NLC has also been studied. The simplest, but most significant case, is that of a nematicon impinging on the graded interface between two differently oriented NLC regions [196, 202]. Since nematicons are wavepackets which tend to behave as rays and maintain their self-confined character after the interaction, the ray optics considerations can also be exploited for the application of modulation theory to soliton refraction and reflection in NLC [127]. Angular deviations as large as 70° have been predicted by voltage tuning NLC in suitably optimised geometries with a single tunable interface from total internal reflection to refraction [117]. The first experimental demonstration of nematicon refraction/total internal reflection was performed in a $100\mu m$ thick NLC cell [196]. The refraction and trajectory bending of nematicons by localised refractive index changes were also studied by applying modulation theory and particularly, circular, elliptical, and rectangular index changes were considered [118]. The large NLC birefringence results in a reflection angle different from the incidence angle turned non-specular reflection [66]. In addition, incoming and reflected Poynting vectors undergo different walk-offs as they depend on the direction of propagation [66]. Hence, this interface geometry results in a non-specular nematicon total internal reflection, as demonstrated in Peccianti *et al* [202], where a nematicon total internal reflection non-specularity as large as 4.5° was reported. Upon total internal reflection, the penetration of a nematicon in the lower index NLC region results in a lateral

shift of the reflected soliton, depending on the index mismatch across the interface [66]. When the interface is graded, as for electrically induced between differently oriented NLC regions, the penetration depth can be significant [66]. Moreover, accounting for the variation of the nonlinearity across the interface, the nonlinear index perturbation can affect the index contrast and give rise to a power-tunable soliton penetration and lateral shift upon total internal reflection, i.e. a nonlinear Goos-Hänchen effect [23], albeit at a smooth interface with a transition length larger than the beam waist [66]. The nonlinear Goos-Hänchen effect was previously reported in laser cavities with shifts of the order of the beam spot size [119]. The nonlinear Goos-Hänchen effect for a nematicon was experimentally demonstrated with nonlinear lateral shifts exceeding $500\mu m$ by changing the nematicon power from 1.6 up to 9.3 mW [203].

Stability is a central issue in nonlinear wave propagation. Modulational instability is often considered the precursor of soliton formation and is a fundamental issue in nonlinear optics [120, 121]. A number of experimental studies of modulational instability have been performed in planar NLC cells [122, 123, 168]. Dark spatial solitons are intensity notches in a uniformly bright background, with a π phase jump across their transverse profile, on axis [66]. They can exist in self-defocusing media and share with bright solitons their character of self-induced waveguides as a positive graded index profile results in the notch due to an all-optical refractive index decrease in the surrounding illuminated regions [135]. An observation of dark spatial solitons in NLCs was recently reported in azo-doped NLC exhibiting a self-defocusing response for extraordinary waves [124]. Excellent agreement with the experimental results was obtained by modelling dark nematicons with a one-dimensional NLS equation, including the inherent losses owing to the resonant absorption and a saturable nonlinear self-defocusing change in index due to the limited doping [124]. Modulation theory was also employed successfully to model dark nematicons and their evolution [129].

1.4 Optical Vortices

In physics, wave propagation is traditionally analyzed by means of exact solutions of wave equations [131]. These solutions often possess singularities, points or lines in space on which mathematical quantities that describe physical properties of the waves become infinite or change abruptly [132]. A phase singularity is a zero of a field. The phase of the field circulates around these points of zero intensity. Research into the properties of phase singularities has thrived since the discussion in depth in a seminal paper by Nye and Berry [133] in 1974.

For a light wave, the phase singularity forms an optical vortex. The wave rotates around the vortex core in a given direction in a spiral. At the centre, the velocity of this rotation becomes infinite and the light intensity is zero [131]. This twisted light, like a corkscrew around its dark centre, when projected onto a flat surface looks like a ring of light [136]. The vortex is given a number, called the topological charge, according to how many twists the light does in one wavelength [137]. A topological charge (also called topological quantum number) is any quantity in a physical theory that takes on only one of a discrete set of values due to topological considerations [137]. Most commonly, topological quantum numbers are topological invariants associated with topological defects or soliton-type solutions of some set of differential equations modelling a physical system [137].

The topological charge of the vortex is always an integer and can be positive or negative, depending on the direction of the twist. The higher the number of the twist, the faster the light

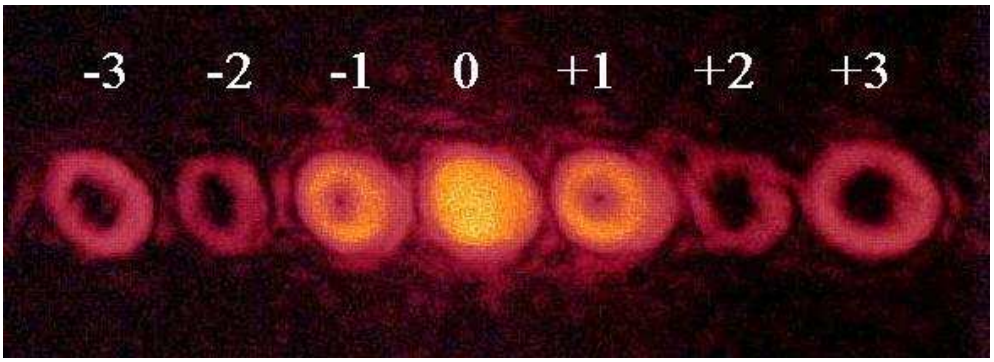

Figure 1.19: Vortices created by computer-generated holograms (Quoted from Wikipedia, the free encyclopaedia; Photo by Azure Hansen, Stony Brook University, 2004; Released into the public domain by the author.)

is spinning around the axis [137, 138]. This spinning carries orbital angular momentum with the wave train. Recalling that a light wave can be represented by a scalar function u, an envelope of an electric field varying smoothly in space and/or time, phase singularities appear at the points (or lines in space) at which u's modulus vanishes, i.e., $\mathrm{Re}\, u = \mathrm{Im}\, u = 0$. Such points are referred to as wave front screw dislocations or optical vortices [131]. An optical vortex is associated with zero light intensity (a black spot) and can be recognized by a specific helical wave front [131]. If the complex wave function is represented as $u(\mathbf{r}, t) = \rho(\mathbf{r}, t)e^{i\chi(\mathbf{r},t)}$ in terms of its real modulus $\rho(\mathbf{r}, t)$ and phase $\chi(\mathbf{r}, t)$, the dislocation strength (or vortex topological charge) is defined by the circulation of the phase gradient around the singularity, $S = 2\pi^{-1} \oint \nabla\chi d\mathbf{r}$ [131]. The result is an integer because the phase changes by a multiple of 2π [131]. It also measures an orbital angular momentum of the vortex associated with the helical wave front structure [131].

Optical vortices can be generated in both linear and nonlinear media, for example, via using computer-generated holograms [131, 134], see Figure 1.19. However, in nonlinear media with a local response optical vortices usually become unstable and break up into filaments because of a symmetry-breaking azimuthal instability [139]. Nevertheless, for instance, when higher order nonlinearities, such as quintic, dominate over the usual cubic nonlinearity vortices in local media can be stabilized [140]. Furthermore, vector vortices in off-resonant saturable Raman media have been shown to be stable [141].

In optics, one is interested in the response of media to applied electromagnetic fields [142]. Optics proceeded quite successfully for many years on the assumption that the response of optical materials was linear in the applied electric field E [142]. In 1875, John Kerr, a lecturer at the Free Church Training College in Glasgow, UK, discovered the first nonlinear optical effect, which is now known as the DC Kerr effect [144]. Since then, more and more phenomena of nonlinear optics have been observed by scientists. Nonlinear optical media are characterized by a dielectric polarization P which responds nonlinearly to the electric field E of the light [142, 143]. This nonlinearity is typically only observed at very high light intensities, such as those provided by pulsed lasers [142]. Nonlinear effects fall into two qualitatively different categories, parametric and non-parametric effects [145]. A parametric non-linearity is an interaction in which the quantum state of the nonlinear material is not changed by the interaction with the optical field [145]. As a consequence of this, the process is 'instantaneous', and energy and momentum are conserved, phase matching is important and is polarization dependent [142, 143, 145]. When the optical fields are not too large, this parametric phenomenon can be

described by a Taylor series expansion of the dielectric polarization density of the medium

$$P \propto \chi_1 E + \chi_2 E^2 + \chi_3 E^3 + \cdots, \tag{1.96}$$

where the coefficients characterize both the linear and nonlinear response of the medium [131, 142, 143, 145]. χ_n are the n-th order susceptibilities of the medium and the presence of such terms is generally referred to as an n-th order nonlinearity. χ_1 describes the linear refractive index of the medium. When χ_2 vanishes (as happens in the case of centrosymmetric media) and the main nonlinear effect is produced by the third term, an intensity dependent nonlinearity leads to the spontaneous focusing of a beam due to the lensing property of a self-focusing ($\chi_3 > 0$) medium [131]. This focusing action of a nonlinear medium can precisely balance the diffraction of a laser beam, resulting in the creation of optical solitons, which are self-trapped light beams that do not change shape during propagation [135]. However, optical vortices become highly unstable in self-focusing nonlinear media due to a symmetry breaking azimuthal instability and they decay into a number of bright spatial solitons [131, 146]. The resulting field distribution does not preserve the radial symmetry, although a stable bright spatial soliton is radially symmetric and has no nodes in its intensity profile [131]. Fortunately, it has been found that the symmetry breaking azimuthal instability of vortex beams can be suppressed and even completely eliminated by a nonlocal, nonlinear response [146]. It has been found that many physical systems are characterized by a nonlocal nonlinear response [147].

A nonlocal response is a key feature of the orientational nonlinearity in liquid crystals due to long-range molecular interactions [147]. For γ_0 small and the limit $\epsilon\nu\frac{\partial^2\theta}{\partial z^2} = 0$, i.e. for small ϵ or in the case of slowly varying envelope along z, in an alternative scaling equations (1.93) and (1.94) are

$$i\frac{\partial E}{\partial z} + \frac{1}{2}\nabla^2 E + \theta E = 0, \tag{1.97}$$

$$\nu\nabla^2\theta - \theta = -|E|^2, \tag{1.98}$$

where $E(x, y, z)$ is the electric-field envelope, $\theta(x, y, z)$ is the director angle perturbation and $\nabla^2 = \partial^2/\partial x^2 + \partial^2/\partial y^2$ is the transverse Laplacian [146]. In the limit $\nu \ll 1$, we can neglect the first term in the equation for the field θ of equation (1.98) and reduce this system to the standard local nonlinear Schrödinger equation with cubic nonlinearity. The opposite case, i.e., $\nu \gg 1$, will be referred to as the strongly nonlocal regime of beam propagation.

The director field in the second equation of the system (1.97) and (1.98) can be solved for a radially symmetric intensity distribution $|E|^2$ as [146]

$$\theta(r, z) = a\int_0^{+\infty} |E(\xi, z)|^2 G_0(r, \xi; a)\xi d\xi, \tag{1.99}$$

where $r = \sqrt{x^2 + y^2}$ is the radial coordinate and G_0 is the Green's function defined at $l = 0$ from the general expression

$$G_l(\xi_1, \xi_2; a) = \begin{cases} K_l(a\xi_2)I_l(a\xi_1), & 0 \le \xi_1 < \xi_2, \\ I_l(a\xi_2)K_l(a\xi_1), & \xi_2 < \xi_1 < +\infty, \end{cases} \tag{1.100}$$

where $a = 1/\sqrt{\nu}$. I_l and K_l are the modified Bessel functions of the first and second kinds, respectively.

It can be assumed that the stationary solutions of the system (1.97) and (1.98) are of the form $E(x,y,z) = E'(r)exp(im\varphi + i\lambda z)$, where φ and $r = \sqrt{x^2+y^2}$ are the azimuthal angle and the radial coordinate, respectively, and λ is the beam propagation constant [146]. Such solutions describe either the fundamental optical soliton, when $m = 0$, or a vortex soliton with topological charge m when $m \neq 0$ [146]. Via substitution, a system of ordinary differential equations is obtained for the steady vortex [146]

$$-\lambda E' + \frac{1}{2}\Delta_r^{(m)} E' + \theta E' = 0, \tag{1.101}$$

$$\theta - \nu \Delta_r^{(0)} \theta = |E'|^2, \tag{1.102}$$

where $\Delta_r^{(m)} = d^2/dr^2 + (1/r)(d/dr) - (m^2/r^2)$. The boundary conditions are $E'(\infty) = E'(0) = 0$ for a vortex, and for the director field, $d\theta/dr_{r=0} = 0$ and $\theta(\infty) = 0$ [146]. Therefore, equations (1.101) and (1.102) are equivalent to a single integrodifferential equation obtained from equations (1.101) and (1.102) when the function $\theta(r)$ is eliminated, or to a single integral equation [146]

$$E'(r) = \int_0^{+\infty} \theta(\eta) E'(\eta) G_m(r, \eta; \sqrt{\lambda}) \eta d\eta, \tag{1.103}$$

where G_m is defined by equation (1.100) and θ is given by equation (1.99).

The nonlinear integral equation (1.103) can be solved by using a stabilized relaxation procedure similar to that employed in Ref. [148]. Important information on the stability of vortex solitons can be obtained from an analysis of the stationary states [146]. z effectively plays the role of time, so the solution can be regarded as non-stationary. A linear perturbation can be represented as a superposition of the modes with different azimuthal symmetry [146]. Assuming the perturbation is small, then a nonstationary solution in the vicinity of the stationary state can be represented as [146]

$$\begin{aligned} &E(\mathbf{r}, z) = \{E'(r) + \delta E'\} e^{i\lambda z + im\varphi}, \quad \Theta(\mathbf{r}, z) = \theta(r) + \delta\theta, \\ &\delta E' = \varepsilon_+(r)\Phi + \varepsilon_-^*(r)\Phi^*, \quad \delta\theta = \theta_+(r)\Phi + \theta_-^*(r)\Phi^*, \end{aligned} \tag{1.104}$$

where $\Phi(\varphi, z) = e^{i\omega z + iL\varphi}$, $|\varepsilon_\pm| \ll E'$, $\theta_\pm \ll \theta$, E', θ are assumed to be real without loss of generality. Linearising equations (1.97) and (1.98), the system of linear equations [146]

$$\pm\{-\lambda + \Delta_r^{(m\pm L)} + \theta(r) + \hat{g}_L\}\varepsilon_\pm \pm \hat{g}_L \varepsilon_\mp = \omega \varepsilon_\pm, \tag{1.105}$$

is obtained, where

$$\hat{g}_L \varepsilon_\pm = E'(r) \int_0^\infty \xi E'(\xi) G_L(r, \xi; a) \varepsilon_\pm(\xi) d\xi.$$

The Hankel spectral transform can be applied to reduce the integrodifferential eigenvalue problem (1.105) to linear algebraic equations. $\operatorname{Im}\omega, \operatorname{Im}\omega < 0$, is the growth rate of the linear perturbation modes [146]. Calculating it as a function of ν, information on the stability of the vortex can be found. When $m = 1$ (a single-charge vortex), for $\nu \ll 1$, all growth rates for $L = 1, 2, 3$ saturate in the local regime and the largest growth rate, as well as the widest instability region, occurs for $L = 2$ [146]. Importantly, above a bifurcation point $\nu_{cr} \approx 90.7$, the growth rate $\operatorname{Im}(\omega)$ vanishes, which means the symmetry-breaking azimuthal instability is eliminated in the highly nonlocal regime($\nu > \nu_{cr}$) [146]. While performing the same stability analysis for $m = 2$ and $m = 3$ vortices, it is found that multicharge vortices remain unstable

with respect to decay into fundamental solitons, even in the limit $\nu \to \infty$ [146].

In contrast, in a self-defocusing nonlinear medium ($\chi_3 < 0$), bright solitons are not supported because a lensing effect cannot be produced. Nevertheless, a negative change of the refractive index can be compensated by a spreading dip in light intensity, thus creating a dark soliton [135], a self-trapped, localised low-intensity state (a dark hole) in a uniformly illuminated background [131]. A dark soliton strip presents an edge dislocation which is however unstable against transverse modulations, and subsequently decays into localised dark spots or optical vortex solitons, as reported by Tikhonenko *et al* [149]. Similar effects for the stripe break-up and generation of optical vortex solitons can also be observed as a result of the interaction of the stripe with a different optical vortex [150]. It can be seen that on propagating through a nonlinear self-defocusing medium, such a vortex-carrying beam creates a self-trapped state, a vortex soliton [131]. Vortex solitons have been observed experimentally in different materials with self-defocusing nonlinearity, such as slightly absorbent liquids, vapors of alkali metals, and photorefractive crystals [151, 152, 153]. Optical vortex solitons in a defocusing saturable medium have been analysed in the framework of the $(2 + 1)$-dimensional generalised NLS equation [154]. Stationary, radially symmetric, localized solutions with nonvanishing asymptotics and a phase singularity (vortex solitons) were found to agree well with the experimental results for a beam in a rubidium vapor, known to be a nonlinear medium with strong saturation of the nonlinear refractive index [154]. In 1998, the first experimental demonstration of the azimuthal self-breaking of intense beams containing a vortex phase dislocation into sets of optical spatial solitons in a quadratic nonlinear material was reported [155]. In 1999, D. Voloschenko and O. D. Lavrentovich reported the observation of optical vortices in a laser beam propagating through the stripe pattern of a cholesteric liquid crystal [156]. The liquid crystal was confined in a cell and optical vortices were produced by edge dislocations of the cholesteric grating [156]. The vortices showed up as spots of zero light intensity in the diffraction maxima and there was one spot in each $+1$ and -1 diffraction maximum and two spots in diffraction maxima $+2$ and -2 [156], similar to Figure 1.19. Stable spatiotemporal optical vortices were found in a bimodal cubic-quintic medium [157] in 2003. In 2005, it is revealed that spatially localized vortex solitons become stable in self-focusing nonlinear media when the vortex symmetry breaking azimuthal instability is eliminated by a nonlocal, nonlinear response [158]. As for solitons, vortices form when the nonlocal, nonlinear response balances diffraction and self-focusing. In 2006, optical vortices were produced by diffraction from dislocations in two-dimensional colloidal crystals by researchers at two Universities in Scotland [159]. In 2007, modulation theory was employed to study the evolution of vortex solitons in optical media with a nonlocal, nonlinear response [160]. The azimuthal evolution of both the vortex width and diffractive radiation was analysed and the physical mechanism for vortex stabilization was described [160]. Vortex solitons in an off-resonant Raman medium were investigated and a detailed analysis was presented to demonstrate the formation of stable and unstable vortex solitons [141] in 2008. In the same year, the nonlinear dynamics of two colour optical vortices was experimentally studied in an iron-doped lithium niobate crystal [161]. In 2009, optical vortices were experimentally demonstrated from liquid crystal droplets, which means a robust self-aligned micro-optical device for orbital angular momentum conversion was realized [162].

As is known, NLCs are an excellent material platform for solitons. In recent years, much research has been done on optical vortices in NLCs. In 2009, the existence and stability of two-component vector solitons were analysed in NLCs, for which one of the components carries

angular momentum and describes a vortex beam [163]. It was demonstrated that the nonlocal, nonlinear response can dramatically enhance the field coupling, leading to the stabilization of the vortex beam when the amplitude of the second beam exceeds some threshold value [163]. A variational approach was developed to describe this effect analytically [163]. It was shown that a localized beam in one colour can stabilise a vortex in the other colour, with the stability threshold in ν reduced by a factor of 10 over that for a single vortex [164]. In this context, it was found that a different type of nematicon instability can arise, one for which a ring structure developes at its peak due to the influence of vortex [164]. Approximate modulation solutions gave good quantitative agreement with direct numerical simulations [164]. In 2010, the stability of an optical vortex in a cell with a circular cross section containing NLC was studied [165]. Modulation theory again gave excellent agreement with numerical results. It was found that the vortex is stable unless the radius of the cell is very small, nearly the width of the vortex itself [165]. Based on the analysis of a stationary vortex, the stability of a low amplitude vortex in a large cell under the influence of its orbital angular momentum and the repelling effect of the cell boundary was studied [165]. Optical vortices in NLCs were experimentally demonstrated and astigmatic transformation of vortex beams into spiralling dipole azimuthons accompanied by power dependent charge flipping of the on-axis phase singularity was observed [166].

Optical vortices have a number of applications in scientific fields ranging from biology to astronomy [167]. In particular, the amplitude of the vortex is 0 at its centre, compensating for the phase singularity there, so that it can be used to trap and manipulate small objects, such as cells [167]. The angular momentum of the vortex can be used to rotate small objects. It is expected that optical vortices will have more and more applications in future.

Chapter 2

Mathematical Methods

2.1 Analytical Methods

2.1.1 Governing equations

The classical Maxwell equations are the essential base of classical electrodynamics, classical optics and electrical circuits. They are a set of partial differential equations (PDEs) which describe the electric and magnetic fields arising from varying distributions of electric charges and currents, and how those fields change in time. These famous four equations are

$$\begin{aligned} \nabla \cdot \mathbf{D} &= \rho \\ \nabla \cdot \mathbf{B} &= 0 \\ \nabla \times \mathbf{E} &= -\frac{\partial \mathbf{B}}{\partial t} \\ \nabla \times \mathbf{H} &= \mathbf{J} + \frac{\partial \mathbf{D}}{\partial t} \end{aligned} \tag{2.1}$$

where $\mathbf{D}$ is electric displacement field, ρ is total charge density, $\mathbf{B}$ is magnetic field, $\mathbf{E}$ is electric field, $\mathbf{H}$ is magnetizing field, $\mathbf{J}$ is total current density and t is time. Developed from Maxwell equations, equations governing electromagnetic wave evolution can be developed, including for soliton evolution on which our research focus. However, Maxwell's four PDEs could only be solved in general by numerical methods which is computationally intensive. In addition, beams travelling in a nonlocal nematic liquid crystal (NLC) are affected by other factors, such as the response of the medium. About the time when nematicons were first discovered, Peccianti *et al* [68] undertook an asymptotic analysis of Maxwell's equations and found that the equations closely resembling the (2 + 1)-D NLS equation govern the electric field of the light beam in the presence of an applied static/low-frequency electric field [68]. Schrödinger's equation describes how the quantum state of a physical system changes with time. The form of the Schrödinger equation depends on the physical situation. The most general form of the time-dependent Schrödinger equation is

$$i\hbar\frac{\partial}{\partial t}\Psi = \hat{H}\Psi, \tag{2.2}$$

where Ψ is the wave function of the quantum system, i is the imaginary unit, $\hbar$ is the reduced Planck constant, and $\hat{H}$ is the Hamiltonian operator which characterizes the total energy of any

given wave function. The NLS equation is a nonlinear version of Schrödinger's equation, but unlike the Schrödinger equation, it does not describe the time evolution of a quantum state. It is a classical field equation and widely used to optics and water waves. The NLS equation in dimensionless form is

$$i\Psi_t = -\frac{1}{2}\Psi_{xx} - \kappa|\Psi|^2\Psi, \tag{2.3}$$

for the complex field $\Psi(x,t)$. The NLS equation is integrable and thus can be solved with the IST. These NLS-like governing equations discovered by Peccianti *et al* cast nematicon evolution as propagation in the time-like coordinate z. For a single optical beam propagating in a NLC with an applied static/low-frequency electric field, its governing equations are a coupled system which contains an NLS-like equation for the beam and a Poisson equation for the director[71, 168], and are

$$2ik\frac{\partial E}{\partial Z} + \nabla^2_{XY}E + (\frac{2\pi}{\lambda})^2\varepsilon_a(\sin^2\phi - \sin^2\hat{\theta})E = 0, \tag{2.4}$$

$$4K\nabla^2\phi + 2\Delta\epsilon_{RF}E_S^2\sin(2\phi) + \varepsilon_0\varepsilon_a\sin(2\phi)|E|^2 = 0, \tag{2.5}$$

where E is the magnitude of the electric field of the beam and $\phi = \hat{\theta} + \theta$ is the total mean director rotation. $\hat{\theta}$ is the pre-tilt caused by the applied static/low-frequency electric field and θ is the optically-induced reorientation of the director caused by the beam, where $\theta \ll \hat{\theta}$ for milliwatt beam. k is the propagation constant of the beam and λ is the input wavelength of the beam. The constant ε_0 is the permittivity of the nematic. The constant $\varepsilon_a = n_\parallel^2 - n_\perp^2$ is the birefringence of NLCs, where $n_\parallel$ and $n_\perp$ are the refractive indices for an optical beam parallel and normal to the director alignment, respectively [169]. E_S is the static/low frequency external electric field and ϵ_{RF} is the static/low frequency anisotropy. K is the elastic constant of the medium and is taken equal for splay, twist and bend deformations of the NLC molecules [66].

The governing equations (2.4) and (2.5) can be nondimensionalised. Set the new variables x, y, z and $u(x,y,z)$ with $X = Ax$, $Y = Ay$, $Z = Bz$ and $E = Cue^{iDz}$, where D is used to eliminate constant factors in (2.4). Substituting the new variables into (2.4) and (2.5), choosing the constants A, B, C and D appropriately and simplifying the equations yields

$$iu_z + \frac{1}{2}\nabla^2_{xy}u - \cos(2\phi)u = 0, \tag{2.6}$$

$$\nu'\nabla^2\phi + p\sin(2\phi) + 2|u|^2\sin(2\phi) = 0, \tag{2.7}$$

where

$$\nu' = \frac{8Kk}{\varepsilon_0\varepsilon_a}, \qquad p = \frac{4\Delta\epsilon_{RF}E_S^2}{\varepsilon_0\varepsilon_a}. \tag{2.8}$$

p is the nondimensional square of the static/low-frequency electric field strength and equation (2.6) is called the Foch-Leontovich equation. At the boundaries $x = \pm L$ of the NLC cell ϕ vanishes, so that

$$\phi(-L) = \phi(L) = 0. \tag{2.9}$$

ϕ varies from $\phi = 0$ at the boundaries to $\phi \approx \pi/2$ when the applied electric field is strong, so that the molecules of the NLC align with the direction of the field.

Equations (2.6) and (2.7) can be further simplified by separating the contributions to the total director orientation ϕ of the pre-tilt $\hat{\theta}$ and the reorientation θ. Substituting $\phi = \hat{\theta} + \theta$ into

the director equation (2.7) gives the expanded equation

$$\nu'\nabla^2\hat{\theta}+\nu'\nabla^2\theta+p\sin(2\hat{\theta})\cos(2\theta)+p\cos(2\hat{\theta})\sin(2\theta)+2|u|^2\sin(2\hat{\theta})\cos(2\theta)+2|u|^2\cos(2\hat{\theta})\sin(2\theta)=0. \tag{2.10}$$

To first order in small $|\theta|$, the director equation (2.10) becomes

$$\nu'\nabla^2\hat{\theta}+\nu'\nabla^2\theta+p\sin(2\hat{\theta})+2\theta p\cos(2\hat{\theta})+2|u|^2\sin(2\hat{\theta})+4\theta|u|^2\cos(2\hat{\theta})=0. \tag{2.11}$$

When there is no beam travelling inside the NLC, the director angle satisfies the equation

$$\nu'\nabla^2\hat{\theta}+p\sin(2\hat{\theta})=0. \tag{2.12}$$

Using the static director equation (2.12), the director equation (2.11) reduces to

$$\nu'\nabla^2\theta+2\theta p\cos(2\hat{\theta})+2|u|^2\sin(2\hat{\theta})+4\theta|u|^2\cos(2\hat{\theta})=0. \tag{2.13}$$

The maximal self-focusing response is achieved when Freédericks threshold in the NLC is zero, which occurs at a pre-tilt of $\hat{\theta}=\pi/4$. The electric field can be adjusted so that the pre-tilt angle $\hat{\theta}$ is above $\pi/4$ but close to it. Using the approximation of $\hat{\theta}$ close to $\pi/4$ and noting that $\cos(2\hat{\theta})<0$ since the static/low-frequency field has been chosen so that $\hat{\theta}>\pi/4$, but close to $\pi/4$ in the centre of the cell, equation (2.13) becomes

$$\nu'\nabla^2\theta-2p\theta+2|u|^2=0. \tag{2.14}$$

Rescaling equation (2.14) yields the final director equation

$$\nu\nabla^2\theta-\theta=-|u|^2. \tag{2.15}$$

In a similar manner, expanding the Foch-Leontovich equation (2.6) using $\phi=\hat{\theta}+\theta$ gives

$$iu_z+\frac{1}{2}\nabla^2_{xy}u-\cos(2\hat{\theta})\cos(2\theta)u+\sin(2\hat{\theta})\sin(2\theta)u=0. \tag{2.16}$$

Again using the approximations of $\hat{\theta}$ close to $\pi/4$ and $|\theta|$ small equation (2.16) can be recast in the form

$$iu_z+\frac{1}{2}\nabla^2_{xy}u+\theta u=0. \tag{2.17}$$

The coupled system of equations (2.15) and (2.17)

$$\begin{aligned} &iu_z+\frac{1}{2}\nabla^2_{xy}u+\theta u=0,\\ &\nu\nabla^2\theta-\theta=-|u|^2 \end{aligned}$$

are the basic governing equations describing nematicon evolution and can be developed to investigate a wide range of nematicon behaviour. There are no exact solutions of equations (2.15) and (2.17). Any variants developed from these nematicon governing equations consequently have no exact solutions either. To determine the evolution of these beams one can solve the governing equations numerically which provides an accurate portrayal of beam evolution, but it yields few insights into nematicon dynamics. Or one can solve the governing equations using approximate methods, which gives more insight into nematicon dynamics.

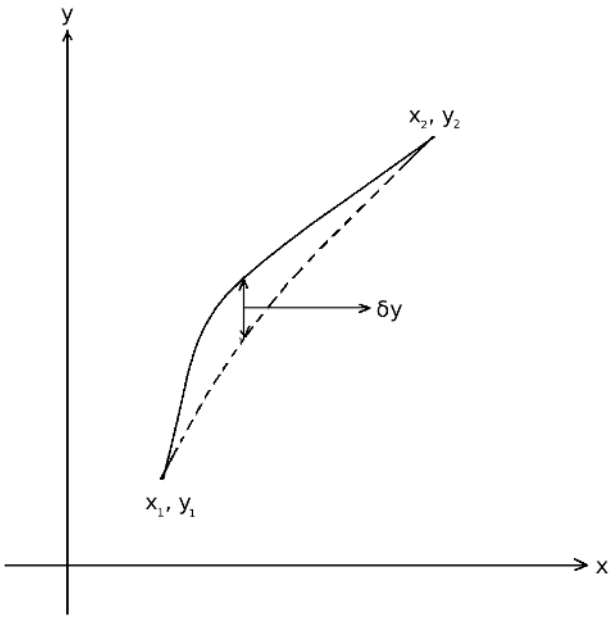

Figure 2.1: A varied path.

2.1.2 Approximate Method

As discussed in section 1.1.2, the main nonlinear effect of nonlinear dispersion is not the difference in the dispersion relation, but the appearance of amplitude dependence in the dispersion relation, which leads to new qualitative behaviour. Then superposition of solutions is not available to generate more general wavetrains. In the absence of exact solutions, variational approximations have been found to be useful to obtain insight and good agreement with numerical and experimental results. This method was the first applied by Anderson in 1983 to approximate nonlinear pulse propagation in optical fibres as governed by the NLS equation [170, 171]. Ever since the method has been utilised in a variety of different areas of optics, such as for multidimensional solitons in media with different nonlinearities [172, 173], and for discrete systems [174].

Before Anderson, the variational method has been used in studying dynamical systems for decades. It is a highly useful tool, although this technique has the potential to be inaccurate if some simplification imposed on the beam profiles and governing equations remove key features of the real beam evolution or form. Nevertheless, if the results obtained by approximately solving the governing equations compare well to numerically determined solutions, insight into the mechanics of beam formation can be gained, as well as its propagation and dynamical behaviour. In our work, a variational method which yields modulation equations will be used to steady nematicon and vortex refraction.

The calculus of variations are used for addressing problems in which the quantity to be minimized (or maximized) appears as a stationary integral, a functional, is a function $y(x, \alpha)$ needs to be determined from a class described by an infinitesimal parameter α. As the simplest case of the calculus of variations, let

$$J = \int_{x_1}^{x_2} f(y, y_x, x)dx, \tag{2.18}$$

where J is the quantity that takes on a stationary value and f is a known function of the indicated variables x and α, as are $y(x,\alpha)$, $y_x(x,\alpha)$, but the dependence of y on x (and α) is not yet known. So the exact path of integration through points (x_1, y_1) to (x_2, y_2) is not known, as shown in Figure 2.1. The path of integration has to be chosen to minimize J. The existence of an optimum path is assumed. In Figure 2.1, two possible paths are shown, although there are an infinite number of possibilities. The difference between these two for a given x is called the variation of y, δy. For convenience, a new function, $\eta(x)$, is introduced to define the arbitrary deformation of the path and a scale factor, α, to give the magnitude of the variation. Then, with the path described by α and $\eta(x)$,

$$y(x,\alpha) = y(x,0) + \alpha\eta(x) \tag{2.19}$$

and

$$\delta y = y(x,\alpha) - y(x,0) = \alpha\eta(x), \tag{2.20}$$

where $y(x, \alpha = 0)$ is chosen as the unknown path that will minimize J and then $y(x,\alpha)$ for nonzero α describes a neighbouring path. In equation (2.18), J is now a function of our parameter α

$$J = \int_{x_1}^{x_2} f[y(x,\alpha), y_x(x,\alpha), x]dx. \tag{2.21}$$

The condition for an extreme value is

$$\left[\frac{\partial J(\alpha)}{\partial \alpha}\right]_{\alpha=0} = 0. \tag{2.22}$$

Now

$$\frac{\partial J(\alpha)}{\partial \alpha} = \int_{x_1}^{x_2} \left[\frac{\partial f}{\partial y}\frac{\partial y}{\partial \alpha} + \frac{\partial f}{\partial y_x}\frac{\partial y_x}{\partial \alpha}\right]dx. \tag{2.23}$$

From equation (2.19),

$$\frac{\partial y(x,\alpha)}{\partial \alpha} = \eta(x),$$
$$\frac{\partial y_x(x,\alpha)}{\partial \alpha} = \frac{d\eta(x)}{dx},$$

so equation (2.23) becomes

$$\frac{\partial J(\alpha)}{\partial \alpha} = \int_{x_1}^{x_2} \left[\frac{\partial f}{\partial y}\eta(x) + \frac{\partial f}{\partial y_x}\frac{d\eta(x)}{dx}\right]dx. \tag{2.24}$$

Integrating the second term by parts to get $\eta(x)$ yields

$$\int_{x_1}^{x_2} \frac{d\eta(x)}{dx}\frac{\partial f}{\partial y_x}dx = \eta(x)\frac{\partial f}{\partial y_x}\bigg|_{x_1}^{x_2} - \int_{x_1}^{x_2} \eta(x)\frac{d}{dx}\frac{\partial f}{\partial y_x}dx. \tag{2.25}$$

It is easily seen from Figure 2.1 that

$$\eta(x_1) = \eta(x_2) = 0, \tag{2.26}$$

so equation (2.24) becomes

$$\int_{x_1}^{x_2} \left[\frac{\partial f}{\partial y} - \frac{d}{dx}\frac{\partial f}{\partial y_x}\right]\eta(x)dx = 0. \tag{2.27}$$

In this form α is no longer part of the problem because it has been set equal to zero corresponding to the solution path. Since $\eta(x)$ is arbitrary, it may be chosen to have the same sign as the bracketed expression in equation (2.27) whenever the latter differs from zero. Therefore the integrand is always nonnegative. Then equation (2.27), the condition for the existence of a stationary value, can be satisfied only if the bracketed term itself is zero. The condition for the stationary value is thus a PDE,

$$\left(\frac{\partial f}{\partial y} - \frac{d}{dx}\frac{\partial f}{\partial y_x}\right) = 0, \tag{2.28}$$

known as the Euler equation.

Based on this calculus of variations, in our work firstly the governing equations must be rewritten in their equivalent Lagrangian formulation, $L(u_z, u_{\mathbf{x}}, u)$, where $\mathbf{x}$ represents the spatial coordinates of the system, not including the time-like coordinate z in this case. The Lagrangian, named after Joseph Louis Lagrange, is a function that summarizes the dynamics of the system and describes the system in terms of its kinetic and potential energy. Then the averaged Lagrangian $\mathcal{L}$ can be defined by

$$\mathcal{L} = \int L d\mathbf{x}. \tag{2.29}$$

Following the principle of stationary action introduced above, a functional is taken the trajectory of the system as its argument and whose integrand is the averaged Lagrangian

$$A = \int_{z_0}^{z_f} \mathcal{L} dz, \tag{2.30}$$

where z_0 and z_f are the initial and final z points respectively.

If the principle of stationary action is satisfied by the averaged Lagrangian, the next step is to substitute an appropriate trial function into the averaged Lagrangian, as the exact solution is not known. So far, no mathematical rules are dictated for choosing trial functions and also no direct relationship is connected with the (unknown) steady state solutions of optical waves. The trial function must be chosen either as a good match to solutions obtained from numerical simulations or by experience, or a combination of both. Generally speaking, trial functions take the form of a basic beam profile with certain parameters such as amplitude, width and phase, which are allowed to vary with z. Some research have been done on how critical the choice of trial functions to the approach [175, 116, 111, 118]. If slightly different trial functions are chosen, such as comparing a sech trial function with a Gaussian trial function, the results are basically insensitive [175, 116, 111, 118]. Once the trial function is inserted into the averaged Lagrangian, the resultant averaged Lagrangian equation is a function of the variable parameters and their derivatives [170]. Let these variable parameters be $p_i(z)$, where $i = 1, ..., N$ and N is the total number of parameters. Consequently, based on equation (2.28), variational equations for optical waves, also known as modulation equations, of the form of Euler-Lagrangian equation

$$\frac{d}{dz}\frac{\partial \mathcal{L}}{\partial(dp_i/dz)} - \frac{\partial \mathcal{L}}{\partial p_i} = 0, \tag{2.31}$$

representing modulations of the beam parameters can be extracted from the averaged La-

grangian and after simplification these modulation equations can be reduced to a group of ordinary differential equations (ODEs) and then be solved by simple numerical methods.

Proved by Emmy Nöther in 1915 and published in 1918 [176] and known as a fundamental tool of modern theoretical physics and the calculus of variations, Nöther's (first) theorem states that any differentiable symmetry of the action of a physical system has a corresponding conservation law relating to some fundamental property of the system. The action of a physical system is the integral over time of a Lagrangian function. Associated with the principle of stationary action, the variational method are therefore closely linked to conservation equations found in integrable systems. Then each of the variational equations, in effect, can be obtained by calculating the corresponding conserved quantity related to the governing equations [1].

When applied in a system, the variational approach needs to be justified. It is sufficient to explain the justification in detail using the case of one dimensional waves described by a variational principle

$$\delta \int \int L(u_t, u_x, u)\, dxdt = 0, \tag{2.32}$$

where $u(x,t)$ is a one dimensional wave function with x and t as its space and time variables, respectively, L is its Lagrangian and δ is a small change of the Lagrangian. The cases of more dimensions, more dependent variables and nonuniform media can all be treated similarly [1]. The Euler equation for (2.32) is

$$\frac{\partial}{\partial t} L_1 + \frac{\partial}{\partial x} L_2 - L_3 = 0, \tag{2.33}$$

where the L_j denote the derivatives

$$L_1 = \frac{\partial L}{\partial u_t}, \qquad L_2 = \frac{\partial L}{\partial u_x}, \qquad L_3 = \frac{\partial L}{\partial u}. \tag{2.34}$$

It can be seen that equation (2.33) is a second order partial differential equation for $u(x,t)$. Therefore, for a nonlinear wave equation $f(u_t, u_x, u) = 0$, if a right form of Lagrangian is found for it, substituting its Lagrangain into the equation (2.33) and simplifying it should get the form of the wave equation $f(u_t, u_x, u) = 0$ back.

The basic variational method, due to Anderson [171], has been applied to approximate a variety of physical systems [170, 172, 173, 174]. However, the usefulness of such approximations is limited due to the neglect of radiation modes. An extension to the averaged Lagrangian method to include radiation was first introduced by Kath and Smyth [96]. In this work they analysed (1 + 1)-D solitons in nonlinear optic fibres. They noticed that although variational approximations matched physical systems well over small intervals of the evolutionary variable, they gradually became less accurate over larger intervals. They found that numerical solutions were exhibiting losses to radiation, so they linked these losses to the evolution of parameters to the steady state by adding a radiation loss term incorporated into one or more of the modulation equations [96, 177]. The inclusion of loss terms allows oscillations of various parameters to settle to steady values in a manner which closely matches that of numerical simulations, so that this extended variational method has a wide range of applications.

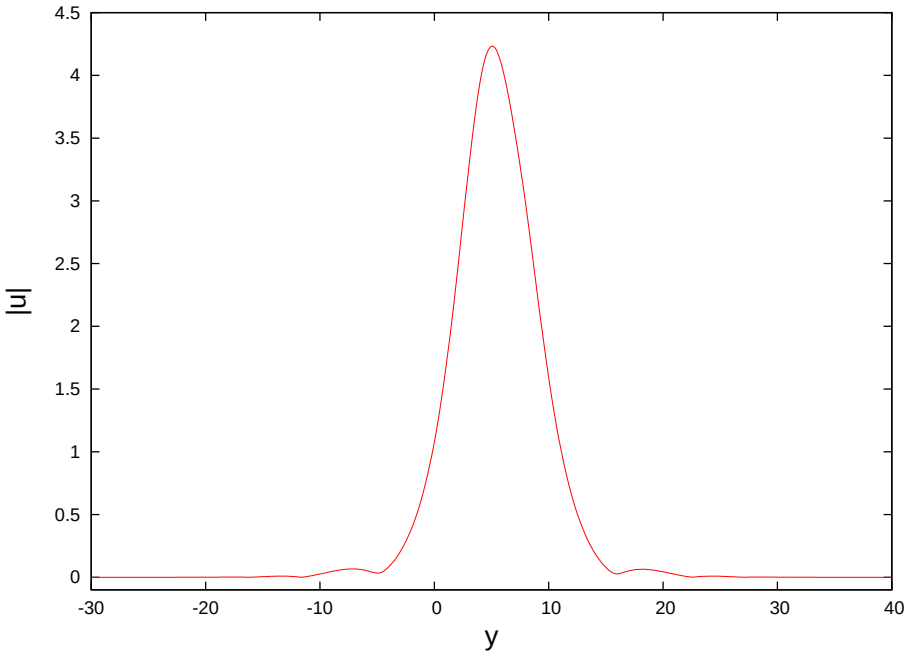

Figure 2.2: Numerically calculated nematicon exhibiting a shelf of radiation during evolution for which equations (3.3) and (3.4).

A Simple System

The basic equation governing many optical phenomena is the generalised NLS equation

$$i\frac{\partial u}{\partial z} + \frac{1}{2}\nabla^2 u + F(|u|^2)u = 0, \tag{2.35}$$

where u represents the envelope of the electric field of the light beam, z is the propagation direction and F depends on the specific medium. The Laplacian ∇^2 is with respect to the variables x and y. The simplest equation governing soliton evolution in a nonlinear optical medium is the NLS equation with $F(|u|^2) = |u|^2$

$$i\frac{\partial u}{\partial z} + \frac{1}{2}\frac{\partial^2 u}{\partial x^2} + |u|^2 u = 0. \tag{2.36}$$

This (1+1)-D NLS equation can be solved exactly using the inverse scattering transform (IST) [11, 96],

$$u(x, z) = a\,\mathrm{sech}(ax)e^{ia^2 z/2}, \tag{2.37}$$

where a is the amplitude of the soliton. The solution shows that a general initial condition evolves into a fixed number of solitons plus decaying dispersive radiation. Practically, however, although the final steady solitons can be determined fairly easily, the evolution of the initial condition to these solitons is very difficult to determine by the IST. The reason for this is the transient evolution is driven by interactions between the emerging solitons and the dispersive radiation and the dispersive radiation is very difficult to determine from the integral equation (Marchenko equation) which is part of the inverse scattering solution. Therefore, as an alternative, Smyth and Kath [96] derived an approximate method to describe this transient evolution via a Lagrangian formulation of the NLS equation. This method will be outlines here as its application to the NLS equation is simpler than for the nematicon equation.

Firstly, to use the modulation theory, a trial function has to be chosen. The form of the exact solution (2.37) of the NLS equation suggests that a sech profile will match the soliton profile well. Also, from the analytical analysis and numerical simulations conducted by Kath and Smyth [96], it was shown that a relatively flat (low amplitude) shelf of dispersive radiation, shed by the beam as it evolves, developes in its vicinity. The existence of this shelf of low wavenumber radiation under the pulse was further demonstrated from soliton perturbation theory and perturbed inverse scattering [96, 178]. The group velocity for linear waves for the NLS equation (2.36) is $C(\kappa) = \kappa$ (κ is the wavenumber, as introduced in last Chapter), so that low wavenumber waves have low group velocity and thereby remain in the vicinity of the soliton. The soliton and the shelf continually interact [96]. This shelf can be observed for any NLS-type equations, for example for nematicons, which will be studied in next Chapter, whose radiation shelf can be seen in Figure 2.2. Hence, we employ a trial function which consists of a soliton-like beam with variable parameters, plus a term which represents linear dispersive radiation which accumulates under the evolving soliton, namely

$$u = \left(a \operatorname{sech} \frac{x}{w} + ig\right) e^{i\sigma}. \tag{2.38}$$

Here the amplitude a, width w, phase σ and radiation shelf height g are functions of z. The shelf of radiation under the evolving soliton must have finite length, otherwise, for instance, the mass of the evolving soliton (2.38) would be infinite. Hence, it is assumed that g is non-zero in the interval $-\ell/2 \leq x \leq \ell/2$ [96]. As the height of the shelf of radiation is small compared with the amplitude of the soliton $|g| \leq a$. The Lagrangian density for the NLS equation (2.36) is

$$L = i(u^* u_z - u u_z^*) - |u_x|^2 + |u|^4, \tag{2.39}$$

where u^* is the complex conjugate of u.

As mentioned in Section 2.1.2, the NLS equation possesses an infinite number of conservation equations. These conservation equations are derived from the integrals of motion [37]. The first three conserved densities are

$$\frac{d}{dt}\int_{-\infty}^{\infty} \rho \, dx = 0, \tag{2.40}$$

$$\frac{d}{dt}\int_{-\infty}^{\infty} J \, dx = 0, \tag{2.41}$$

$$\frac{d}{dt}\int_{-\infty}^{\infty} E_n \, dx = 0, \tag{2.42}$$

where

$$\rho = \int_{-\infty}^{\infty} |u|^2 dx, \qquad J = \frac{i}{2}(u u_x^* - u^* u_x), \qquad E_n = |u_x|^2 - |u|^4, \tag{2.43}$$

are generally referred to as the mass density, mass flux (or momentum) density, and energy density. In the optical context mass is physically optical power. They are related to invariances of Lagrangian: mass conservation to invariances with respect to phase changes, momentum conservation to invariances with respect to translations in x and energy conservation to invariances with respect to translations in z.

Substituting the trial function (2.38) into the Lagrangian (2.39) gives

$$L = -2g^2\sigma' + 2(ga' - g'a)\operatorname{sech}\frac{x}{w} - 2\sigma' a^2 \operatorname{sech}^2\frac{x}{w} + 2\frac{gaw'}{w^2}x\operatorname{sech}\frac{x}{w}\tanh xw$$
$$-\frac{a^2}{\sigma^2}\operatorname{sech}^2\frac{x}{w}\tanh^2\frac{x}{w} + a^4\operatorname{sech}^4\frac{x}{w},$$

to $O(g^2)$. Integrating in x from $-\infty$ to $+\infty$ gives the averaged Lagrangian [1]

$$\mathcal{L} = \int_{-\infty}^{+\infty} L\,\mathrm{d}x$$
$$= 2[\pi g(wa' + aw') - \pi awg' - 2a^2w\sigma' - lg^2\sigma' - \frac{1}{3}\frac{a^2}{w} + \frac{2}{3}a^4w].$$

To calculate the variational, or modulation, equations for this averaged Lagrangian we use the Euler-Lagrange equation (2.31). The modulation equations determining the evolution of the soliton are then

$$\delta a : -\pi wg' - 2aw\sigma' - \frac{1}{3}\frac{a}{w} + \frac{4}{3}a^3w = 0, \tag{2.44}$$

$$\delta w : -2\pi ag' - 2a^2\sigma' + \frac{1}{3}\frac{a^2}{w^2} + \frac{2}{3}a^4 = 0, \tag{2.45}$$

$$\delta\sigma : \frac{d}{dt}(2a^2w + lg^2) = 0, \tag{2.46}$$

$$\delta g : \pi(aw)' - lg\sigma' = 0. \tag{2.47}$$

It should be noted that the equation due to variation with respect to σ, equation (2.46), expresses conservation of mass, equation (2.40).

After some algebra, these modulation equations can be written in the simplified form

$$(aw)' = \frac{lg}{\pi}(a^2 - \frac{1}{2}w^{-2}), \tag{2.48}$$

$$g' = -\frac{2}{3\pi}a(a^2 - w^{-2}), \tag{2.49}$$

$$\sigma' = a^2 - \frac{1}{2}w^{-2}, \tag{2.50}$$

$$\frac{d}{dt}\left(2a^2w + \ell g^2\right) = 0.. \tag{2.51}$$

Substituting (2.48) and (2.49) into (2.51) we obtain the equation for conservation of energy

$$(\frac{2a'}{w} - \frac{aw'}{w^2}) - 2(4a^2a'w + a^3w') = 0,$$
$$(\frac{2aa'}{w} - \frac{a^2w'}{w^2}) - 2(4a^3a'w + a^4w') = 0,$$
$$(\frac{a^2}{w} - 2a^4w)' = 0.$$

The initial partial differential equation (2.36) is then reduced to a finite dynamical system of

comparatively simple ordinary differential equations for the evolution of the soliton

$$\frac{d}{dt}(aw) = \frac{l}{\pi}g(a^2 - \frac{1}{2}w^{-2}), \tag{2.52}$$

$$\frac{dg}{dt} = -\frac{2}{3\pi}a(a^2 - w^{-2}), \tag{2.53}$$

$$\frac{d\sigma}{dt} = a^2 - \frac{1}{2}w^{-2}, \tag{2.54}$$

$$\frac{d}{dt}(\frac{a^2}{w} - 2a^4 w) = 0. \tag{2.55}$$

Note that equation (2.55), merely expresses conservation of energy, equation (2.42). The fixed point at $\hat{a} = \hat{w}^{-1}$ of these modulation equations is in excellent agreement with full numerical solutions and the inverse scattering solution of the NLS equation [11, 96]. The length parameter l is determined by the requirement that the frequency of the oscillations of the linearised solution about this critical point matches the soliton oscillation frequency. Then [96]

$$l = \frac{3\pi^2}{8\hat{a}}. \tag{2.56}$$

The fixed point $\hat{a}$ can be found from the energy conservation equation (2.42) as

$$\hat{a} = \left(2a_0^4 w_0 - \frac{a_0^2}{w_0}\right)^{1/3}, \tag{2.57}$$

with a_0 and w_0 the initial values of a and w.

However, the solution of these modulation equations does not decay to this fixed point as the fixed point is a centre. Physically, this is because the effect of the dispersive radiation shed as the soliton evolves has not been included in the modulation equations.

Since the amplitude of the shed radiation is small compared with the soliton, away from the pulse the nonlinear term in the NLS equation (2.36) is negligible. Therefore, the equation governing the radiation propagating away from the pulse is

$$iu_z + \frac{1}{2}u_{xx} = 0. \tag{2.58}$$

Then to find the mass shed to the dispersive radiation from the evolving soliton, we calculate the mass flux to the right of the soliton, which by symmetry is the same as the mass shed to the left. Integrating the differential form of the mass conservation equation from $x = l/2$ to $x = \infty$ gives the mass radiated to the right away from the vicinity of the pulse as

$$\frac{d}{dt}\int_{l/2}^{\infty} |u|^2 dx \quad = \quad Im(u^* u_x)|_{x=l/2}. \tag{2.59}$$

By Laplace transforming the Schrödinger equation (2.58), we obtain

$$is\tilde{u} + \frac{1}{2}\frac{d^2\tilde{u}}{dx^2} = 0 \tag{2.60}$$

The solution of this ODE is $\tilde{u} = Ae^{\lambda x}$ and the characteristic equation of the ODE is

$$\lambda^2 + 2is = 0 \Rightarrow \lambda^2 = -2is = 2se^{-i\frac{\pi}{2}} \Rightarrow \lambda = -\sqrt{2s}e^{-i\frac{\pi}{4}} \tag{2.61}$$

The negative root for λ has been chosen so as to obtain decay as $x \to \infty$. Hence

$$\tilde{u}_x = L(u_x) = \lambda A e^{\lambda x} = \lambda \tilde{u} = -\sqrt{2}e^{-i\pi/4} \cdot s \cdot \frac{u^*}{\sqrt{s}} = -\sqrt{2}e^{-i\pi/4} \cdot s \cdot H(s), \tag{2.62}$$

where $H(s) = L\{h(t)\} = F(s)G(s)$, $F(s) = L\{f(t)\} = 1/\sqrt{s}$ and $G(s) = L\{g(t)\} = \tilde{u}$, so $f(t) = 1/\sqrt{\pi t}$ and $g(t) = u$. By the convolution theorem

$$h(t) = \int_0^t f(t-\tau)g(\tau)d\tau = \int_0^t \frac{u(\tau)}{\sqrt{\pi(t-\tau)}}\, d\tau. \tag{2.63}$$

Multiplying by s is the same as differentiating with respect to t. Hence from (2.62) we have the final result

$$u_x(l/2, t) = -\sqrt{2}e^{-i\pi/4}\frac{d}{dt}\int_0^t \frac{u(l/2,\tau)}{\sqrt{\pi(t-\tau)}}\, d\tau. \tag{2.64}$$

Substituting equation (2.64) into equation (2.59) gives

$$\frac{d}{dt}\int_{l/2}^{\infty} |u|^2 dx = -\sqrt{2}Im\left[e^{-\pi i/4}u^*(l/2,z) \times \frac{d}{dt}\int_0^t \frac{u(l/2,\tau)}{\sqrt{\pi(t-\tau)}}\, d\tau\right]. \tag{2.65}$$

The mass radiated into the two regions $x > l/2$ and $x < -l/2$ must be lost from the mass contained in the solution in the vicinity of the soliton [96]. Therefore, combining the mass conservation equation in the neighbourhood of the pulse (2.46) and twice the result of (2.65), a modified equation for total mass conservation, including loss to shed radiation, can be obtained

$$\frac{d}{dt}\left(2a^2 w + \frac{3\pi^2}{8\hat{a}}g^2\right) = 2\sqrt{2}Im\left[e^{-\pi i/4}u^*(l/2,z) \times \frac{d}{dt}\int_0^t \frac{u(l/2,\tau)}{\sqrt{\pi(t-\tau)}}\, d\tau\right]. \tag{2.66}$$

The solution at the edge of the shelf, $u(l/2, \tau)$, and can then be calculated with the radiation loss added to the modulation equations (2.52)–(2.55) [96]. The final set of modulation equations, including loss to dispersive radiation, is then [96]

$$\frac{dg}{dt} = \frac{2}{3\pi}\frac{a}{w^2}(1 - a^2w^2) - 2\alpha g, \tag{2.67}$$

$$\frac{d}{dt}(aw) = \frac{3\pi}{8\hat{a}}(a^2 - \frac{1}{2}w^{-2})g, \tag{2.68}$$

$$\frac{d}{dt}(\frac{a^2}{w} - 2a^4 w) = 0, \tag{2.69}$$

$$\frac{d\sigma}{dt} = a^2 - \frac{1}{2}w^{-2}. \tag{2.70}$$

The loss coefficient is

$$\alpha = \frac{3\hat{a}}{8}\frac{1}{r}\frac{d}{dt}\int_0^t \frac{r(\tau)}{\sqrt{\pi(t-\tau)}}d\tau, \tag{2.71}$$

where

$$r^2 = \frac{3\hat{a}}{8}\left(2a^2 w + \frac{3\pi^2}{8\hat{a}}g^2 - 2\hat{a}\right). \tag{2.72}$$

Nematicons in liquid crystals

As shown in Figure 2.3, let us consider the propagation of a polarised, coherent light beam (laser light) through a cell filled with a nematic liquid crystal. The direction down the cell

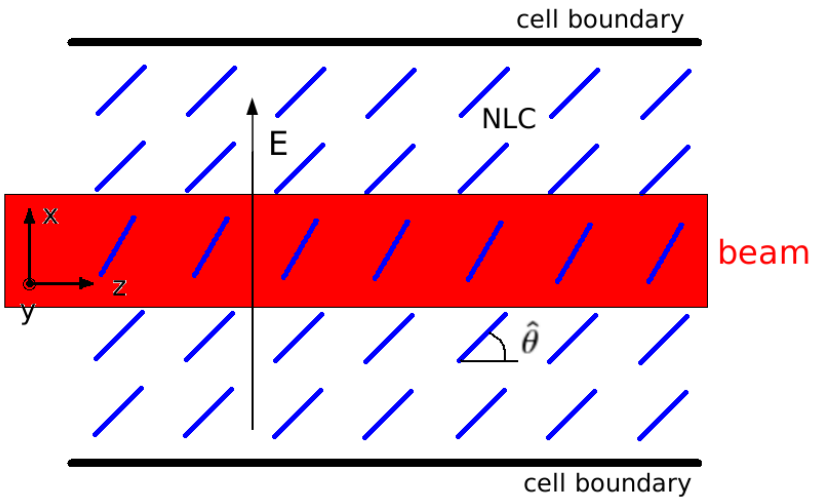

Figure 2.3: Schematic diagram of a liquid crystal cell with a propagating polarised light beam. Reproduced from [104].

is the z direction and the (x, y) plane is orthogonal to this. The beam is polarised in the x direction and an external static electric field is applied in the x direction to pre-tilt the nematic molecules at an angle $\hat{\theta}$ to the z direction. This external field helps overcome the Freédericksz threshold for the nematic so that a low power light beam can self-focus as the total electric field, external plus the electric field of the electromagnetic radiation, is above the threshold [63]. The perturbation of the director angle from the pre-tilt is denoted by θ. The envelope of the electric field of the light is denoted by E. Typical dimensions are $\sim 100\mu m$ for the cell width, $\sim 1mm$ for the cell length and $\sim 5\mu m$ for the beam width [168]. Due to the small size of the beam relative to the cell, if the beam is launched near the centre of the cell the effect of the cell boundaries on its propagation can be ignored. In non-dimensional form the equations governing the propagation of the beam are [104]

$$i\frac{\partial E}{\partial z} + \frac{1}{2}\nabla^2 E + 2\theta E = 0, \tag{2.73}$$

$$\nu\nabla^2\theta - 2q\theta = -2|E|^2, \tag{2.74}$$

where q is related to the square of the external static electric field and ν is the normalized elastic coefficient [78, 179, 204].

The trial functions for the electric field E and director angle θ are taken in the form [104]

$$\begin{aligned} E &= a\,\mathrm{sech}(r/w)e^{i\sigma} + ige^{i\sigma}, \\ \theta &= \alpha\,\mathrm{sech}^2(r/\beta), \end{aligned} \tag{2.75}$$

in analogy with that for the NLS equation (2.38) [104]. Here a is the electric field amplitude, w is the beam width, σ is the propagation constant, α is the director amplitude and β is the director width. All the parameters are functions of z. The Lagrangian for the nematicon equations (2.73)

and (2.74) for a circularly symmetric nematicon is (2.73)–(2.74) in polar coordinates is [104]

$$L = \int_0^Z \int_0^\infty [ir(E^* E_z - E E_z^*) - r|E_r|^2 + 4r\theta|E|^2 - \nu r\theta_r^2 - 2qr\theta^2] dr dz, \tag{2.76}$$

where $*$ represents complex conjugate. Substituting the trial functions (2.75) into the Lagrangian (2.76) and integrating in r from 0 to ∞ results in the averaged Lagrangian [104]

$$\begin{aligned} \mathcal{L} &= -2(a^2 w^2 I_2 + \Lambda g^2)\sigma' - 2I_1 a w^2 g' + 2I_1 g w^2 a' + 4I_1 a w g w' \\ &\quad - a^2 I_{22} - 4\nu I_{42}\alpha^2 - 2qI_4\alpha^2\beta^2 + \frac{2\alpha a^2 A^2 B^2 w^2 \beta^2}{A^2\beta^2 + B^2 w^2}. \end{aligned} \tag{2.77}$$

The various integrals I_i and I_{ij} are

$$I_2 = \int_0^\infty x \operatorname{sech}^2 x dx = \ln 2, \tag{2.78}$$

$$I_{x32} = \int_0^\infty x^3 \operatorname{sech}^2 x dx = 1.352301002\ldots, \tag{2.79}$$

$$I_{22} = \int_0^\infty x \operatorname{sech}^2 x \tanh^2 x dx = \frac{1}{3}\ln 2 + \frac{1}{6}, \tag{2.80}$$

$$I_1 = \int_0^\infty x \operatorname{sech} x dx = 2C, \tag{2.81}$$

$$I_{42} = \int_0^\infty x \operatorname{sech}^4 x \tanh^2 x dx = \frac{2}{15}\ln 2 + \frac{1}{60}, \tag{2.82}$$

$$I_4 = \int_0^\infty x \operatorname{sech}^4 x dx = \frac{2}{3}\ln 2 - \frac{1}{6}, \tag{2.83}$$

where C is the Catalan constant $C = 0.915965594$ [207]. Here $\Lambda = \frac{1}{2}l^2$ is the area of the shelf under the beam, modulo 2π. Furthermore

$$A = \frac{\sqrt{2}I_2}{\sqrt{I_{x32}}} \quad \text{and} \quad B = \sqrt{2I_2}. \tag{2.84}$$

In the above calculation of the averaged Lagrangian (2.77), all the resulting integrals can be simply evaluated, except for the cross integral

$$\int_0^\infty 4r\theta|E|^2 dr = 4\alpha a^2 \int_0^\infty r \operatorname{sech}^2 \frac{r}{\beta} \operatorname{sech}^2 \frac{r}{w} dr. \tag{2.85}$$

Integrals such as

$$I = \int_0^\infty r \operatorname{sech}^2 \frac{r}{\beta} \operatorname{sech}^2 \frac{r}{w} dr \tag{2.86}$$

cannot be evaluated exactly as functions of the parameters unless $\beta = w$. To obtain useful, explicit approximate equations, the concept of equivalent functions is introduced [97]. The function $\operatorname{sech}^2(r/\beta)$ is then replaced by the Gaussian $\exp(-r^2/(A\beta)^2)$, and $\operatorname{sech}^2(r/w)$ is replaced by the Gaussian $\exp(-r^2/(Bw)^2)$, so that the integral (2.86) can be evaluated explicitly. The constants A, B will be evaluated later to make the areas under the curves the same.

Let $r = wr'$. Then

$$I = \int_0^\infty wr' \operatorname{sech}^2(\frac{w}{\beta}r') \operatorname{sech}^2 r' \, w dr' = w^2 \int_0^\infty r' \operatorname{sech}^2(\frac{w}{\beta}r') \operatorname{sech}^2 r' \, dr' = w^2 F(\frac{w}{\beta}). \tag{2.87}$$

The funtion F is

$$F(c) = \int_0^\infty r' \operatorname{sech}^2(cr') \operatorname{sech}^2 r' \, dr'. \tag{2.88}$$

Due to nonlocal limit $c = w/\beta \ll 1$, F(c) can be expanded in a Taylor series about 0 for $c \ll 1$

$$F(c) = F(0) + F'(0)c + \frac{1}{2}F''(0)c^2 + \cdots \tag{2.89}$$

The values of $F(0)$, $F'(0)$ and $F''(0)$ can be evaluated by differentiating with respect to c under the integral sign, giving

$$F(0) = \int_0^\infty r' \operatorname{sech}^2 0 \operatorname{sech}^2 r' \, dr' = \int_0^\infty r' \operatorname{sech}^2 r' \, dr' = I_2, \tag{2.90}$$

$$F'(c) = \int_0^\infty -2r'^2 \operatorname{sech}^2 r' \tanh(cr') \operatorname{sech}^2(cr') dr', \qquad F'(0) = 0, \tag{2.91}$$

$$F''(c) = \int_0^\infty 2x^3 \operatorname{sech}^2 r' \operatorname{sech}^2(cr')[\tanh^2(cr') - 1] dr', \qquad F''(0) = -2I_{x32}. \tag{2.92}$$

Substituting these values into equation (2.89) yields

$$F(c) = I_2 + \frac{1}{2}(-2I_{x32})c^2 + \cdots \approx I_2 - I_{x32}c^2, \tag{2.93}$$

Then substituting $F(c)$ (2.93) into the integral (2.87) and setting $c = \frac{w}{\beta}$, we get

$$I \approx I_2 w^2 - I_{x32}\frac{w^4}{\beta^2}. \tag{2.94}$$

Now the Gaussian equivalent functions are going to be used to explicitly calculate a good approximation of the integral I (2.86). The result obtained above (2.94) will be compared with the Gaussian result to fix the constants A and B. Replacing hyperbolic secants in the integral I (2.86) by the Gaussians gives

$$\begin{aligned} I &= \int_0^\infty r e^{-\frac{r^2}{A^2\beta^2}} e^{-\frac{r^2}{B^2w^2}} dr \\ &= \int_0^\infty r e^{-(\frac{1}{A^2\beta^2} + \frac{1}{B^2w^2})r^2} dr \\ &= \frac{A^2B^2\beta^2w^2}{2(A^2\beta^2 + B^2w^2)} \\ &= \frac{B^2}{2}w^2 - \frac{B^4}{2A^2}\frac{w^4}{\beta^2} + \cdots \end{aligned} \tag{2.95}$$

on expanding in $\omega/\beta \ll 1$. Setting (2.95) equal to (2.94), we obtain

$$\frac{B^2}{2} = I_2, \tag{2.96}$$

$$\frac{B^4}{2A^2} = I_{x32}. \tag{2.97}$$

Solving equations (2.96) and (2.97) gives the values of the constants A and B as in (2.84).

Substituting the values of I_2 and I_{x32} as in (2.78) and (2.79) gives

$$A = 0.842949746, \tag{2.98}$$

$$B = 1.177410023. \tag{2.99}$$

Via the above replacement the cross integral can be explicitly evaluated and then the whole averaged Lagrangian can be calculated simply. The next step is taking variations of the averaged Lagrangian (2.77), and after some algebra, the modulation equations for the evolution of a nematicon are

$$\begin{aligned}
\frac{d}{dz}(I_2 a^2 w^2 + \Lambda g^2) &= 0, \\
\frac{d}{dz}(I_1 a w^2) &= \Lambda g \frac{d\sigma}{dz}, \\
I_1 \frac{dg}{dz} &= \frac{I_{22} a}{2w^2} - \frac{A^2 B^4 \alpha a w^2 \beta^2}{(A^2\beta^2 + B^2 w^2)^2}, \\
I_2 \frac{d\sigma}{dz} &= -\frac{I_{22}}{w^2} + \frac{A^2 B^2 \alpha \beta^2 \left(A^2\beta^2 + 2B^2 w^2\right)}{\left(A^2\beta^2 + B^2 w^2\right)^2}, \\
\alpha &= \frac{A^2 B^2 \beta^2 w^2 a^2}{2(A^2\beta^2 + B^2 w^2)(2\nu I_{42} + q I_4 \beta^2)}, \\
\beta^2 &= \frac{q I_4 B^2 w^2 + \sqrt{q^2 I_4^2 B^4 w^4 + 16 \nu q I_{42} I_4 A^2 B^2 w^2}}{2 q A^2 I_4}.
\end{aligned} \tag{2.100}$$

Nöther's Theorem gives the equation for the conservation of energy as [181]

$$\begin{aligned}
&\frac{\partial}{\partial z}\left[\frac{\partial E}{\partial z}\frac{\partial L}{\partial E_z} + \frac{\partial E^*}{\partial z}\frac{\partial L}{\partial E_z^*} + \frac{\partial \theta}{\partial z}\frac{\partial L}{\partial \theta_z} - L\right] + \frac{\partial}{\partial x}\left[\frac{\partial E}{\partial z}\frac{\partial L}{\partial E_x} + \frac{\partial E^*}{\partial z}\frac{\partial L}{\partial E_x^*} + \frac{\partial \theta}{\partial z}\frac{\partial L}{\partial \theta_x}\right] \\
&+ \frac{\partial}{\partial y}\left[\frac{\partial E}{\partial z}\frac{\partial L}{\partial E_y} + \frac{\partial E^*}{\partial z}\frac{\partial L}{\partial E_y^*} + \frac{\partial \theta}{\partial z}\frac{\partial L}{\partial \theta_y}\right] = 0.
\end{aligned}$$

The equation for the conservation of x momentum is

$$\begin{aligned}
&\frac{\partial}{\partial z}\left[\frac{\partial E}{\partial x}\frac{\partial L}{\partial E_z} + \frac{\partial E^*}{\partial x}\frac{\partial L}{\partial E_z^*} + \frac{\partial \theta}{\partial x}\frac{\partial L}{\partial \theta_z}\right] + \frac{\partial}{\partial x}\left[\frac{\partial E}{\partial x}\frac{\partial L}{\partial E_x} + \frac{\partial E^*}{\partial x}\frac{\partial L}{\partial E_x^*} + \frac{\partial \theta}{\partial x}\frac{\partial L}{\partial \theta_x} - L\right] \\
&+ \frac{\partial}{\partial y}\left[\frac{\partial E}{\partial x}\frac{\partial L}{\partial E_y} + \frac{\partial E^*}{\partial x}\frac{\partial L}{\partial E_y^*} + \frac{\partial \theta}{\partial x}\frac{\partial L}{\partial \theta_y}\right] = 0.
\end{aligned}$$

And the equation for the conservation of y momentum is

$$\begin{aligned}
&\frac{\partial}{\partial z}\left[\frac{\partial E}{\partial y}\frac{\partial L}{\partial E_z} + \frac{\partial E^*}{\partial y}\frac{\partial L}{\partial E_z^*} + \frac{\partial \theta}{\partial y}\frac{\partial L}{\partial \theta_z}\right] + \frac{\partial}{\partial x}\left[\frac{\partial E}{\partial y}\frac{\partial L}{\partial E_x} + \frac{\partial E^*}{\partial y}\frac{\partial L}{\partial E_x^*} + \frac{\partial \theta}{\partial y}\frac{\partial L}{\partial \theta_x}\right] \\
&+ \frac{\partial}{\partial y}\left[\frac{\partial E}{\partial y}\frac{\partial L}{\partial E_y} + \frac{\partial E^*}{\partial y}\frac{\partial L}{\partial E_y^*} + \frac{\partial \theta}{\partial y}\frac{\partial L}{\partial \theta_y} - L\right] = 0.
\end{aligned}$$

Therefore, from Nöther's theorem the averaged form of the energy conservation equation can be obtained from the Lagrangian (2.76) from invariances in z, resulting in the averaged energy conservation equation

$$\frac{dH}{dz} = \frac{d}{dz}\int_0^\infty r\left[|E_r|^2 - 4\theta|E|^2 + \nu\theta_r^2 + 2q\theta^2\right]\, dr = 0. \tag{2.101}$$

The set of modulation equations governing the evolution of the nematicon is then equations.

(2.100) [104].

2.2 Numerical Methods

2.2.1 Numerical method of solving modulation equations

The modulation equations, which are a system of first order ODEs, need to be solved numerically. The standard fourth order Runge-Kutta method or a suitable equivalent technique can be used. Write the modulation equations in the form of a matrix equation

$$\mathbf{A}\mathbf{x}' = \mathbf{b}, \tag{2.102}$$

where $\mathbf{x}'$ is the vector of derivatives of each of the beam parameters as a function of z, $\mathbf{A}$ is the matrix of coefficients of $\mathbf{x}'$ and $\mathbf{b}$ is the vector of the right-hand sides of each of the differential equations. To solve equation (2.102) using the fourth order Runge-Kutta method the system must be inverted to the form

$$\mathbf{x}' = \mathbf{f}(z, \mathbf{x}). \tag{2.103}$$

Suppose the matrix $\mathbf{A}$ can be decomposed as a product of two matrices

$$\mathbf{L}\mathbf{U} = \mathbf{A}, \tag{2.104}$$

where $\mathbf{L}$ is lower triangular (has elements only on the diagonal and below) and $\mathbf{U}$ is upper triangular (has elements only on the diagonal and above). For a $n \times n$ matrix $\mathbf{A}$, equation (2.104) would be

$$\begin{bmatrix} \alpha_{11} & 0 & 0 & 0 & \dots & 0 \\ \alpha_{21} & \alpha_{22} & 0 & 0 & \dots & 0 \\ \alpha_{31} & \alpha_{32} & \alpha_{33} & 0 & \dots & 0 \\ \vdots & \vdots & \vdots & \vdots & \ddots & \vdots \\ \alpha_{n1} & \alpha_{n2} & \alpha_{n3} & \alpha_{n4} & \dots & \alpha_{nn} \end{bmatrix} . \begin{bmatrix} \beta_{11} & \beta_{12} & \beta_{13} & \beta_{14} & \dots & \beta_{1n} \\ 0 & \beta_{22} & \beta_{23} & \beta_{24} & \dots & \beta_{2n} \\ 0 & 0 & \beta_{33} & \beta_{34} & \dots & \beta_{3n} \\ \vdots & \vdots & \vdots & \vdots & \ddots & \vdots \\ 0 & 0 & 0 & 0 & \dots & \beta_{nn} \end{bmatrix}$$
$$= \begin{bmatrix} a_{11} & a_{12} & a_{13} & a_{14} & \dots & a_{1n} \\ a_{21} & a_{22} & a_{23} & a_{24} & \dots & a_{2n} \\ a_{31} & a_{32} & a_{33} & a_{34} & \dots & a_{3n} \\ \vdots & \vdots & \vdots & \vdots & \ddots & \vdots \\ a_{41} & a_{42} & a_{43} & a_{44} & \dots & a_{nn} \end{bmatrix} . \tag{2.105}$$

This is known as an LU decomposition. The matrix $\mathbf{A}$ then can be factorised into lower and upper triangular matrices respectively

$$\mathbf{A}\mathbf{x}' = (\mathbf{L}\mathbf{U})\mathbf{x}' = \mathbf{L}(\mathbf{U}\mathbf{x}') = \mathbf{b}. \tag{2.106}$$

Now the system can be solved firstly for the introduced vector $\mathbf{y}$, such that

$$\mathbf{L}\mathbf{y} = \mathbf{b}, \tag{2.107}$$

and then for $\mathbf{x}'$

$$\mathbf{U}\mathbf{x}' = \mathbf{y}. \tag{2.108}$$

The advantage of breaking up one linear set into two successive ones is that the solution of a triangular set of equations is quite trivial[186]. Numerical forward substitution is used to solve equation (2.107) for $\mathbf{y}$ as

$$\begin{aligned} y_1 &= \frac{b_1}{\alpha_{11}} \\ y_i &= \frac{1}{\alpha_{ii}}\left[b_i - \sum_{j=1}^{i-1} \alpha_{ij} y_j\right] \qquad i = 2, 3, ..., N \end{aligned}$$

and then backward substitution solves equation (2.108) for $\mathbf{x}'$ as

$$\begin{aligned} x'_N &= \frac{y_N}{\beta_{NN}} \\ x'_i &= \frac{1}{\beta_{ii}}\left[y_i - \sum_{j=i+1}^{N} \beta_{ij} x_j\right] \qquad i = N-1, N-2, ..., 1. \end{aligned}$$

Compared with LU decomposition, if Gaussian elimination were used to compute $\mathbf{x}'$ for each b_i the computation would be dramatically slowed [187].

The system (2.103) for the initial value problem is now solved using the standard fourth order Runge-Kutta scheme for $\mathbf{x}'$ using the initial values of the beam parameters. Compared with traditional Euler method and improved Euler method, Runge-Kutta method is relatively simple to use and is sufficiently accurate to handle many problems efficiently. Involving a weighted average of values of $\mathbf{f}(z, \mathbf{x})$ at different points in the interval $z_n \leq z \leq z_{n+1}$, the Runge-Kutta formula is given by

$$\begin{aligned} \mathbf{x}_{m+1} &= \mathbf{x}_m + \frac{1}{6}(\mathbf{k}_1 + 2\mathbf{k}_2 + 2\mathbf{k}_3 + \mathbf{k}_4), \\ z_{m+1} &= z_m + h, \end{aligned} \tag{2.109}$$

where

$$\begin{aligned} \mathbf{k}_1 &= \mathbf{f}(z_m, x_m), \\ \mathbf{k}_2 &= \mathbf{f}(z_m + \frac{1}{2}h, x_m + \frac{1}{2}h\mathbf{k}_1), \\ \mathbf{k}_3 &= \mathbf{f}(z_m + \frac{1}{2}h, x_m + \frac{1}{2}h\mathbf{k}_2), \\ \mathbf{k}_4 &= \mathbf{f}(z_m + h, x_m + h\mathbf{k}_3). \end{aligned} \tag{2.110}$$

Here h is the step of length and the sum $(\mathbf{k}_1 + 2\mathbf{k}_2 + 2\mathbf{k}_3 + \mathbf{k}_4)/6$ can be interpreted as an average slope. $\mathbf{k}_1$ is the slope at the left end of the interval, $\mathbf{k}_2$ is the slope at the midpoint using the Euler formula to go from t_n to $t_n + h/2$, $\mathbf{k}_3$ is a second approximation to the slope at the midpoint, and finally $\mathbf{k}_4$ is the slope at $t_n + h$ using the Euler formula and the slope $\mathbf{k}_3$ to go from t_n to $t_n + h$. $\mathbf{x}_m$ are the values of the n parameters at the position z_m after m steps and $\mathbf{x}_{m+1}$ are the values of the parameters $\mathbf{x}$ at the next z step determined by the step length h. This method is fourth order accurate in h and solves the modulation ODE system [111].

2.2.2 Full numerical method of solving governing equations

Various numerical approaches have been employed to numerically solve the NLS equation (2.3), such as the classical explicit method, hopscotch method, implicit-explicit method, Crank-Nicolson implicit scheme, the Ablowitz-Ladik scheme, the split step Fourier method (F. Tappert) and pseudospectral Fourier method (Fornberg and Whitham) [180]. Generally speaking, numerical methods for initial value problems fall into two categories: finite difference methods and function approximation methods. For finite difference methods, the original function $\Psi(x,t)$ is approximated by Ψ_n^m at a set of points x_n, t_m on a rectangular grid in the x,t plane, where $x_n = hn$, $t_m = km$, h and k are the increments in x and t, respectively. Expanding function values at grid points in a Taylor series gives the approximations to the differential equation involving algebraic relations between grid point values. Methods such as the classical explicit method, hopscotch method, implicit-explicit method, Crank-Nicolson implicit scheme and Ablowitz-Ladik scheme mentioned above, are finite difference methods. The function approximation method approximates the exact solution $\Psi(x,t)$ by an approximate solution defined on a finite dimensional subspace

$$\Psi(x,t) \approx \tilde{\Psi}(x,t) = \sum_{i=1}^{n} C_i(t)\Phi_i(x), \tag{2.111}$$

where $\Phi_i(x)$ are basis functions. Commonly, appropriate choices for the basis functions are trigonometric functions, which leads to a finite Fourier transform or pseudospectral method and piecewise polynomial functions with a local basis, giving a finite element method [180]. The pseudospectral method of Fornberg and Whitham transforms $\Psi(x,t)$, its derivatives and other operators into Fourier space with respect to x [182]. For convenience the spatial period can be normalized to $[0, 2\pi]$. With this scheme, Ψ_{xx} can be evaluated as $F^{-1}[i^2k^2F(\Psi)]$. Combined with a leap frog time step the NLS equation is then approximated by

$$\Psi(X,t+\Delta t) = \Psi(X,t-\Delta t) - 4i\Delta t\frac{\pi^2}{L^2}F^{-1}(k^2F(\Psi(X,t))) - 2\kappa\Delta t|\Psi|^2\Psi, \tag{2.112}$$

where L is the length of the interval of interest, $X = 2\pi k/L$ and $k = -\frac{N}{2}+1, ..., -1, 0, 1, ...\frac{N}{2}$ given by the discretised interval with N equidistant points. Fornberg and Whitham [182] showed that a modification can be used for equation (2.112)

$$\Psi(X,t+\Delta t) = \Psi(X,t-\Delta t) - iF^{-1}(\sin(\frac{4k^2\pi^2}{L^2}\Delta t)F(\Psi(X,t))) - 2\kappa\Delta t|\Psi|^2\Psi \tag{2.113}$$

to give better stability characteristics. Then the linear part of equation (2.113) will be exactly satisfied for any solution of

$$i\Psi_t = \frac{4\pi^2}{L^2}\Psi_{xx}, \tag{2.114}$$

and equation (2.113) is unconditionally stable according to a linear stability analysis.

The numerical solution of the full nematicon equations is used in order to compare with the modulation solutions. Considering proven accuracy and efficiency, a pseudo-spectral method based on the method developed by Fornberg and Whitham [182] will be applied. Fornberg and Whitham's Fourier method has been analysed and compared with other numerical techniques by various authors and has been found to be competitive, yielding accurate solutions with

low computational cost compared to other popular methods, such as finite difference or finite element methods [183].The numerical scheme introduced here is developed from the one derived by Fornberg and Whitham as the z integration is calculated using a fourth order Runge-Kutta method in Fourier space, instead of the original stepping in z of Fornberg and Whitham, which is a second order scheme in physical space. Additionally, a damping layer has to be included to reduce the effects of wave reflection at the boundaries of the computational domain [184]. Adding damping terms to equation (2.3) yields

$$\begin{aligned} &i\Psi_t + \frac{1}{2}\Psi_{xx} - \kappa|\Psi|^2\Psi + i\epsilon(x)\Psi = 0 \qquad \text{where,} \\ &\epsilon(x) = \epsilon_0[sech^2(\eta(x - L/2)) + sech^2(\eta(x + L/2))]. \end{aligned} \tag{2.115}$$

Here ϵ_0 and $1/\eta$ are the strength and width of the damping layer, respectively. The inclusion of a damping term allows smaller spatial intervals to be chosen, which in turn leads to faster computational speed. To solve the modified NLS equation (2.115), firstly it needs to be transformed into Fourier space via the Fourier transform, which gives

$$\frac{d\bar{\Psi}}{dt} + \frac{i}{2}\omega^2\bar{\Psi} - i\kappa F\{|\Psi|^2\Psi\} + F\{\epsilon\Psi\} = 0, \tag{2.116}$$

where the finite Fourier transform of $\Psi(x,t)$ and its inverse respectively are defined by

$$\bar{\Psi}_\omega = F(\Psi) = \sum_{j=-\frac{N}{2}+1}^{\frac{N}{2}} \Psi_j e^{i2\pi\frac{\omega}{L}j}, \tag{2.117}$$

$$\Psi_j = F^{-1}(\bar{\Psi}) = \frac{1}{L}\sum_{\omega=-\frac{N}{2}+1}^{\frac{N}{2}} \bar{\Psi}_\omega e^{-i2\pi\frac{\omega}{L}j}, \tag{2.118}$$

where ω is the discrete Fourier transform dummy variable. Using discrete fast Fourier transform (FFT), equation (2.116) can now be rewritten in Fourier space by multiplying by an integrating factor, $e^{i\omega^2 t/2}$, from which the name of the method was taken, and which yields a first order ODE

$$\frac{d}{dt}(\bar{\Psi}_j e^{i\omega_j^2 t/2}) = (i\kappa F\{|\Psi|^2\Psi\} - F\{\epsilon\Psi\})e^{i\omega_j^2 t/2}, \tag{2.119}$$

where

$$\omega_j = \frac{2\pi j}{L}, \qquad j = \frac{-N}{2} + 1, ..., \frac{N}{2}. \tag{2.120}$$

To solve this system, firstly, calculate the Fourier transforms by the standard forward FFT algorithm [185]; secondly, use the Runge-Kutta method or an equivalent iterative method in Fourier space to calculate $\bar{\Psi}$ at the next t step; then $\bar{\Psi}$ is multiplied by the inverse integrating factor and finally the backward FFT algorithm calculates the inverse Fourier transform of $\bar{\Psi}$, namely Ψ.

The (1 + 1)-D NLS equation has been used here as an example to highlight the main features of the full numerical method. The extension of the numerical method to the $(2 + 1)$-D nematicon governing equation will now be discussed. The nematicons presented here have governing equations which contain a director equation that also needs to be solved for. The director equation is tackled using a standard FFT-based boundary value numerical method [185]. Further details of the method, and the algorithms, will be described below for the

governing equations used in Chapter 3 and 4

$$i\frac{\partial E}{\partial z} + ip\Delta\frac{\partial E}{\partial y} + \frac{1}{2}\nabla^2 E + \sin(2\psi_b)\theta E = 0, \tag{2.121}$$
$$\nu\nabla^2\theta - 2q\theta + \sin(2\psi_b)|E|^2 = 0,$$

where p, Δ, ν, q and ψ_b are constants whose meanings are not needed in this Chapter. Adding a damping term to equation (2.121), the system of governing equations becomes

$$i\frac{\partial E}{\partial z} + ip\Delta\frac{\partial E}{\partial y} + \frac{1}{2}\nabla^2 E + \sin(2\psi_b)\theta E + i\epsilon E = 0, \tag{2.122}$$
$$\nu\nabla^2\theta - 2q\theta + \sin(2\psi_b)|E|^2 = 0. \tag{2.123}$$

Taking the Fourier transform of equation (2.122) yields

$$\frac{\partial \bar{E}}{\partial z} + ip\Delta\omega_x\bar{E} - \frac{i}{2}\omega_x^2\bar{E} - \frac{i}{2}\omega_y^2\bar{E} - iF\{\sin(2\psi_b)\theta E\} + F\{\epsilon E\} = 0. \tag{2.124}$$

where $\omega_x(\omega_y)$ is the Fourier transform dummy variable corresponding to spatial variable $x(y)$.

In equation (2.124), $F\{\sin(2\psi_b)\theta E\}$ requires the computation of θ from the director equation (2.123) with $\theta = 0$ at the boundaries $x = \pm L/2$, $y = \pm L/2$. On taking FFTs of (2.123) in the x direction this reduces to a two-point boundary value problem in y

$$\begin{cases} \dfrac{d^2\bar{\theta}}{dy^2} = \omega^2\bar{\theta} + \dfrac{2q}{\nu}\bar{\theta} - \dfrac{2}{\nu}F\{\sin(2\psi_b)|E|^2\} \\ \\ \theta(-L/2) = 0, \quad \theta(L/2) = 0 \end{cases} . \tag{2.125}$$

An approach to two-point boundary-value problems is the finite-difference method. As the problem (2.125) is nonlinear, it is solved by using finite differences combined with Picard iteration. Firstly, discretise the second derivative using second order differences to obtain the system

$$\bar{\theta}_{i+1} - 2\bar{\theta}_i + \bar{\theta}_{i-1} = \Delta y^2\omega^2\bar{\theta}_i + \Delta y^2 f(\bar{\theta}_i),$$

where f includes all the nonlinear terms. This is then written in matrix form

$$A\bar{\theta} = b.$$

Given an initial guess $\bar{\theta}_0$ for $\bar{\theta}$, then iterate

$$A\bar{\theta}_{i+1} = b(\bar{\theta}_i),$$

until $\bar{\theta}_i$ converges.

The integrating factor method is used in an identical fashion to the previous NLS example, which reduces equation (2.124) to

$$\frac{d}{dz}(\bar{E}_{jk}e^{i(\omega_j^2+\omega_k^2)z/2}) = [iF\{\sin(2\psi_b)\theta E\} - F\{\epsilon u\}]e^{i(\omega_j^2+\omega_k^2)z/2}, \tag{2.126}$$

where

$$\omega_j = \frac{2\pi j}{L_x}, \qquad \omega_k = \frac{2\pi k}{L_y}, \tag{2.127}$$

$$j = \frac{-N_x}{2} + 1, ..., \frac{N_x}{2}, \qquad k = \frac{-N_y}{2} + 1, ..., \frac{N_y}{2}. \tag{2.128}$$

L_x, N_x are the interval length and number of points respectively in the x direction and L_y, N_y the same in the y direction. Fornberg and Whitham used a leapfrog z stepping scheme whereby E_z was approximated by $E_z \approx (E(x, z + \Delta z) - E(x, z - \Delta z))/(2\Delta z)$ [182]. However, here we use the fourth order Runge-Kutta method to calculate E as it is more accurate. To calculate E at the next space step $(z + \Delta z)$, the right hand side of equation (2.126) is calculated at z, $z + \Delta z/2$ and $z + \Delta z$. Equation (2.126) is estimated for a step $\Delta z/2$ from z as

$$\frac{d}{dz}(\phi_{jk}) = \eta(E_{jk}) e^{\frac{i}{4}(\omega_j^2 + \omega_k^2)\Delta z} = G(E, z), \tag{2.129}$$

where

$$\phi = \bar{E} e^{i(\omega_x^2 + \omega_y^2)z/2}, \qquad \eta(E) = iF\{\sin(2\psi_b)\theta E\} - F\{\epsilon E\}. \tag{2.130}$$

The nonlinear part of equation (2.126) is firstly calculated in physical space, then transformed to Fourier space numerically using the forward FFT algorithm. With these definitions at the current step n, the Runge-Kutta method takes ϕ_{jk}^n and computes ϕ_{jk}^{n+1} at the next z step $n+1$. The algorithm is explained in detail as follows

- $$U_1 = \phi_j^n + \frac{\Delta z}{2} G(E, z). \tag{2.131}$$

$G(E, z)$ is easily calculated when E is known at z. U_1 is an Euler step of length $\Delta z/2$, yielding an estimate of ϕ at $z + \Delta z/2$.

- $$U_2 = \phi_j^n + \frac{\Delta z}{2} G(F^{-1}(U_1), z + \frac{\Delta z}{2}). \tag{2.132}$$

Multiplying U_1 by the inverse integrating factor and then taking the inverse Fourier transform of U_1, yields an estimate of E at $z + \Delta z/2$. Consequently $G(E, z + \Delta z/2)$ can be calculated.

- $$U_3 = \phi_j^n + \Delta z G(F^{-1}(U_2), z + \frac{\Delta z}{2}). \tag{2.133}$$

- $$U_4 = -\phi_j^n + \frac{\Delta z}{2} G(F^{-1}(U_3), z + \Delta z). \tag{2.134}$$

Then, ϕ_{jk}^{n+1}, the solution at $n + 1$, is given by a weighted average of the estimates U_1 to U_4, namely

$$\phi_{jk}^{n+1} = \frac{1}{3}U_1 + \frac{2}{3}U_2 + \frac{1}{3}U_3 + \frac{1}{3}U_4. \tag{2.135}$$

Finally E at the next z step, E^{n+1}, is extracted from ϕ_{jk}^{n+1} by multiplying by the inverse integrating factor and $\bar{E}$ is inverted via the backward FFT algorithm to return E to physical space. This process is repeated until the final z value has been reached.

Chapter 3

Soliton Refraction at an Interface in a Liquid Crystal

3.1 Background

In optics, nematicons are spatial optical solitons (self-trapped light beams) in nematic liquid crystalline materials which form due to a balance between diffraction and self-focusing via nonlinear molecular reorientation as explained in Chapter 2. Several proposed applications of nematicons, such as routers and switches, are based on controlling the trajectories of nematicons [103, 111, 118, 188, 189, 190, 191, 192, 193, 194, 195], e.g. by altering the refractive index distribution in the liquid crystalline sample. This can be achieved in a number of ways, including the use of an external low-frequency electric field [101, 191, 196] and/or extra optical beams to perturb the solitary wave environment [103, 111, 118, 188, 190, 192, 193, 194, 195]. The present Chapter will be concerned with nematicon control and steering through index changes caused by an external low-frequency or static electric field (voltage). Extensive theoretical studies of one dimensional solitary wave refraction and reflection at interfaces were carried out for local [197] and nonlocal media [198] by Aceves *et al.* This research used both numerical beam propagation solvers and asymptotic solutions based on treating solitary waves as particles [199], which provided results in good agreement with numerical solutions. These studies are equivalent to the modulation theory approach used here. Most studies of the refraction of spatial solitary waves at interfaces have dealt with bright solitary waves, while dark and grey solitary waves in self-defocusing dielectrics also show refraction at interfaces separating media with different optical properties [200, 201].

The present work will investigate the refraction and reflection of nematicons at a (straight) interface between regions in a liquid crystal cell with different refractive indices and walk-off. These regions can be formed experimentally by employing a planar glass cell equipped with separate electrodes on the top slide (see Figure 3.1), which results in two background pre-tilt orientations of the director [196, 202, 203].

As shown in Figure 3.1, a thick layer (several optical wavelengths thick) of uniaxial nematic liquid crystal (NLC) occupying a planar cell, with boundary conditions arranged such that the optic axis, or molecular director, lies in the plane xz everywhere in the cell, as introduced in Figure 1.14 and Figure 1.15 in Section 1.3.1. The cell is configured so that two independent biasing static, external electric fields can be applied across its thickness [196] and by reorientation

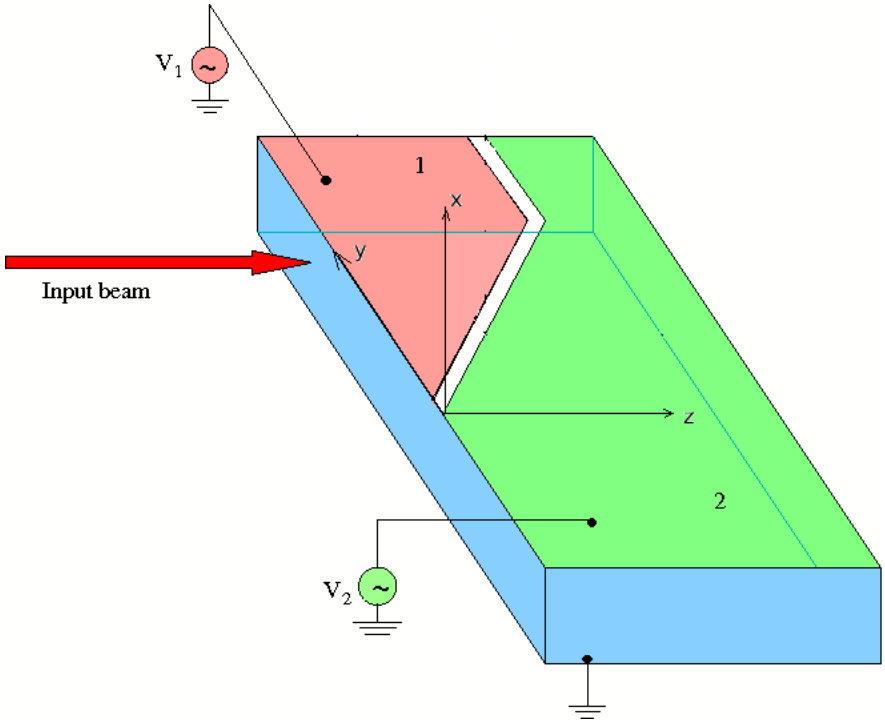

Figure 3.1: (**The sample**) Schematic diagram of the liquid crystalline cell with two regions 1 and 2. On the top side, two electrodes are separated by a straight gap. Unequal voltages V_1 and V_2 applied to regions 1 and 2, respectively, inducing different reorientations of the director. Reproduced from [196, 202, 203].

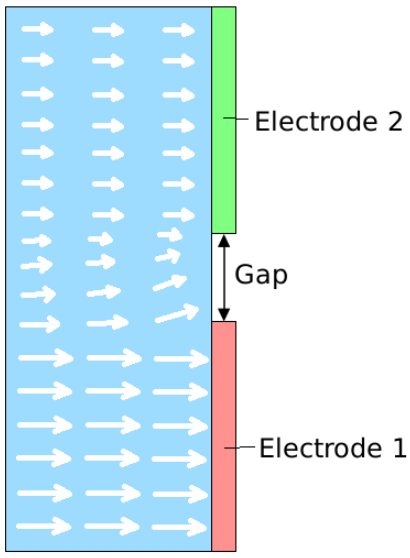

Figure 3.2: The gap separating the electrodes. Reproduced from [196].

the angle between the optic axis and the direction z is adjusted down the cell. A coherent beam of light is launched into the cell and propagates in the volume of this nonlinear dielectric. The electrode gap is shown in Figure 3.2 and its width is $100\mu m$. A coordinate system is defined such that the applied electric fields are in the x direction (i.e. across the NLC thickness), the same direction as the polarisation of the extraordinary input beam launched in the principal plane xz. The transverse direction y completes the right handed Cartesian coordinate system. In the paraxial approximation the non-dimensional equation governing the envelope of the input extraordinarily polarised light beam is [78, 79, 204]

$$i\frac{\partial E}{\partial z} - i\Delta\frac{\partial E}{\partial y} + \frac{1}{2}\nabla^2 E + \left[\sin^2\psi - \sin^2\psi_b\right] E = 0, \tag{3.1}$$

where ψ is the angle the NLC molecular director makes with the z axis, with ψ_b the pre-tilt angle due to the external bias. The angle ψ_b can be non-uniform. The walk-off angle δ between the Poynting vector and the wavevector of the extraordinary beam is given by

$$\Delta = \tan\delta = \frac{\Delta n^2 \sin 2\psi}{\Delta n^2 + 2n_\perp^2 + \Delta n^2 \cos 2\psi}, \tag{3.2}$$

where $\Delta n^2 = n_\parallel^2 - n_\perp^2$ is the optical birefringence and $n_\parallel$ and $n_\perp$ are the refractive indices for fields parallel and perpendicular to the optic axis, respectively [204]. In the present work, the typical values $n_\parallel = 1.6954$ and $n_\perp = 1.5038$ will be used, which refer to the nematic E7 at room temperature in the near infrared at wavelength 1.604 μm [204]. In experiments the nematicon propagation is fully three dimensional [196], while in the present work the two dimensional approximation is used, as introduced in Section 1.3.2 that the terms $\nu\frac{\partial^2\theta}{\partial z^2}$ and $\frac{\partial^2 E}{\partial z^2}$ can be neglected. For full three dimensional propagation of a nematicon, the walk-off Δ is the projection of the walk-off onto the observation plane yz [202].

The Laplacian ∇^2 is in the (x, y) plane. The input beams used in experiments have milliwatt power levels [205], so that the reorientation of the NLC due to light is substantially less than that due to the bias field(s). Let us then take $\psi = \psi_b + \theta$, where $|\theta| \ll |\psi_b|$. In this limit, a Taylor series expansion in the electric field equation (3.1) results in

$$i\frac{\partial E}{\partial z} - i\Delta\frac{\partial E}{\partial y} + \frac{1}{2}\nabla^2 E + \sin(2\psi_b)\theta E = 0 \tag{3.3}$$

to first order in $|\theta|$. In a similar manner, the non-dimensional equation governing the director orientation is

$$\nu\nabla^2\theta - 2q\theta = -\sin(2\psi_b)|E|^2 \tag{3.4}$$

to first order in $|\theta|$ [78, 79, 98]. Here ν measures the elastic response of the NLC. The usual experimental operating regime has ν large, $\nu = O(100)$ [101], the so-called nonlocal regime in which the NLC response extends far beyond the beam waist. The parameter q is proportional to the square of the static electric field [78, 79]. While the system of equations (3.3) and (3.4) has been derived in the context of nonlinear beam propagation in nematic liquid crystals, it is general and describes nonlinear propagation in a diverse range of media for which the nonlinearity is accompanied by some diffusive phenomena [197].

To complete the description of the NLC cell and the equations governing the propagation of the extraordinary beam, the external bias configuration of the cell needs to be specified. The geometry assumed will be the same as for the experimental set-up of Peccianti *et al* [196, 203]

for which the two different static fields were applied through thin film electrodes with a straight gap separating them. This gap lies at a slope in the (y, z) plane and can be described by $y = \mu_1 z + \mu_2$. The change in biasing field, and so the change in the pre-tilting angle, is modelled with a sharp discontinuity. This is consistent with experiments for which the electric field was found to vary smoothly between two constant values over a distance of the order of the gap between the electrodes, of about $50\mu m$ [202, 203]. Hence the background pre-tilt is approximated by

$$\psi_b = \begin{cases} \psi_{br}, & y < \mu_1 z + \mu_2, \\ \psi_{bl}, & y > \mu_1 z + \mu_2, \end{cases} \tag{3.5}$$

and q takes the two values

$$q = \begin{cases} q_r, & y < \mu_1 z + \mu_2, \\ q_l, & y > \mu_1 z + \mu_2. \end{cases} \tag{3.6}$$

3.2 Analysis

3.2.1 Modulation Equations

The simplified nematicon equations (3.3) and (3.4) do not possess an exact solitary wave solution, even in the case for which ψ_b and q are constants. To obtain an analytical model for nematicon evolution a modulation theory based on suitable trial functions for the electric field and director distribution profiles has been found useful [104] and will be employed here. The nematicon equations (3.3) and (3.4) have the Lagrangian

$$L = i\left(E^* E_z - E E_z^*\right) - i\Delta\left(E^* E_y - E E_y^*\right) - |\nabla E|^2 + 2\sin(2\psi_b)\theta|E|^2 - \nu|\nabla\theta|^2 - 2q\theta^2. \tag{3.7}$$

Suitable trial functions for the electric field and director distribution [104] are

$$E = a\,\mathrm{sech}\,\frac{\sqrt{x^2 + (y-\xi)^2}}{w}\, e^{i\sigma + iV(y-\xi)} + ige^{i\sigma + iV(y-\xi)} \tag{3.8}$$

$$\theta = \alpha\,\mathrm{sech}^2\,\frac{\sqrt{x^2 + (y-\xi)^2}}{\beta}. \tag{3.9}$$

Here a and w are the amplitude and waist of the nematicon, α and β are the amplitude and width of the director distribution, ξ is the nematicon position (beam axis), V is the propagation constant, giving the angle of propagation of the nematicon in the (y, z) plane, and σ is the nematicon phase. We have ν large and are in the nonlocal limit, $\beta \geq w$. The first term in the trial function (3.8) for the electric field represents a varying soliton with the profile of the exact soliton solution of the $(1 + 1)$ dimensional NLS equation. The second term represents the low wavenumber diffractive radiation which accumulates under the nematicon as it evolves [96]. The existence of this shelf of radiation under the beam can be shown from perturbed inverse scattering theory in the case of the $(1 + 1)$-D NLS equation [96] or from a perturbation analysis of the governing equations [178, 206], as described in Chapter 2. However, it is simplest to note that the group velocity of waves for the linearised electric field equation (3.3) is $C(\kappa) = \kappa$, where κ is the wavenumber. Hence, low wavenumber waves cannot leave the vicinity of the evolving nematicon. The parameter g measures the height of the shelf of low wavenumber diffractive radiation which accumulates under the solitary wave as it evolves [96, 104]. An input beam evolves to a steady state nematicon through the shedding of conserved quantities

via radiation. The shelf then does not remain flat, but matches into diffractive radiation propagating away from the nematicon. Hence, g is assumed to be non-zero in the disc of radius R, $0 \leq \sqrt{x^2+(y-\xi)^2} \leq R$, centred on the nematicon. All the nematicon parameters are functions of z. In the nonlocal limit the diffractive radiation shed by a nematicon has a significant effect on its evolution only for large values of z [104]. As propagation will be considered here for $z = O(10)$, the effect of this shed radiation will be ignored in the present work.

Substituting the trial functions (3.8) and (3.9) into the Lagrangian (3.7) and averaging by integration in x and y from $-\infty$ to ∞ results in the averaged Lagrangian [1]

$$\begin{aligned}\mathcal{L} &= -2\left(I_2 a^2 w^2 + \Lambda g^2\right)\left[\sigma' - V\xi' - \frac{1}{2}V^2\right] - 2I_1 a w^2 g' \\ &+ 2I_1 w^2 g a' + 4I_1 a w g w' - I_{22} a^2 - 4\nu I_{42}\alpha^2 \\ &+ \frac{A^2B^2\alpha\beta^2 a^2 w^2}{2Q}\left[\sin(2\psi_{bl})\operatorname{erfc}(\lambda_1) \;\; + \sin(2\psi_{br})\operatorname{erfc}(-\lambda_1)\right] \\ &+ \frac{1}{2}B^2 a^2 w^2 V\left[\Delta_l \operatorname{erfc}(\lambda_2) + \Delta_r \operatorname{erfc}(-\lambda_2)\right] \\ &- \frac{1}{4}D^2\alpha^2\beta^2\left[q_l \operatorname{erfc}(\lambda_3) + q_r \operatorname{erfc}(-\lambda_3)\right]. \end{aligned} \tag{3.10}$$

Here $\Delta_l = \Delta(\psi_{bl})$, $\Delta_r = \Delta(\psi_{br})$ and $\operatorname{erfc}(\zeta)$ is the complementary error function [207]. The arguments of the complementary error functions are

$$\begin{aligned}&\lambda_1 = \frac{\sqrt{A^2\beta^2 + B^2 w^2}}{AB\beta w}\left(\mu_1 z + \mu_2 - \xi\right), \lambda_2 = \frac{\mu_1 z + \mu_2 - \xi}{Bw}, \quad \lambda_3 = \frac{\sqrt{2}\left(\mu_1 z + \mu_2 - \xi\right)}{D\beta}, \\ &Q = A^2\beta^2 + B^2 w^2. \end{aligned} \tag{3.11}$$

$\Lambda = R^2/2$ is the area of the shelf of low wavenumber radiation under the beam, modulo 2π and the integrals I_i and $I_{i,j}$ in the modulation equations are

$$\begin{aligned} I_1 &= \int_0^\infty \rho f(\rho)\, d\rho, \qquad I_2 = \int_0^\infty \rho f^2(\rho)\, d\rho, \\ I_{22} &= \int_0^\infty \rho \left[\frac{df}{d\rho}\right]^2 d\rho, \qquad I_{x32} = \int_0^\infty \rho^3 f^2(\rho)\, d\rho, \\ I_{42} &= \frac{1}{4}\int_0^\infty \rho \left[\frac{d}{d\rho} f^2(\rho)\right]^2 d\rho, \qquad I_4 = \int_0^\infty \rho f^4(\rho)\, d\rho. \end{aligned} \tag{3.12}$$

For $f(\rho) = \operatorname{sech}\rho$

$$\begin{aligned} &I_1 = 2C, \quad I_2 = \ln 2, \quad I_{22} = \frac{1}{3}\ln 2 + \frac{1}{6}, I_{x32} = 1.352314016\ldots, \\ &I_{42} = \frac{2}{15}\ln 2 + \frac{1}{60}, \quad I_4 = \frac{2}{3}\ln 2 - \frac{1}{6}. \end{aligned} \tag{3.13}$$

Here C is the Catalan constant $C = 0.915965594\ldots$ [207].

The constants A, B and D arising in the modulation equations are

$$A = \frac{I_2\sqrt{2}}{\sqrt{I_{x32}}}, \quad B = \sqrt{2I_2} \quad \text{and} \quad D = 2\sqrt{I_4}. \tag{3.14}$$

Again, it should be noted that when the above averaged Lagrangian is evaluated, all the resulting integrals can be simply evaluated, except for the piecewise integration

$$\begin{aligned}
&\int_{-\infty}^{+\infty}\int_{-\infty}^{+\infty} q\,\mathrm{sech}^4\,\frac{\sqrt{x^2+(y-\xi)^2}}{\beta}\,dxdy\\
&=q_r\int_{-\infty}^{+\infty}\int_{-\infty}^{\mu_1 z+\mu_2}\mathrm{sech}^4\,\frac{\sqrt{x^2+(y-\xi)^2}}{\beta}\,dydx\\
&+q_l\int_{-\infty}^{+\infty}\int_{\mu_1 z+\mu_2}^{+\infty}\mathrm{sech}^4\,\frac{\sqrt{x^2+(y-\xi)^2}}{\beta}\,dydx. \qquad (3.15)
\end{aligned}$$

The integrals in (3.15) cannot be evaluated exactly. So a replacement by an equivalent Gaussian has to be used here in a similar fashion as in Section 2.1.2. The function $\mathrm{sech}^4\,\frac{\sqrt{x^2+(y-\xi)^2}}{\beta}$ is then replaced by the Gaussian $e^{-\frac{2(x^2+(y-\xi)^2)}{D^2\beta^2}}$, so that the piecewise integration becomes

$$\begin{aligned}
&q_r\int_{-\infty}^{+\infty}\int_{-\infty}^{\mu_1 z+\mu_2} e^{-\frac{2(x^2+(y-\xi)^2)}{D^2\beta^2}}\,dydx+q_l\int_{-\infty}^{+\infty}\int_{\mu_1 z+\mu_2}^{+\infty} e^{-\frac{2(x^2+(y-\xi)^2)}{D^2\beta^2}}\,dydx\\
&=q_r\int_{-\infty}^{+\infty} e^{-\frac{2x^2}{D^2\beta^2}}\,dx\int_{-\infty}^{\mu_1 z+\mu_2} e^{-\frac{2(y-\xi)^2}{D^2\beta^2}}\,dy+q_l\int_{-\infty}^{+\infty} e^{-\frac{2x^2}{D^2\beta^2}}\,dx\int_{\mu_1 z+\mu_2}^{+\infty} e^{-\frac{2(y-\xi)^2}{D^2\beta^2}}\,dy\\
&=q_r\cdot\frac{\sqrt{2\pi}}{2}D\beta\cdot\frac{\sqrt{2\pi}}{4}D\beta\,\mathrm{erfc}(\frac{\sqrt{2}(\xi-\mu_1 z-\mu_2)}{D\beta})\\
&+q_l\cdot\frac{\sqrt{2\pi}}{2}D\beta\cdot\frac{\sqrt{2\pi}}{4}D\beta\,\mathrm{erfc}(\frac{\sqrt{2}(\mu_1 z+\mu_2-\xi)}{D\beta})
\end{aligned}$$

The constants A and B were determined in section 2.1.2. The constant D will be determined in a similar fashion by equating integrals in the nonlocal limit $\beta \gg \omega$. The matching of areas is done for the limit in which the cell is uniform, that is $z \to \infty$, as the integrals can then be evaluated. Let us set $Y = y - \xi$ and evaluate the integral of the hyperbolic secant first

$$\begin{aligned}
&\int_{-\infty}^{+\infty}\int_{-\infty}^{+\infty}\mathrm{sech}^4\,\frac{\sqrt{x^2+Y^2}}{\beta}\,dxdY\\
&=\int_0^{2\pi}\int_0^{\infty} r\,\mathrm{sech}^4\,\frac{r}{\beta}\,drd\theta \qquad \text{changed to polar coordinates}\\
&=2\pi\beta^2 I_4. \qquad (3.16)
\end{aligned}$$

Then the integral of the Gaussian is

$$\begin{aligned}
&\int_{-\infty}^{+\infty}\int_{-\infty}^{+\infty} e^{-\frac{2(x^2+Y^2)}{D^2\beta^2}}\,dxdY\\
&=\int_{-\infty}^{+\infty} e^{-\frac{2Y^2}{D^2\beta^2}}\,dY\int_{-\infty}^{+\infty} e^{-\frac{2x^2}{D^2\beta^2}}\,dx\\
&=\sqrt{\frac{\pi}{2}}D\beta\cdot\sqrt{\frac{\pi}{2}}D\beta\\
&=\frac{\pi}{2}D^2\beta^2. \qquad (3.17)
\end{aligned}$$

We now equate (3.16) and (3.17), so that the value of the constant D can be obtained as

$$D = 2\sqrt{I_4}.$$

Taking variations of the averaged Lagrangian (3.10) with respect to the parameters results in the modulation equations governing the refraction of the nematicons at the interface. These modulation equations are

$$\frac{d}{dz}\left(I_2 a^2 w^2 + \Lambda g^2\right) = 0, \tag{3.18}$$

$$\frac{d\xi}{dz} = V - \frac{1}{2}\left[\Delta_l \operatorname{erfc}(\lambda_2) + \Delta_r \operatorname{erfc}(-\lambda_2)\right], \tag{3.19}$$

$$\begin{aligned}\frac{dV}{dz} &= \frac{BV}{2\sqrt{\pi} I_2 w}\left(\Delta_l - \Delta_r\right) e^{-\lambda_2^2} + \frac{AB\alpha\beta}{2\sqrt{\pi} I_2 w\sqrt{Q}}\left(\sin 2\psi_{bl} - \sin 2\psi_{br}\right) e^{-\lambda_1^2} \\ &- \frac{\sqrt{2} D\alpha^2\beta}{4\sqrt{\pi} I_2 a^2 w^2}\left(q_l - q_r\right) e^{-\lambda_3^2},\end{aligned} \tag{3.20}$$

$$I_1 \frac{d}{dz} a w^2 = \Lambda g\left(\sigma' - V\xi' + \frac{1}{2}V^2\right), \tag{3.21}$$

$$\begin{aligned}I_1 \frac{dg}{dz} &= \frac{I_{22} a}{2w^2} - \frac{A^2 B^4 \alpha\beta^2 a w^2}{4Q^2}\left[\sin(2\psi_{bl}) \operatorname{erfc}(\lambda_1) \ + \sin(2\psi_{br}) \operatorname{erfc}(-\lambda_1)\right] \\ &+ \frac{A^3 B\alpha\beta^3 a}{4\sqrt{\pi} w Q^{3/2}}\left[\sin 2\psi_{bl} - \sin 2\psi_{br}\right] e^{-\lambda_1^2} \\ &+ \frac{BaV}{4\sqrt{\pi} w}\left(\mu_1 z + \mu_2 - \xi\right)\left(\Delta_l - \Delta_r\right) e^{-\lambda_2^2},\end{aligned} \tag{3.22}$$

$$\begin{aligned}&\frac{d\sigma}{dz} - V\frac{d\xi}{dz} + \frac{1}{2}V^2 = -\frac{I_{22}}{I_2 w^2} \\ &+ \frac{A^2\alpha\beta^2\left(A^2\beta^2 + 2B^2 w^2\right)}{2Q^2}\left[\sin(2\psi_{bl}) \operatorname{erfc}(\lambda_1) \ + \sin(2\psi_{br}) \operatorname{erfc}(-\lambda_1)\right] \\ &- \frac{A^3 B\alpha\beta^3}{4 I_2 w Q^{3/2}}\left(\sin 2\psi_{bl} - \sin 2\psi_{br}\right) e^{-\lambda_1^2} + \frac{1}{2}V\left[\Delta_l \operatorname{erfc}(\lambda_2) + \Delta_r \operatorname{erfc}(-\lambda_2)\right] \\ &- \frac{BV}{4\sqrt{\pi} I_2 w}\left(\mu_1 z + \mu_2 - \xi\right)\left(\Delta_l - \Delta_r\right) e^{-\lambda_2^2},\end{aligned} \tag{3.23}$$

together with the algebraic equations

$$\alpha = \frac{A^2 B^2 \beta^2 a^2 w^2}{Q} \times \frac{\sin(2\psi_{bl}) \operatorname{erfc}(\lambda_1) + \sin(2\psi_{br}) \operatorname{erfc}(-\lambda_1)}{16\nu I_{42} + D^2\beta^2\left[q_l \operatorname{erfc}(\lambda_3) + q_r \operatorname{erfc}(-\lambda_3)\right]}, \tag{3.24}$$

and

$$\begin{aligned}&\frac{A^2 B^4 \beta a^2 w^4}{Q^2}\left[\sin(2\psi_{bl}) \operatorname{erfc}(\lambda_1) + \sin(2\psi_{br}) \operatorname{erfc}(-\lambda_1)\right] \\ &+ \frac{AB^3 a^2 w^3}{\sqrt{\pi} Q^{3/2}}\left(\sin 2\psi_{bl} - \sin 2\psi_{br}\right)\left(\mu_1 z + \mu_2 - \xi\right) e^{-\lambda_1^2} \\ &- \frac{1}{2} D^2\alpha\beta\left[q_l \operatorname{erfc}(\lambda_3) + q_r \operatorname{erfc}(-\lambda_3)\right] - \frac{D}{\sqrt{2\pi}}\alpha(q_l - q_r)\left(\mu_1 z + \mu_2 - \xi\right) e^{-\lambda_3^2} \\ &= 0.\end{aligned} \tag{3.25}$$

The modulation equation (3.18) is the equation for conservation of optical power, which is termed mass conservation in the sense of the scale invariance of the Lagrangian (3.7) [199]. The modulation equation (3.20) is the equation for conservation of linear momentum. The trajectory of the beam is governed by this momentum equation and the modulation equation

(3.19). Unlike previous studies of the refraction of nematicons by changes in the liquid crystal medium, the trajectory equations (3.19) and (3.20) are not independent of the amplitude and width evolution of the nematicon as the position equations explicitly depend on the waist w of the nematicon via the complementary error functions in these equations [118]. The medium changes across the interface, so that the amplitude a and width w of the nematicon show significant adjustments.

The shelf radius R is given by Minzoni *et al* [104]. However, due to the different scalings used in the nematicon equations (3.3) and (3.4), R must be replaced by $R\sqrt{2/\sin(2\psi_b)}$ and q must be replaced by $2q/\sin(2\psi_b)$ [104].

3.2.2 Adjustments to Numerical Code

As outlined in Section 2.2.1, the governing equation (3.3) was solved using a pseudo-spectral method similar to that of Fornberg and Whitham [182]. The director equation (3.4) was solved as a two-point boundary value problem using Picard iteration in Fourier space. The modulation equations were solved using the standard fourth order Runge-Kutta scheme [185] in an identical manner to that described in Section 2.2.1. It is noted that the discontinuities in ψ_b and q across $y = \mu_1 z + \mu_2$ were smoothed using tanh to link the two levels. If this smoothing were not used, nonphysical oscillations in the nematicon position occur. In order to eliminate spurious numerical effects, the discontinuities in ψ_b and q across $y = \mu_1 z + \mu_2$ were smoothed using $\tanh(y - \mu_1 z - \mu_2)/w_t$ to link the orientations ψ_{bl} and ψ_{br} and q_l and q_r, where w_t is the width of the boundary layer. For small w_t this smoothing made no difference to the solutions, other than to eliminate nonphysical beam deformations and possible splitting which occur as $w_t \to 0$. As noted in the previous section, in experiments the pre-tilting field and the background director distribution varied smoothly, and rapidly, between the two constant values [202, 203]. Therefore, smoothing this change for the numerical solution is more appropriate than applying boundary conditions at the interface, as in previous studies of two media with different properties separated by an interface [197, 198].

3.3 Results

In this section numerical solutions of the full governing nematicon equations will be compared with solutions of the modulation equations. In the following discussion numerical solutions of the full governing equations (3.3) and (3.4) are referred to as "full numerical solutions" and numerical solutions of the modulation equations (3.18)-(3.25) are termed "modulation solutions." The position of the maximum of the nematicon was used for its numerical position ξ. The results will be presented for two opposite cases: the beam travels from a less to a more optically dense medium and the beam goes from a more to a less optically dense medium. Unlike the experiments of Peccianti *et al* [196], for which the angle of refraction of the nematicon was changed by varying the relative voltage difference between the two regions of the NLC cell across the interface, in the present work the relative voltage difference will be kept constant for both cases of propagation. The angle of refraction will be changed by varying the input angle of the beam, i.e. the angle of incidence, for a fixed interface. In this context, it should be noted that changing the angle of the interface also changes the incidence angle of the nematicon. The values of the background director angle ψ_b and the other parameter values were chosen to be within the experimental ranges [196]. The propagation of the beam is sketched schematically

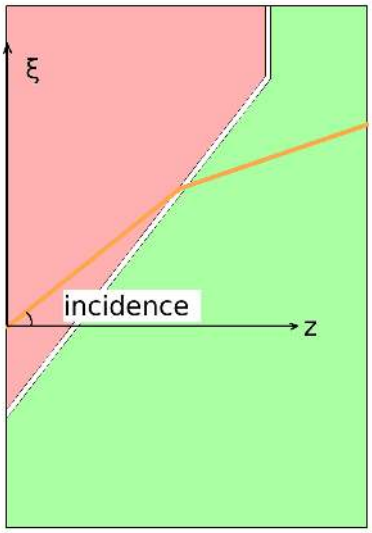

Figure 3.3: The incidence of the beam on the interface

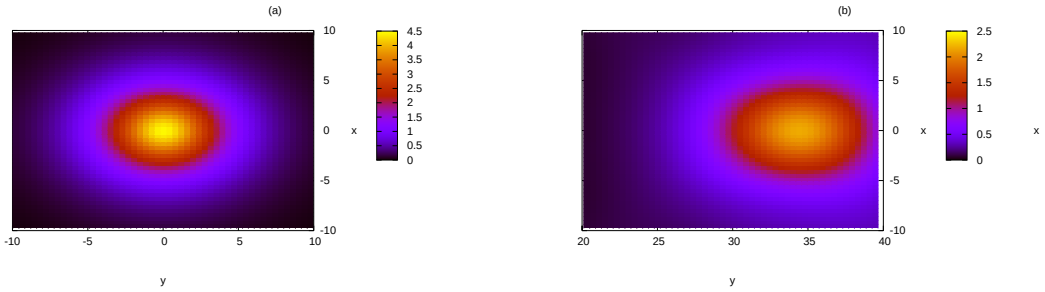

Figure 3.4: Full numerical solution for $|u|$ for the initial values $a = 4.5$, $w = 2.5$, $\xi = 0$, $V = 0.5$ with the parameter values $\nu = 200$, $\psi_{bl} = 0.4$, $\psi_{br} = 0.9$, $q_l = 1.0$, $q_r = 1.3$, $\mu_1 = 2$ and $\mu_2 = -20$. (a) $z = 0$, (b) $z = 200$.

in Figure 3.3. The propagation angle φ of the beam is then given by

$$tan\varphi = \frac{d\xi}{dz}.$$

Taking $\xi = \infty$ in the modulation equation (3.19) gives the angle of incidence φ_l

$$(\frac{d\xi}{dz})_{\xi=\infty} = V - \Delta_l,$$

so that

$$tan\varphi_l = V - \Delta_l. \tag{3.26}$$

Due to the large changes in medium properties, the input nematicon has to be chosen so that it is stable, that is it does not decay into radiation, on propagation across the interface. Such stable cases are shown in Figure 3.4 and Figure 3.5 for propagation to a more and to a less optically dense medium, respectively. The optical beams are stable until the final z, $z = 200$, for propagation to a more optically dense medium and $z = 80$ for propagation to a less optically

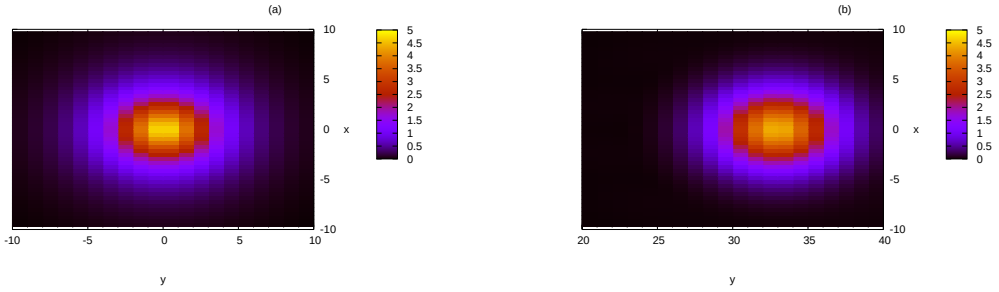

Figure 3.5: Full numerical solution for $|u|$ for the initial values $a = 5.0$, $w = 2.0$, $\xi = 0$, $V = 0.5$ with the parameter values $\nu = 200$, $\psi_{bl} = 0.8$, $\psi_{br} = 0.6$, $q_l = 1.3$, $q_r = 1.0$, $\mu_1 = 2$ and $\mu_2 = -8$. (a) $z = 0$, (b) $z = 80$.

dense medium, respectively. For these z, the beam is far beyond the interface and resembles the input beam.

Firstly, let us consider a typical case of a nematicon propagating from a less to a more optically dense medium. Figure 3.6 shows a comparison of positions as given by the full numerical and modulation solutions. It can be seen from this figure that the position comparison is excellent. Before refraction at the interface, the trajectory of the full numerical solution almost completely coincides with that of the modulation solution. However, when the refraction starts to occur at the interface at around $z = 12.8$ in Figure 3.6(a), the numerical nematicon trajectory shows a sudden change. This is explored further in Figure 3.7, which shows contour plots at $x = 0$ of the evolution of the nematicon on refraction to a more dense medium. It can be seen from Figure 3.7 that on refraction to the denser region the nematicon has undergone significant distortion, then taking a significant distance to settle back to a uniform state, after which the numerical trajectory returns to the modulation one, as visible in Figure 3.6(a). An example for another initial value $V_0 = 1.0$ in Figure 3.6(b) shows the same type of behaviour of the nematicon. The distortion of the nematicon occurs when it is close to the interface, so that different portions of it are in both media. This introduces gradients across its profile, resulting in the distortion, an effect which has been noted in studying the refraction of nematicons by localised refractive index changes [118]. The modulation theory outlined in the previous section assumes that the nematicon is a point particle which does not change its profile, or functional form, as it evolves. While this is an excellent approximation in a uniform medium [104], in a non-uniform case the changes in medium properties can lead to significant beam deformation not accounted for in the modulation theory [118, 130]. Such beam deformations can have an effect on the refraction of nematicons.

Figure 3.8 shows a comparison between the final propagation angle as a function of the input angle as given by the full numerical and modulation solutions. As given by (3.26), the final angles and the input angles are all measured by their tangents with the z axis. V_0 refers to the input value of V and V_f refers to the steady value after passing the interface. It can be seen that the modulation equations give results in excellent agreement with the full numerical solutions for a wide range of input angles. This is further confirmed by the difference between the modulation value of $V_0 - \Delta_r$ and the full numerical value shown in Figure 3.9. The difference between these two values is shown in Figure 3.9(a) and the percentage error in Figure 3.9(b).

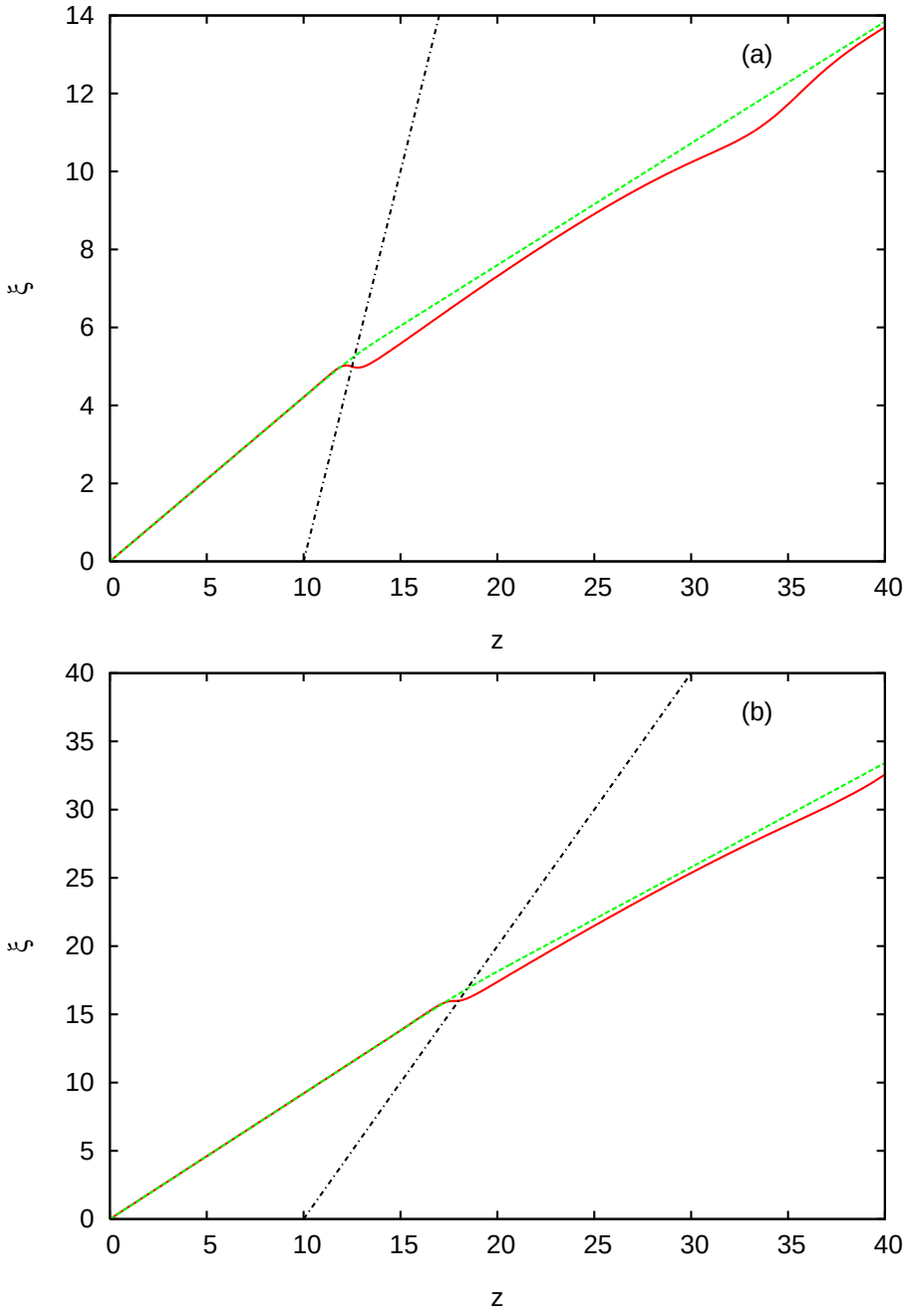

Figure 3.6: Comparison between nematicon trajectories as given by the full numerical and modulation solutions for the initial values $a = 4.5$ and $w = 2.5$, with $\nu = 200$, $\psi_{bl} = 0.4$, $\psi_{br} = 0.9$, $q_l = 1.0$, $q_r = 1.3$, $\mu_1 = 2$ and $\mu_2 = -20$. Full numerical solution: — (red, solid line); modulation solution: – – – (green, dashed line); interface: - · - · (black, dash dot line). (a) $V_0 = 0.5$, (b) $V_0 = 1.0$. (*The most parts of full numerical solution and modulation solution overlap to a high extent. Especially when printed in black and white, the superposition makes a solid line look like a dashed line.)

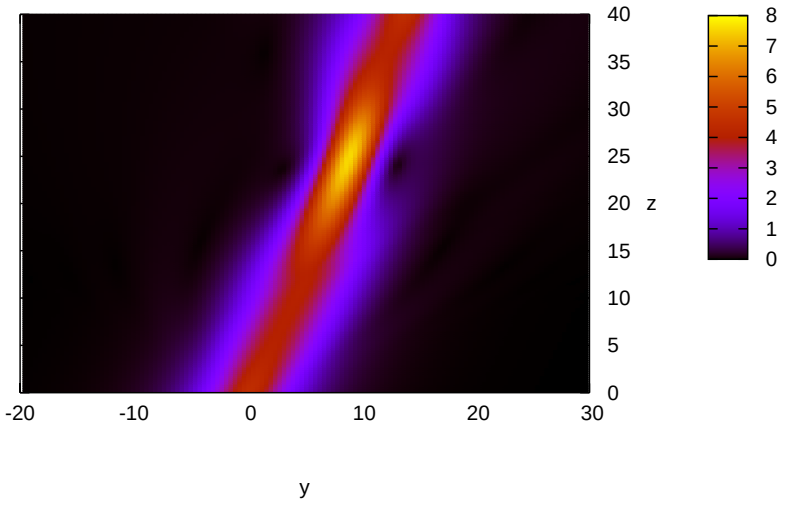

Figure 3.7: Nematicon evolution at $x = 0$ as given by the full numerical solution for the initial value $V_0 = 0.5$, with $\nu = 200$. Initial values $a = 4.5$, $w = 2.5$, with $\psi_{bl} = 0.4$, $\psi_{br} = 0.9$, $q_l = 1.0$, $q_r = 1.3$, $\mu_1 = 2$ and $\mu_2 = -20$.

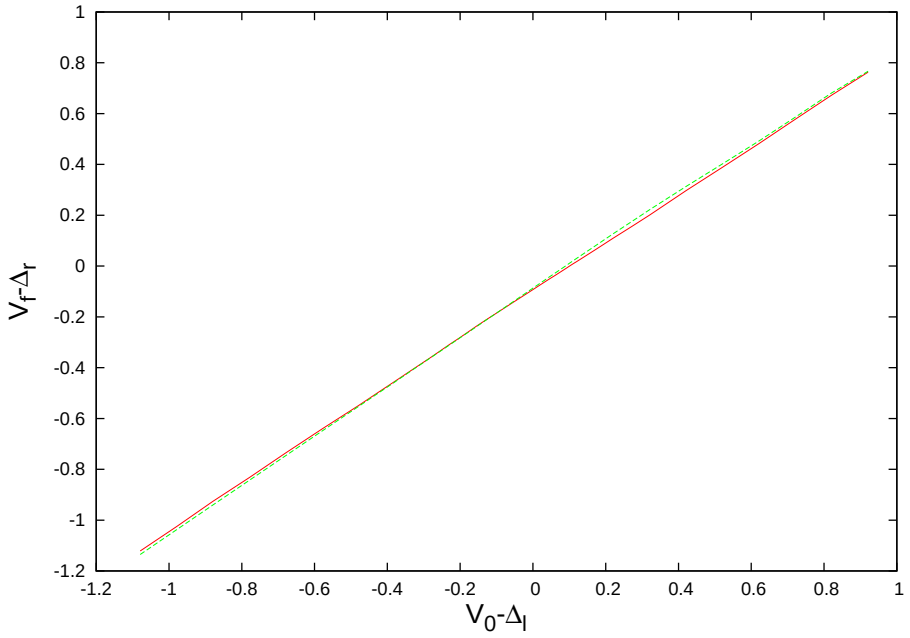

Figure 3.8: Comparison of refracted propagation constant $V_f - \Delta_r$ versus incident propagation constant $V_0 - \Delta_l$ as given by the full numerical and modulation solutions. The initial values are $a = 4.5$, $w = 2.5$, $\xi = 0$, with the parameter values $\nu = 200$, $\psi_{bl} = 0.4$, $\psi_{br} = 0.9$, $q_l = 1.0$, $q_r = 1.3$, $\mu_1 = 2$ and $\mu_2 = -20$. Full numerical solution: — (red, solid line); modulation solution: – – – (green, dashed line). (*The most parts of full numerical solution and modulation solution overlap to a high extent. Especially when printed in black and white, the superposition makes a solid line look like a dashed line.)

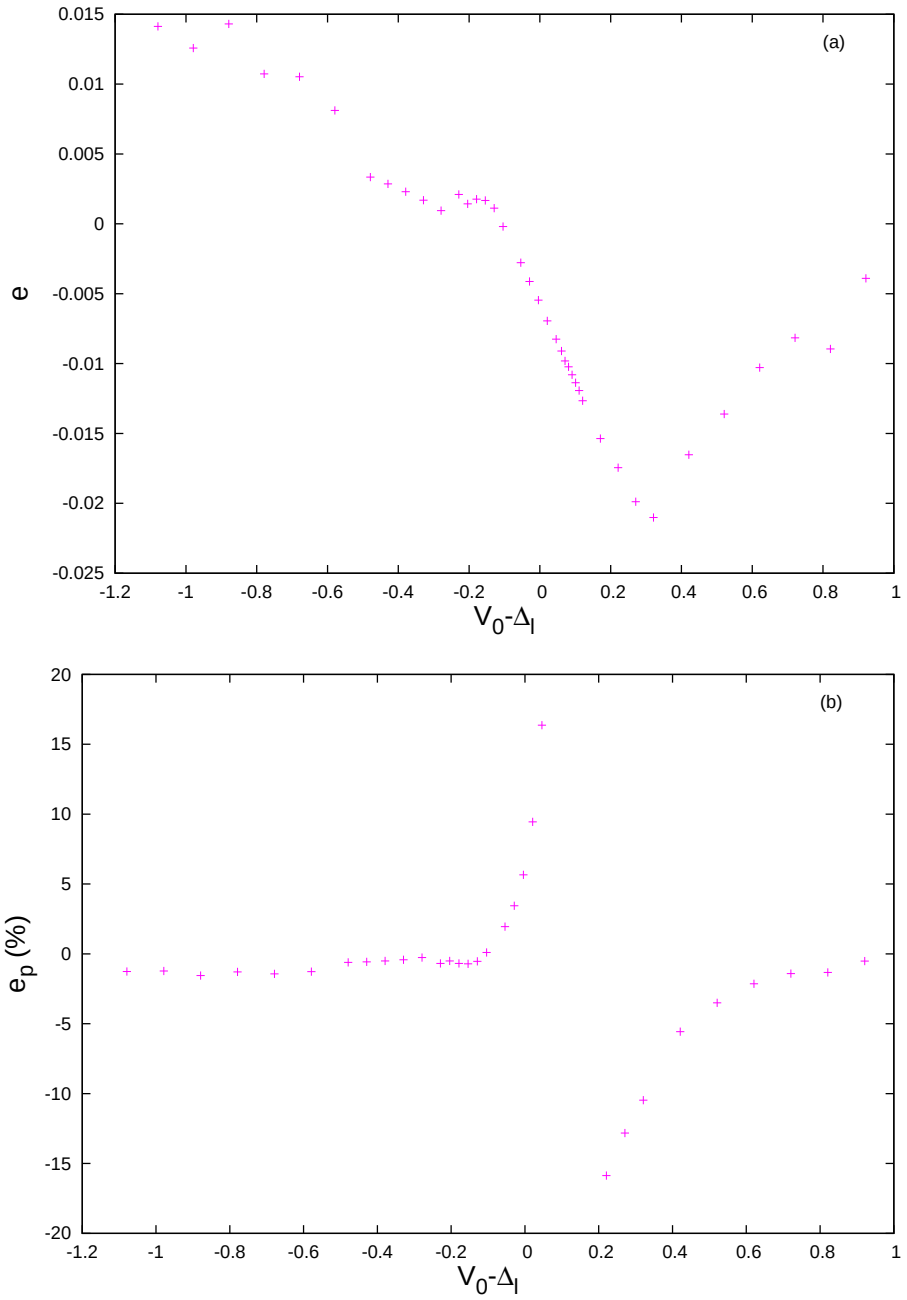

Figure 3.9: The error in the refracted propagation constant $V_f - \Delta_r$ as given by the modulation theory compared with the numerical solution as a function of incident propagation constant $V_0 - \Delta_l$. The initial values are $a = 4.5$, $w = 2.5$, $\xi = 0$, with the parameter values $\nu = 200$, $\psi_{bl} = 0.4$, $\psi_{br} = 0.9$, $q_l = 1.0$, $q_r = 1.3$, $\mu_1 = 2$ and $\mu_2 = -20$. (a) error e, (b) percentage error e_p.

The percentage error in the modulation angle is generally less than 5%. The exception is for input $V_0 - \Delta_l$ between 0.05 and 0.3, which is because the refraction angle is 0 at $V_0 - \Delta_l = 0.1$, so that the percentage error is not a good measure of the difference around this input angle. The change in the angle of propagation across the interface is $O(5^o)$. In experiments on nematicons, changes in the angle of propagation of up to 18^o were obtained [196]. The change in the angle of propagation depends on the jump in the values of ψ and q as these parameters depend on the size of the two pre-tilting electric fields [101, 127]. As shown by the typical result in Figure 3.6, although the refraction process for propagation into a more optically dense medium is nonlinear, in most respects it resembles linear, Snell-type refraction. Nonlinear effects become most apparent when propagation into a less optically dense medium is considered, as will be dealt with now.

Let us now consider a solitary wave beam propagating from a more to a less optically dense medium. Similar to the less-to-more case, Figure 3.10 shows a comparison of positions as given by the full numerical and modulation solutions. Again, the two examples in Figure 3.10 show that the position comparison is excellent. It can be seen from Figure 3.11 that there is little distortion of the nematicon on refraction to the less optically dense medium and that there is no corresponding abrupt change in its numerical trajectory. The reason for this is that there is a smaller change in medium properties for the parameter values used, with the change in ψ_b significantly less. This smaller change in properties means that there is a smaller gradient across the beam when it is near the interface, resulting in reduced distortion. The modulation theory approximation of a fixed beam profile is then good.

Figure 3.12 shows a comparison between the input and output propagation angles as given by the full numerical and modulation solutions. There is again excellent agreement, but it can be seen that there is a slightly increasing difference as $V_0 - \Delta_l$ approaches around 1.5. The difference and percentage differences also confirm this, as shown in Figure 3.13. It is noted that the angle curve in Figure 3.12 has a peak around $V_0 - \Delta_l = 1.7$. This peak is due to the nematicon changing from refraction to total internal reflection, which will be explained in detail as follows.

For a change from a more to a less optically dense medium, a linear wave either refracts following Snell's law or undergoes total internal reflection above the critical angle. However, a nematicon is an isolated nonlinear wavepacket with an extended transverse profile. This results in a variety of possible behaviours, which include refraction and total internal reflection, but extend to other behaviours. As schematically illustrated in Figure 3.14, the nematicon can undergo refraction when passing into the less dense medium, type 1 of Figure 3.14, or proceed straight without change in its trajectory if it does not approach the interface, type 5. However, a nematicon is an extended body so that it can overlap the different media on both sides of the interface when it is in its vicinity. This has two consequences, giving two different types of total internal reflection [196, 203]. One is reflection with enhanced Goos-Hänchen shift [208], whereby the nematicon peak enters the less dense medium, but then re-enters the original medium, resulting in total internal reflection [196, 197, 198, 202, 203, 208], type 2 of Figure 3.14. The second is when the beam undergoes total internal reflection without its peak touching the interface, due to its tail crossing the interface and entering the less dense medium. This total internal reflection is of two types. On increasing the angle of incidence, at a specific angle the nematicon undergoes total internal reflection with its axis exactly tangential to the interface, type 3 behaviour. On further increase of the angle of incidence, the nematicon undergoes total

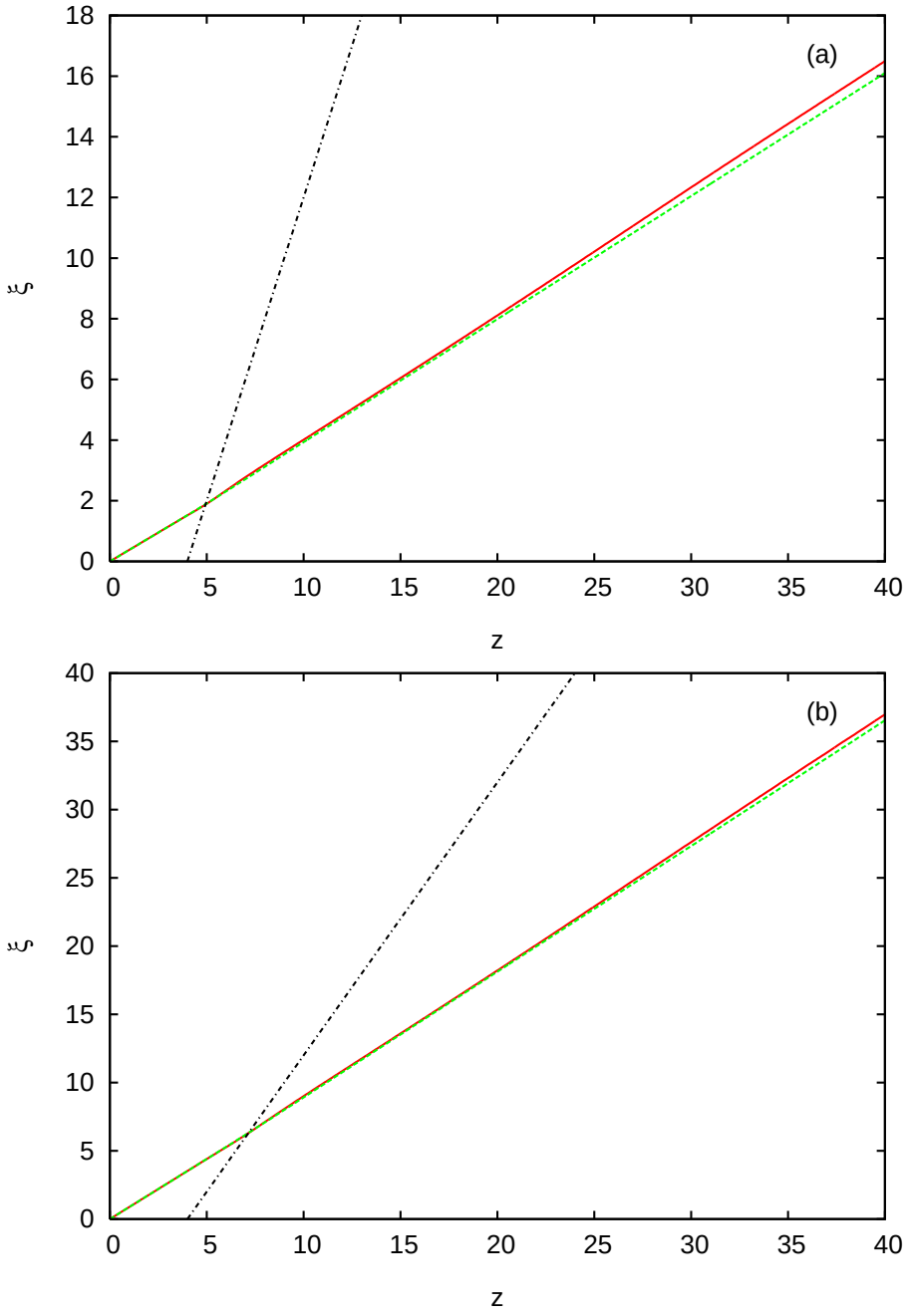

Figure 3.10: Comparison between nematicon trajectories as given by the full numerical and modulation solutions for the initial values $a = 5.0$ and $w = 2.0$, with $\nu = 200$, $\psi_{bl} = 0.8$, $\psi_{br} = 0.6$, $q_l = 1.3$, $q_r = 1.0$, $\mu_1 = 2$ and $\mu_2 = -8$. Full numerical solution: — (red, solid line); modulation solution: – – – (green, dashed line); interface: - · - · (black, dash dot line). (a) $V_0 = 0.5$, (b) $V_0 = 1.0$. (*The most parts of full numerical solution and modulation solution overlap to a high extent. Especially when printed in black and white, the superposition makes a solid line look like a dashed line.)

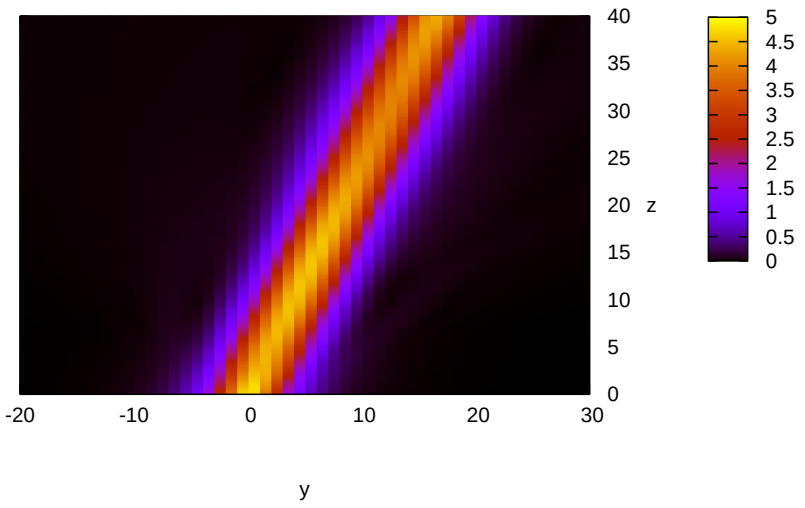

Figure 3.11: Nematicon evolution at $x = 0$ as given by the full numerical solution for the initial value $V_0 = 0.5$, with $\nu = 200$. Initial values $a = 5.0$, $w = 2.0$, with $\psi_{bl} = 0.8$, $\psi_{br} = 0.6$, $q_l = 1.3$, $q_r = 1.0$, $\mu_1 = 2$ and $\mu_2 = -8$.

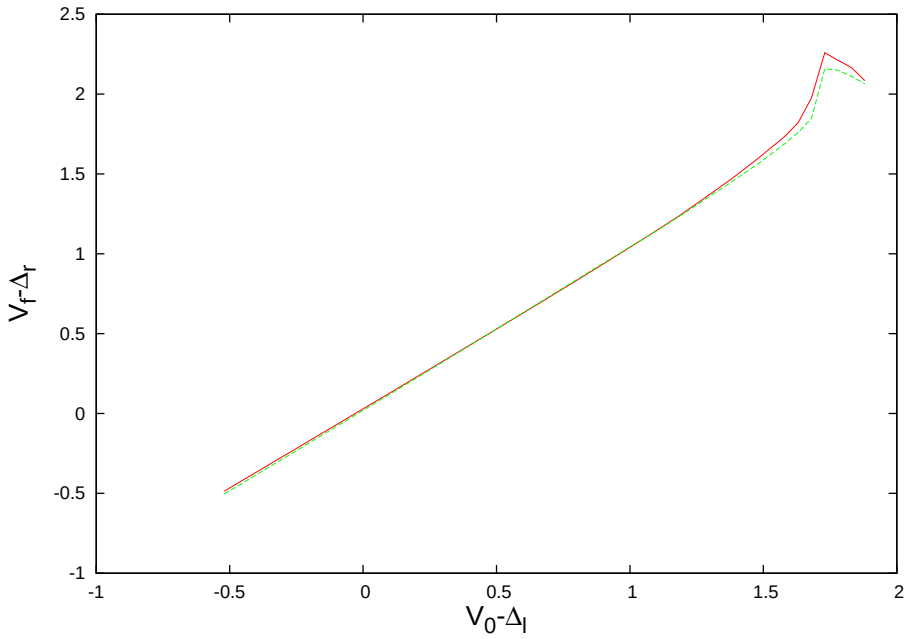

Figure 3.12: Comparison of refracted propagation constant $V_f - \Delta_r$ versus incident propagation constant $V_0 - \Delta_l$ as given by the full numerical and modulation solutions. The initial values are $a = 5.0$, $w = 2.0$, $\xi = 0$, with the parameter values $\nu = 200$, $\psi_{bl} = 0.8$, $\psi_{br} = 0.6$, $q_l = 1.3$, $q_r = 1.0$, $\mu_1 = 2$ and $\mu_2 = -8$. Full numerical solution: — (red, solid line); modulation solution: – – – (green, dashed line). (*The most parts of full numerical solution and modulation solution overlap to a high extent. Especially when printed in black and white, the superposition makes a solid line look like a dashed line.)

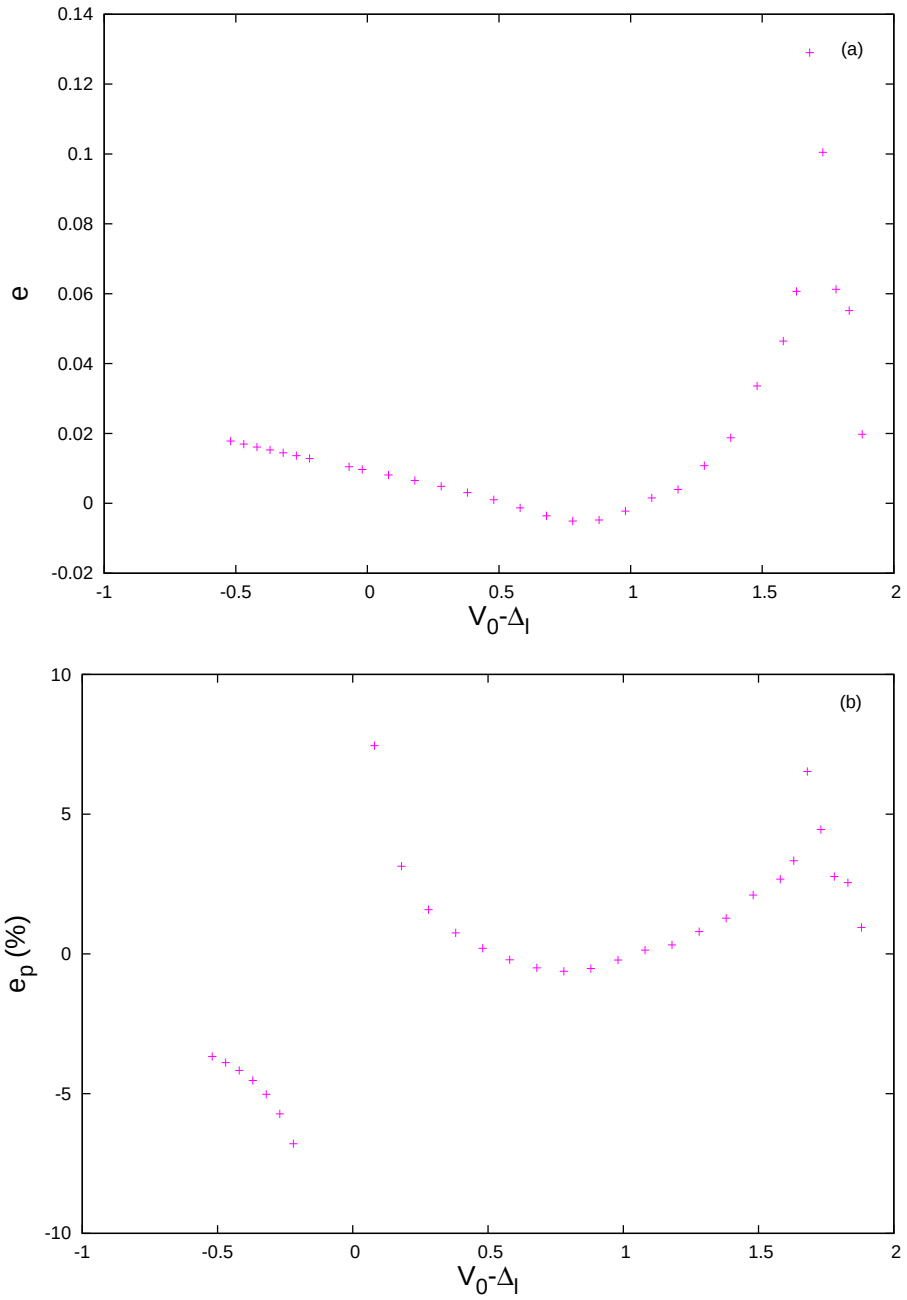

Figure 3.13: The error in the refracted propagation constant $V_f - \Delta_r$ as given by the modulation theory compared with the numerical solution as a function of incident propagation constant $V_0 - \Delta_l$. The initial values are $a = 5.0$, $w = 2.0$, $\xi = 0$, with the parameter values $\nu = 200$, $\psi_{bl} = 0.8$, $\psi_{br} = 0.6$, $q_l = 1.3$, $q_r = 1.0$, $\mu_1 = 2$ and $\mu_2 = -8$. (a) error e, (b) percentage error e_p.

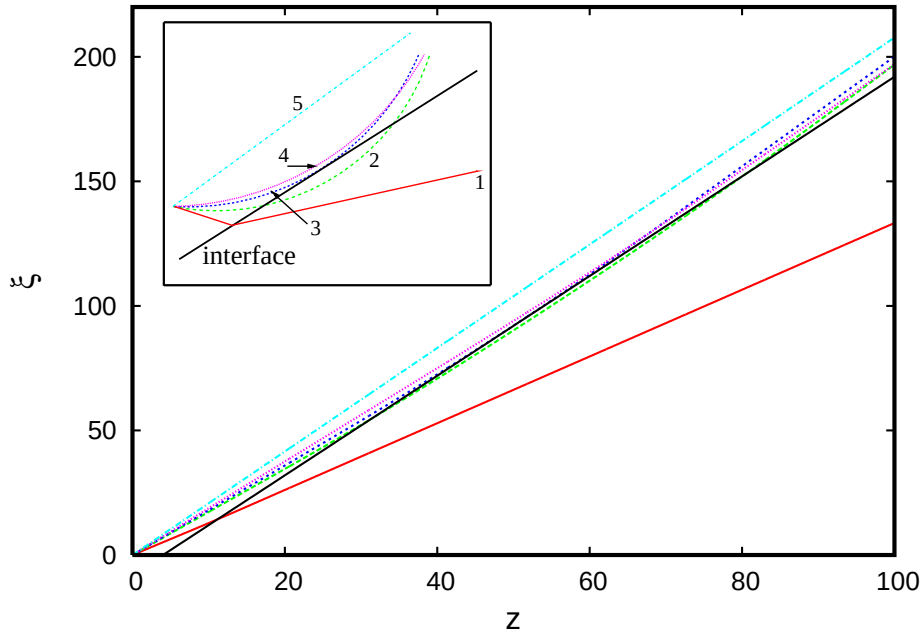

Figure 3.14: Beam behaviour types as it propagates from more to less optically dense medium. Inset shows schematic of possible beam trajectories. 1. refraction: — (full red line), 2. Goos-Hänchen type reflection: — — — (long dash green line), 3. total internal reflection at the interface: – – – (short dash dark blue line), 4. total internal reflection with beam axis in more dense medium: ··· (dotted pink line), 5. unchanged beam path: – - – - – (dash dot light blue line). Interface is the thick straight solid line (black).

refraction type	numerical	modulation
1.	$\mathcal{V}_0 \leq 1.67$	$\mathcal{V}_0 \leq 1.709$
2.	$1.68 \leq \mathcal{V}_0 < 1.812$	$1.71 \leq \mathcal{V}_0 < 1.800$
3.	$\mathcal{V}_0 = 1.812$	$\mathcal{V}_0 = 1.800$
4.	$1.812 < \mathcal{V}_0 \leq 2.02$	$1.800 < \mathcal{V}_0 \leq 2.019$
5.	$\mathcal{V}_0 \geq 2.03$	$\mathcal{V}_0 \geq 2.020$

Table 3.1: $\mathcal{V}_0 = V_0 - \Delta_l$ ranges for refraction types to an optically less dense medium. The behaviour types are classified as in Figure 3.14. The parameter values are $a = 5$ and $w = 2$, with $\nu = 200$, $\psi_{bl} = 0.8$, $\psi_{br} = 0.6$, $q_l = 1.3$, $q_r = 1.0$, $\mu_1 = 2.0$ and $\mu_2 = -8.0$.

internal reflection with its peak remaining in the denser medium, behaviour type 4. In this case, reflection occurs due to the nematicon tail entering the less optically dense medium.

A comparison between the ranges of $V_0 - \Delta_l$ for the different behaviours, illustrated schematically in Figure 3.14, as given by the modulation solution and the full numerical solution is provided in Table 3.1. Excellent agreement for the different regime ranges as predicted by the modulation solution is seen from Table 3.1. Type 1 refraction of Figure 3.14 is when the nematicon undergoes refraction when passing into the less dense medium, and is similar to a linear wave. One example of this refraction type is illustrated in Figure 3.10. For high angles of incidence, the nonlocal nematicon shows three types of total internal reflection. Refraction changes to Goos-Hänchen reflection [196, 197, 198, 202, 203, 208], type 2 behaviour of Figure 3.14, at $V_0 - \Delta_l = 1.67$ for the full numerical solution and $V_0 - \Delta_l = 1.709$ for the modulation solution, with the beam entering the less dense medium, and then passing back through the interface, as observed in experiments [196, 202, 203] and previous theoretical studies [197, 198]. A typical case of Goos-Hänchen reflection is illustrated in Figure 3.15, which is subject to a

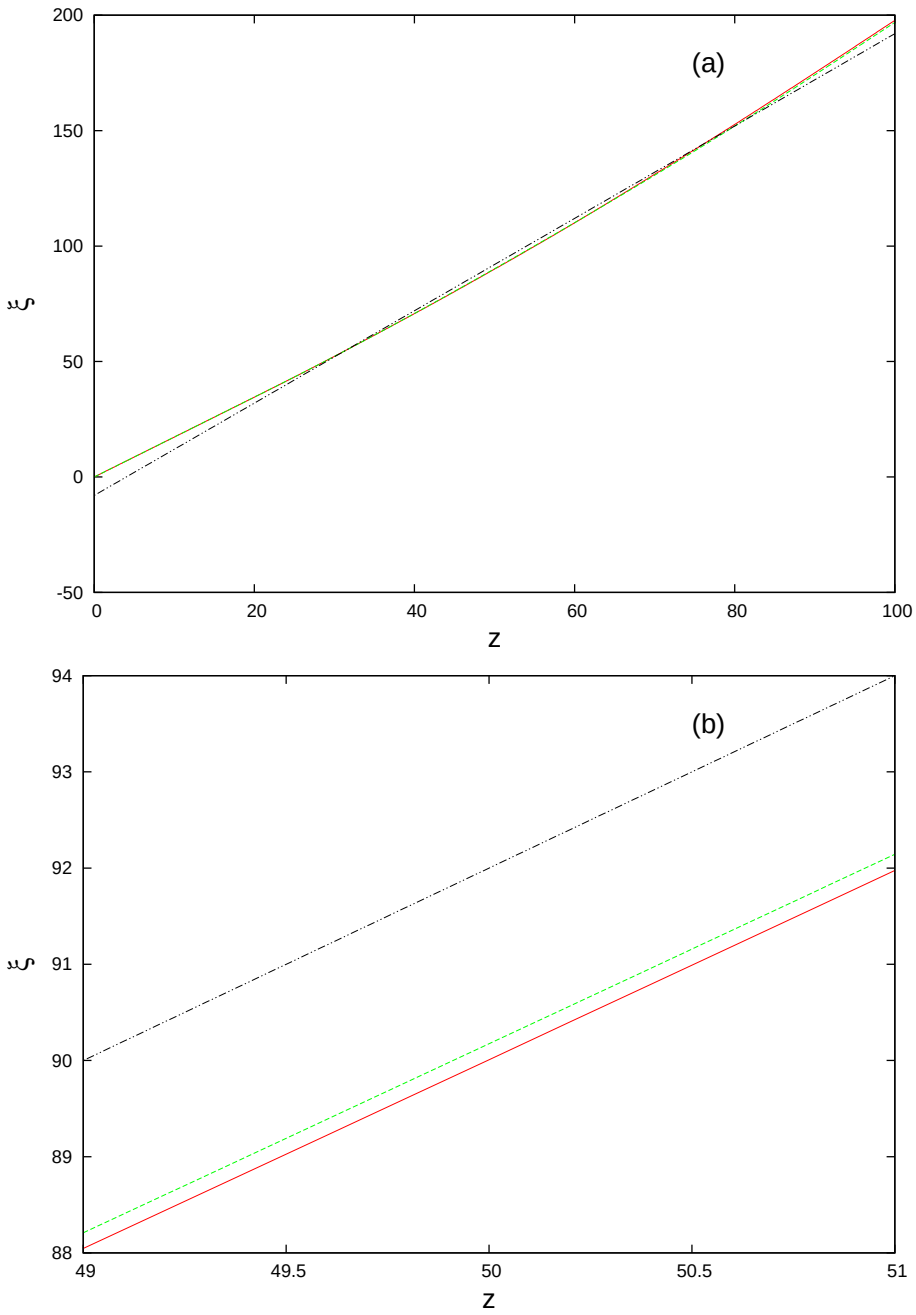

Figure 3.15: Goos-Hänchen type reflection. Comparisons for the initial values $a = 5.0$, $w = 2.0$, $\xi = 0$, $V = 1.85$ with the parameter values $\nu = 200$, $\psi_{bl} = 0.8$, $\psi_{br} = 0.6$, $q_l = 1.3$, $q_r = 1.0$, $\mu_1 = 2$ and $\mu_2 = -8$. Full numerical solution: — (red, solid line); modulation solution: – – – (green, dashed line); interface: – ·· – ·· (black, dash dot dot line). (a) for z ranging from 0 to 100, (b) amplified curves for z ranging from 49 to 51.

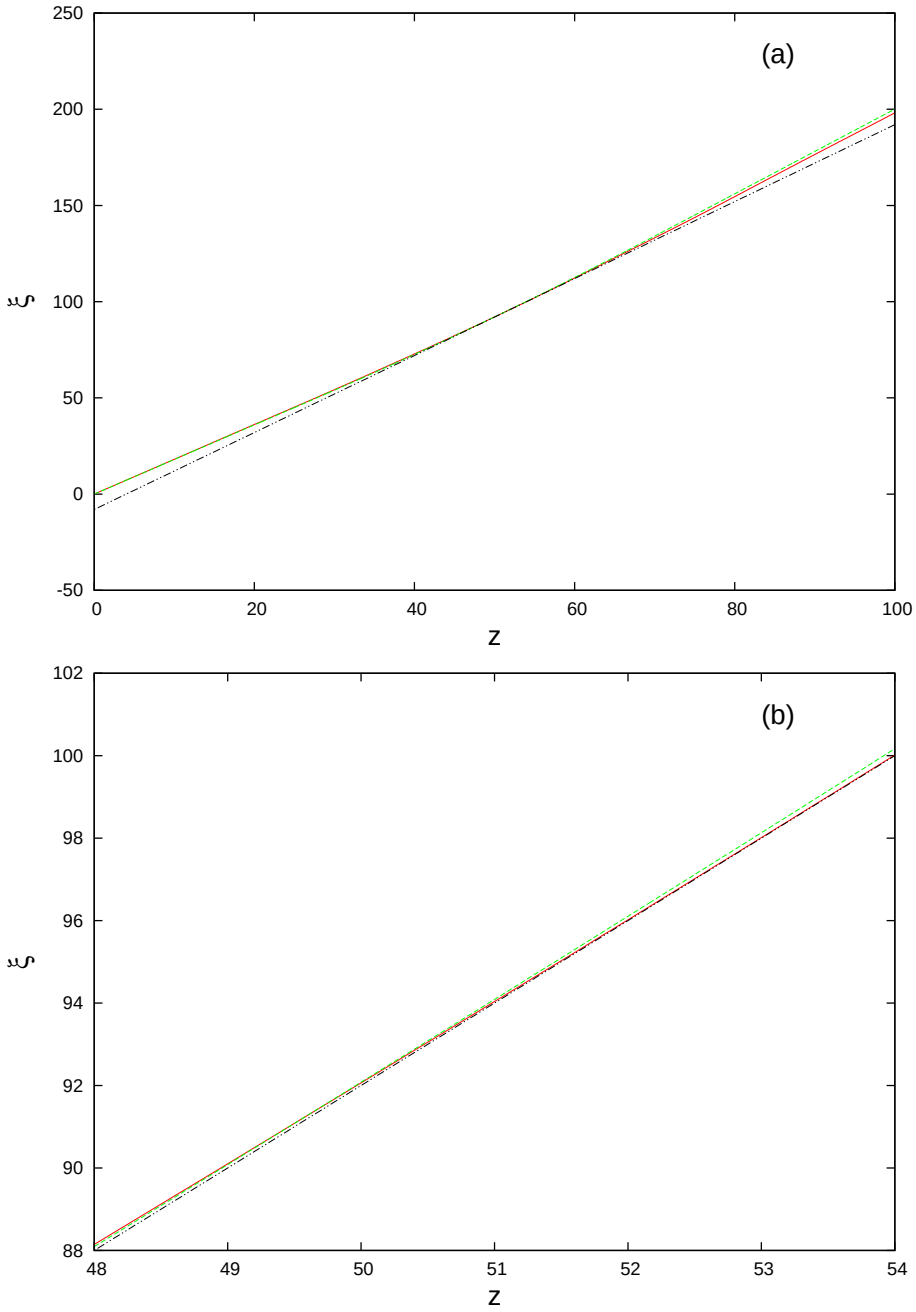

Figure 3.16: Total internal reflection at the interface. Comparisons for full numerical solution with the initial values $a = 5.0$, $w = 2.0$, $\xi = 0$, $V = 1.932$ and the parameter values $\nu = 200$, $\psi_{bl} = 0.8$, $\psi_{br} = 0.6$, $q_l = 1.3$, $q_r = 1.0$, $\mu_1 = 2$, $\mu_2 = -8$ and modulation solution with the initial values $a = 5.0$, $w = 2.0$, $\xi = 0$, $V = 1.92$ and the parameter values $\nu = 200$, $\psi_{bl} = 0.8$, $\psi_{br} = 0.6$, $q_l = 1.3$, $q_r = 1.0$, $\mu_1 = 2$, $\mu_2 = -8$. Full numerical solution: — (red, solid line); modulation solution: – – – (green, dashed line); interface: – · · – · · (black, dash dot dot line). (a) for z ranging from 0 to 100, (b) amplified curves for z ranging from 48 to 54.

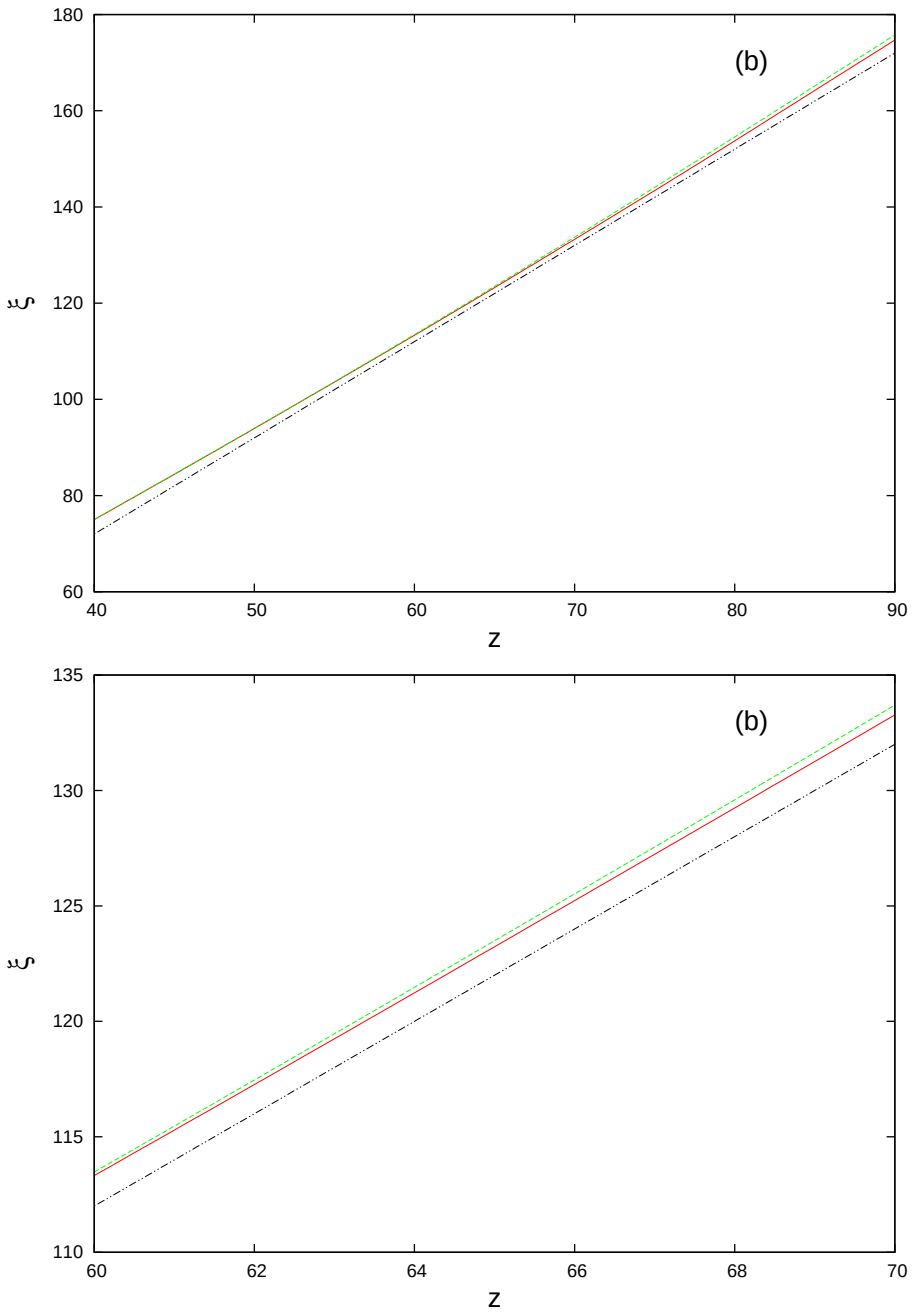

Figure 3.17: Total internal reflection with beam axis in more dense medium. Comparisons for the initial values $a = 5.0$, $w = 2.0$, $\xi = 0$, $V = 2.0$ with the parameter values $\nu = 200$, $\psi_{bl} = 0.8$, $\psi_{br} = 0.6$, $q_l = 1.3$, $q_r = 1.0$, $\mu_1 = 2$ and $\mu_2 = -8$. Full numerical solution: — (red, solid line); modulation solution: – – – (green, dashed line); interface: – ·· – ·· (black, dash dot dot line). (a) for z ranging from 40 to 90, (b) amplified curves for z ranging from 60 to 70.

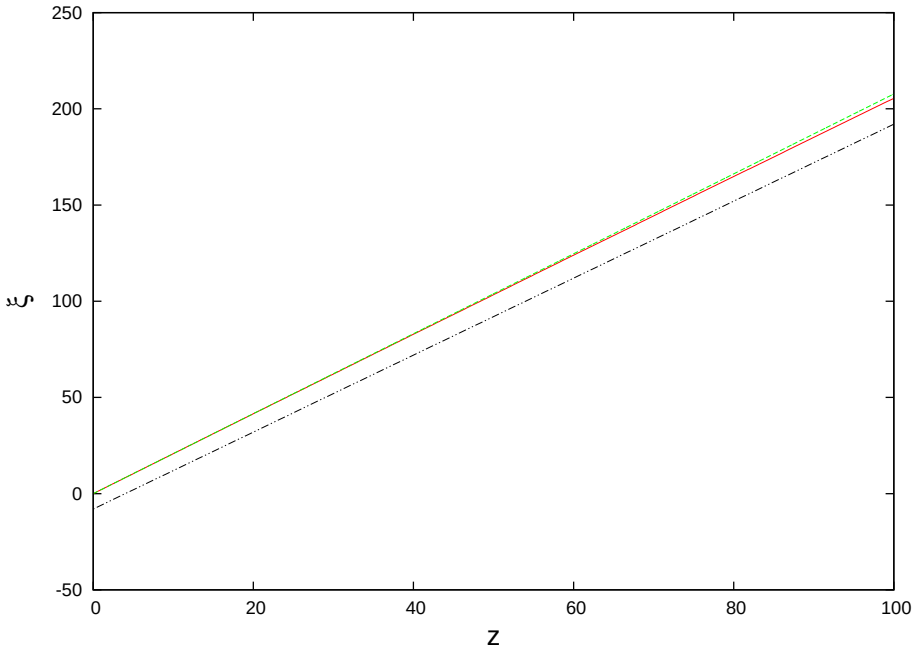

Figure 3.18: Unchanged beam path. Comparisons for the initial values $a = 5.0$, $w = 2.0$, $\xi = 0$, $V = 2.2$ with the parameter values $\nu = 200$, $\psi_{bl} = 0.8$, $\psi_{br} = 0.6$, $q_l = 1.3$, $q_r = 1.0$, $\mu_1 = 2$ and $\mu_2 = -8$. Full numerical solution: — (red, solid line); modulation solution: – – – (green, dashed line); interface: – ·· – ·· (black, dash dot dot line). (*The most parts of full numerical solution and modulation solution overlap to a high extent. Especially when printed in black and white, the superposition makes a solid line look like a dashed line.)

large Goos-Hänchen type shift [208] along the interface [203]. The agreement in the trajectories between the numerical and modulation solutions is again excellent for this non-specular reflection. The observed lateral shift can be of the order of mm thanks to the large nonlocality and the graded character of the interface [203]. Converting the theoretical solution shown in Figure 3.15 to dimensional units [101] gives a Goos-Hänchen shift of around $250\mu m$, compared with the experimental result of around $500\mu m$. The experimental Goos-Hänchen shift is more complicated than the simple theoretical modelling. The beam stays close to the interface for an extended distance. As the interface is graded with a width of $50\mu m$ [202, 203], not the sharp step of the theoretical modelling, close agreement between the experimental and theoretical shifts is not expected, with only order of magnitude agreement expected. Furthermore, the actual shift depends on the power of the beam and the voltage difference across the interface.

On increasing the angle of incidence, at a specific angle $V_0 - \Delta_l = 1.812$ for the full numerical solution and $V_0 - \Delta_l = 1.800$ for the modulation solution, Goos-Hänchen reflection stops and, as shown in Figure 3.16, the nematicon undergoes total internal reflection with its axis exactly tangential to the interface, the type 3 behaviour of Figure 3.14. On further increase of the angle of incidence, the nematicon undergoes total internal reflection with its peak remaining in the denser medium and not reaching the interface, the type 4 behaviour of Figure 3.14. This behaviour is illustrated in Figure 3.17. In this case, reflection occurs due to the nematicon tail, but not its peak, entering the less optically dense medium. The nematicon is an extended structure, so that its tail can then enter the less optically dense medium, feeling the change in refractive index, so resulting in reflection, which gets weaker as a smaller portion of the tail enters the less dense medium, as shown by the smaller angle of reflection after around

$V_0 - \Delta_l = 1.8$ seen in Figure 3.12. Eventually no change in the trajectory occurs for $V_0 - \Delta_l \geq 2.03$ as given by full numerical solution and $V_0 - \Delta_l \geq 2.020$ as given by modulation solution as there is insufficient overlap of the tail with the less optically dense medium to change the trajectory of the nematicon. The Type 5 behaviour of Figure 3.14 shows that the nematicon proceeds straight and its trajectory does not change if it does not approach the interface. This is illustrated in Figure 3.18. It should be added that the total internal reflection of the nematicon is non-specular due to the nonlinear response involved and to the anisotropy of the uniaxial medium with inherent walkoff, with the difference between the angles of incidence and reflection being up to about 2^o for the example considered here, comparable to the 4.5^o for experiments [202], indicating the nonlinear nature of the total internal reflection. The exact value of the difference depends on the operating parameters used, of course.

3.4 Discussion

The refraction of a nonlinear self-guided, nonlinear wave in a nematic liquid crystal, a nematicon, at the interface between two regions with different director orientations, and hence refractive indices, has been investigated using modulation theory and numerical solutions. In previous experimental studies, these two orientations of nematic molecules were produced by applying two different external voltages across the cell [196, 202, 203]. Our modulation theory was based on a Lagrangian formulation of the nematicon equations. The angle of refraction was changed by altering the angle of incidence of the beam on the interface for a fixed external voltage difference, in contrast to experiments in which the input beam angle was not varied. Despite this difference, the present theoretical investigation reproduces the broad features of the experimental ones [196, 202, 203]. Similar changes in the propagation angle of the nematicon were found, ranging between -5^o for refraction from a less to a more optically dense medium and $+10^o$ for total internal reflection from a more to a less optically dense medium. Excellent agreement was found between the full numerical solutions and the predictions of the modulation theory.

The most diverse range of refraction behaviour was found for a beam propagating into a less optically dense medium. In analogy with linear wave refraction, total internal reflection can occur and take a number of forms. The beam axis can enter the less dense medium, refract and re-enter the more dense medium, so-called Goos-Hänchen reflection [197, 198, 208], as found in previous experimental studies [196, 202, 203]. The beam can also reflect without its peak entering the less dense medium, the refraction resulting from its tail interacting with the less dense medium. The reflection of the nematicon was then found to be non-specular, in accord with experimental results [202]. Excellent agreement was found between the ranges for these different types of refraction behaviour as given by full numerical solutions and modulation theory.

This study of nematicon refraction fits in with a number of such studies which show the power and accuracy of modulation theory in giving simple, low dimensional models in excellent agreement with numerical and experimental results [101, 103, 111, 118].

Chapter 4

Vortex Refraction at an Interface in a Liquid Crystal

4.1 Background

The behaviour of optical vortices in nematic liquid crystals has received much less attention than nematicons. Similar to optical solitons, nematic liquid crystals can also support the stable propagation of another type of nonlinear optical beam, the optical vortex, a type of solitary wave with a ring-like structure whose phase increases by an integer multiple n of 2π, the integer n termed the charge of the vortex, as discussed in Chapter 1 [146]. In a local medium, an optical vortex is unstable due to a symmetry breaking azimuthal instability, as discussed in Chapter 1. For the single charge ($m = 1$) vortices to be considered here, the vortex is unstable to a mode 2 azimuthal instability ($L = 2$), so that the vortex pinches off at diagonally opposite points and splits into two solitary waves. However, in nonlocal media with sufficiently strong nonlocality, the nonlocal response can stabilise a single charge ($m = 1$) vortex, but not higher charge vortices ($m > 1$) (see Chapter 1). This instability and restabilisation in nonlocal media has been investigated not only numerically (see section 1.4) [146], but also analytically, as is briefly explained below [113].

The dimensionless equations for the field envelope $E(x, y, z)$ and the director deviation ϕ from its pretilted position can be written in the form [146, 147]

$$i\frac{\partial E}{\partial z} + \frac{1}{2}\nabla^2 E + \phi E = 0, \tag{4.1}$$

$$\nu\nabla^2\phi - \phi = -|E|^2, \tag{4.2}$$

where ∇^2 is the transverse Laplacian with z being the direction of light propagation. ν is the nonlocality parameter, the ratio of the elastic energy of the nematic liquid crystal to the energy of the applied static electric field [97]. Similar to the nematicons of Chapter 3, we use a trial function for the vortex soliton of the form

$$E(r, \theta, z) = are^{-r/w}e^{i\sigma+i\theta} + ig(r, \theta, z)e^{i\sigma+i\theta}, \tag{4.3}$$

where the first term is the vortex soliton and the second term represents low frequency diffractive radiation shed by the vortex as it evolves [146], as for the nematicons of Chapter 3. Let G

represent Green's function for the director equation (4.2), so that

$$G(r,\theta,r',\theta') = \sum_{l=-\infty}^{\infty} G_l(r,r')e^{il(\theta-\theta')}, \tag{4.4}$$

with

$$G_l(r,r') = \begin{cases} I_l(r/\sqrt{\nu})K_l(r'/\sqrt{\nu}), & 0 \le r < r', \\ K_l(r/\sqrt{\nu})I_l(r'/\sqrt{\nu}), & r' < r < \infty, \end{cases} \tag{4.5}$$

and I_l and K_l are modified Bessel functions of order l. The system of equations (4.1) and (4.2) can be reduced to a single equation after using the solution of the director equation (4.2) through this Green's function

$$\theta = \int_{-\infty}^{\infty}\int_{-\infty}^{\infty} G(x,y,x',y')|E(x',y')|^2\,dx'dy'. \tag{4.6}$$

Then the governing equations (4.1) and (4.2) have the Lagrangian

$$L = L_0 + L_\nu, \tag{4.7}$$

where L_0 is independent of the nonlinearity

$$L_0 = ir(E^*E_z - EE_z^*) - r|E_r|^2 - \frac{1}{r}|E_\theta|^2, \tag{4.8}$$

and

$$L_\nu = r|E|^2\int_0^{2\pi}\int_0^{\infty} G(r,\theta,r',\theta')|E(r',\theta')|^2 dr'd\theta'. \tag{4.9}$$

Modulation equations for the vortex parameters can be obtained by averaging the Lagrangian (4.7) and then taking variations with respect to the parameters a, w, σ, and g. The fixed point of the modulation equations corresponds to a stationary vortex. This stationary vortex can be found by setting $g = 0$, $a' = w' = 0$ and σ' a constant and then taking variations [113]. Analysing the system obtained by linearising around this fixed point, it is found that in the local limit $\nu \to 0$ the symmetry breaking unstable modes are $l = 1, 2, 3$, with the most unstable mode at $l = 2$. In the nonlocal limit ν large, a single-charge vortex becomes stable for $\nu \ge \nu_{cr} = 100.5$. These results are in very good agreement with the numerical data of Yakimenko *et al* [146], for which $\nu_{cr} = 90.7$. In a nematic liquid crystal the nonlocal response of the nematic stabilises the vortex due to the optical axis being non-zero in the neighbourhood of the phase singularity [113]. In the local limit of the nematic equations, the optical axis is 0 at the phase singularity, so that the vortex is unstable [113].

Experimentally, optical vortices have been generated in nematic liquid crystals, both singly [209, 210], as incoherently interacting pairs [211] and as arrays [212], in cholesteric liquid crystals [213] and also in colloidal media [159]. The equations governing nonlinear optical beam propagation in colloidal media are similar to those for beam propagation in a nematic liquid crystal [214, 215]. In this chapter the refraction of an optical vortex at a nonlinear refractive index interface in a nematic liquid crystal will be investigated using both modulation theory and numerical solutions. The refractive index interface is made by applying two independent external, biasing static electric fields to pre-tilt the nematic molecules at two different angles, as in the experiments of Peccianti *et al* [196] and as in Chapter 3. The experiments of Peccianti *et al* [196] involved the refraction of a nematicon, rather than an optical vortex, but the exper-

imental set-up is the same, except for the generation of the optical vortex beam. Although in the nematic liquid crystals the refraction of an optical soliton and an optical vortex have some similarities, it can be inferred that they should also have distinct differences due to the different stability properties of a nematicon and a vortex.

To this end, let us consider a planar cell containing a nematic liquid crystal with the boundary condition at the cell walls arranged so that the molecular director, or axis of the nematic molecules, lies in the (x, z) plane. To induce a refractive index change across the nematic, two independent, external biasing static electric fields are applied across its thickness [196]. The nematic director can then have two independent orientations measured from the direction z down the cell, resulting in two regions of different refractive index via the nonlinear dependence of the refractive index of the nematic on the director orientation [147, 204]. A coherent beam of light in the form of an optical vortex is then introduced into the cell and propagates down it. To define the coordinate system, let us take the direction of polarisation of the extraordinary light beam and the external electric fields to be in the x direction, which is across the cell thickness. As stated, the z direction is down the cell and the y direction completes the right handed coordinate system. This configuration is illustrated in Figure 3.1. In the paraxial approximation the nondimensional system of equations governing the evolution of the vortex is [78, 79, 204]

$$i\frac{\partial E}{\partial z} - i\Delta\frac{\partial E}{\partial y} + \frac{1}{2}\nabla^2 E + \sin(2\psi_b)\theta E = 0, \tag{4.10}$$

$$\nu\nabla^2\theta - 2q\theta = -\sin(2\psi_b)|E|^2, \tag{4.11}$$

as for the nematicon of Chapter 3. Here E is the complex valued envelope of the electric field of the optical beam and, as before, the Laplacian ∇^2 is taken with respect to the transverse coordinates x and y. The parameter ν measures the elastic response of the nematic and is large, $O(100)$, in the usual experimental regime [101], so that the response of the nematic is termed nonlocal as it extends far beyond the waist of the beam. The parameter q is proportional to the square of the external biasing electric field [78, 79]. The pre-tilt of the nematic due to the external biasing field is ψ_b. The total angle made by the director to the z direction is $\psi = \psi_b + \theta$. For the usual milliwatt beam power levels [205], the extra rotation caused by the beam is small, $|\theta| \ll |\psi_b|$. As shown in [127], the governing equations (4.10) and (4.11) are valid in this small extra deviation limit. Finally, δ is the walk-off angle between the Poynting vector and the wavevector of the extraordinary beam. In the small deviation limit $|\theta| \ll |\psi_b|$ [127]

$$\Delta = \tan\delta = \frac{\Delta n^2 \sin 2\psi_b}{\Delta n^2 + 2n_\perp^2 + \Delta n^2 \cos 2\psi_b}, \tag{4.12}$$

where $\Delta n^2 = n_\parallel^2 - n_\perp^2$ is the optical birefringence and $n_\parallel$ and $n_\perp$ are the refractive indices for fields parallel and perpendicular to the optic axis, respectively [204]. In the present work the typical values $n_\parallel = 1.6954$ and $n_\perp = 1.5038$ will be used, which are for the nematic E7 at room temperature in the near infrared at wavelength 1.064 μm [204, 216]. While the governing equations (4.10) and (4.11) have been introduced in the context of nonlinear beam propagation in nematic liquid crystals, they are more general and describe nonlinear wave propagation in a diverse range of media for which nonlinearity is coupled with some diffusive phenomena [197].

As stated above, the external biasing electric field takes two values across the cell. The same electric field geometry will be used as in the original experiments [196, 203] and as in

Chapter 3. Then, two different static fields are applied through thin film electrodes separated by a straight gap along the line $y = \mu_1 z + \mu_2$, so that the electric field and the resulting director distribution ψ_b have a jump discontinuity along this line. This approximation of a jump in the media properties is in accord with experiments as the electric field was found to vary smoothly between two constant values over a distance of the order of the gap between the electrodes, about $50\mu m$ [202, 203]. We then set the pre-tilt

$$\psi_b = \begin{cases} \psi_{br}, & y < \mu_1 z + \mu_2, \\ \psi_{bl}, & y > \mu_1 z + \mu_2 \end{cases} \tag{4.13}$$

and also q takes the two values

$$q = \begin{cases} q_r, & y < \mu_1 z + \mu_2, \\ q_l, & y > \mu_1 z + \mu_2. \end{cases} \tag{4.14}$$

4.2 Analysis

4.2.1 Modulation Equations

As in previous work [160, 163, 164] the electric field will be assumed to be a mode (or charge) one optical vortex of the form

$$E = are^{-r/w} e^{i\sigma + iV(y-\xi) + i\phi} + ige^{i\sigma + iV(y-\xi) + i\phi}, \tag{4.15}$$

where $r^2 = x^2 + (y-\xi)^2$ and ϕ is the polar angle relative to the centre of the vortex $(0, \xi)$. The first term in this trial function is an optical vortex of amplitude $A = awe^{-1}$ and width w. Here $A = awe^{-1}$ is the maximum of the function $f_v(r) = are^{-r/w}$, in contrast to the nematicon of Section 3.2.1 of the last Chapter for which the soliton's amplitude is $A = a$, which is the maximum of the function $f_s(r) = a\,\mathrm{sech}(r/w)$. The second term represents the low wavenumber radiation which accumulates under the vortex as it evolves [104, 160]. Linearising the electric field equation (4.10) shows that low wavenumber radiation has low group velocity $C(\kappa) = \kappa$, where κ is the wavenumber [96], so that low wavenumber radiation accumulates under the vortex. Furthermore, this radiation is $\pi/2$ out of phase with the vortex as the in-phase component corresponds to changes in the vortex amplitude and width [96]. Symmetry gives that the shelf as radially symmetric in space, centred about the vortex peak at $r = w$. That is to say, the low wavenumber radiation forms a shelf of length w under the peak of the vortex, so that g is non-zero in $w/2 \leq r \leq 3w/2$ [160]. The radiation shelf then matches to propagating diffractive radiation, the shedding of which allows the vortex to evolve to a steady state. This shed radiation has a significant effect on the vortex only for large z scales for the nonlocal limit with ν large [104]. As such large propagation distances will not be considered here, the form of this propagating diffractive radiation will not be considered further.

In principle, the refraction of an optical vortex can be analysed as for the nematicon. However, the director response to the vortex is more complicated than that for the nematicon due to the nonlocal response causing the optic axis distortion to be non-zero in the vortex core [160, 163, 164], so that a suitable trial function for the director response is not clear. This non-zero perturbed director core, in fact, is the mechanism able to stabilise the vortex [160]. Rather than assuming a trial function for θ, a solution of the director equation (4.11) will be

found.

The electric field equation (4.10) with its director equation (4.11) has the Lagrangian

$$L = L_0 + L_\nu, \tag{4.16}$$

where

$$L_0 = i\left(E^* E_z - E E_z^*\right) - i\Delta\left(E^* E_y - E E_y^*\right) - |\nabla E|^2, \tag{4.17}$$

is independent of the nonlinearity, and has average $\mathcal{L}_0$, while

$$L_\nu = \sin(2\psi_b)|E|^2\theta, \tag{4.18}$$

with average $\mathcal{L}_\nu$, depends on the specific form of the nonlocal nonlinearity.

To calculate L_ν, θ has firstly to be solved from the director equation (4.11) because, as explained above, vortices are more complicated than solitons, so that there is no obvious trial function for θ. Equation (4.11) is expressed in polar coordinates, as the vortex is radially symmetric. For the large nonlocality used in the present work, the response of the director to the optical beam extends far beyond the beam, so that the beam can be approximated at the peak $r = w$ of the vortex relative to the director response [160, 164]. By assuming vortex is wide, i.e. w is big, the term $\frac{1}{r}\frac{\partial\theta}{\partial r}$ in (4.11) can be neglected. The radiation g^2 is much smaller than $\sin(2\psi_b)a^2r^2e^{-\frac{2r}{w}}$, so that it can also be ignored. Then, the director equation (4.11) can be approximated as

$$\nu\frac{d^2\theta}{dr^2} - 2q\theta = -\sin(2\psi_b)a^2r^2e^{-\frac{2r}{w}}. \tag{4.19}$$

Although the ODE (4.19) can be solved exactly, the complicated solution form results in an involved calculation of the averaged Lagrangian in the next step. To obtain a simple averaged Lagrangian, as approximation will be used which is valid in the nonlocal limit with ν large.

The system of equations (4.10) and (4.11) can be reduced to a single equation after using the solution of the director equation (4.11) through a Green's function G,

$$\theta = -\sin(2\psi_b)\int_{-\infty}^{\infty}\int_{-\infty}^{\infty} G(x,y,x',y')|E(x',y')|^2\,dx'dy', \tag{4.20}$$

where G is expressed in terms of the modified Bessel function K_0, as in equation (4.4) and equation (4.5), for a radially symmetric solution [160]. However, the Green's function kernel involves modified Bessel functions, so this solution, as it stands, is difficult to use in calculating an averaged Lagrangian from (4.20). To overcome this difficulty the nonlocal nature of the director response will be used to calculate an asymptotic solution for θ.

For the large nonlocality ν used in the present work, the response of the director to the optical beam extends far beyond the beam, so that the beam can be approximated as a delta function at the peak $r = w$ of the vortex, relative to the director response [160, 164]. An additional consequence of the nonlocal response of the nematic is that the director distribution is slowly varying, so that within the core of the vortex, $r \leq w$, θ can be taken to be constant as the first term in a Taylor series in $r/\sqrt{\nu}$. This can be seen from the solution of the director equation (4.11) as the argument of the Bessel function solution is $r\sqrt{2q}/\sqrt{\nu}$. The final approximation needed to obtain an asymptotic solution of the director equation which can be used to exactly calculate the integrals involved in the averaged Lagrangian is that the vortices used in the

present work are wide enough to be stable [160]. In this case, the derivative θ_r/r in the director equation (4.11) can be neglected, leading to (4.19). With these approximations, the solution of the director equation (4.19) is

$$\theta = \begin{cases} A, & r < w \\ Ae^{-\sqrt{2q/\nu}(r-w)}, & r \geq w \end{cases}, \tag{4.21}$$

for ν large, where

$$A = \frac{a^2 w^3 \sin(2\psi_b)}{4\sqrt{2q\nu}}.$$

The straight boundary delineating the two refractive index regions is $y = \mu_1 z + \mu_2$. Then, to evaluate the averaged Lagrangian term involving θ, the integral

$$\int_{-\infty}^{\infty}\int_{\mu_1 z+\mu_2}^{\infty} \sin(2\psi_b) r^2 e^{\frac{-2r}{w}} \theta \, dxdy \tag{4.22}$$

needs to be calculated. Although in the calculation $e^{-2r/w}e^{-r\sqrt{2q/\nu}}$ can be replaced by an equivalent Gaussian as for the nematicon of Chapter 3, this integral still cannot be evaluated due to the form (4.21) for θ.

Let us for the moment ignore the constant section of the director (4.21) for $r < w$ and extend the solution for $r > w$ into $r < w$. We shall also take the medium to be uniform, so that $z \to -\infty$ in (4.22). The integral we are interested in in the averaged Lagrangian is

$$I = \int_0^{\infty} \theta |E|^2 \, r dr. \tag{4.23}$$

Now extending the form of θ for $r > w$ into $r < w$ and then expanding for ν large gives

$$\begin{aligned} I_e &= \int_0^{\infty} \theta |E|^2 \, r dr \\ &= \int_0^{\infty} A e^{-\sqrt{\frac{2q}{\nu}}(r-w)} \cdot a^2 r^2 e^{-\frac{2r}{w}} \cdot r dr \\ &= 6Aa^2 e^{\sqrt{\frac{2q}{\nu}}w} (\sqrt{\frac{2q}{\nu}} + \frac{2}{w})^{-4} \\ &= 6Aa^2 e^{\sqrt{\frac{2q}{\nu}}w} (\frac{w}{4})^4 (1 + \frac{w}{2}\sqrt{\frac{2q}{\nu}})^{-4} \\ &= 6Aa^2 (1 + \sqrt{\frac{2q}{\nu}}w + \dots)(\frac{w}{4})^4 [1 + (-4)\frac{w}{2}\sqrt{\frac{2q}{\nu}} + \dots] \\ &\approx 6Aa^2 (\frac{w}{4})^4 (1 - w\sqrt{\frac{2q}{\nu}}). \end{aligned} \tag{4.24}$$

Evaluating the integral using the full solution for θ (4.21) and then expanding for ν large gives

$$
\begin{aligned}
I_f &= \int_0^w A \cdot a^2 r^2 e^{-\frac{2r}{w}} \cdot r dr + \int_w^\infty A e^{-\sqrt{\frac{2q}{\nu}}(r-w)} \cdot a^2 r^2 e^{-\frac{2r}{w}} \cdot r dr \\
&= Aa^2(-\frac{19}{8}w^4 e^{-2} + \frac{3}{8}w^4) + Aa^2[\frac{1}{2}w^4 e^{-2}(1 + \frac{w}{2}\sqrt{\frac{2q}{\nu}})^{-1} + \frac{3}{4}w^4 e^{-2}(1 + \frac{w}{2}\sqrt{\frac{2q}{\nu}})^{-2} \\
&\times \frac{3}{4}w^4 e^{-2}(1 + \frac{w}{2}\sqrt{\frac{2q}{\nu}})^{-3} + \frac{3}{8}w^4 e^{-2}(1 + \frac{w}{2}\sqrt{\frac{2q}{\nu}})^{-4}] \\
&= Aa^2(-\frac{19}{8}w^4 e^{-2} + \frac{3}{8}w^4) + Aa^2[\frac{1}{2}w^4 e^{-2}(1 - \frac{1}{2}w\sqrt{\frac{2q}{\nu}} + \cdots) + \frac{3}{4}w^4 e^{-2}(1 - w\sqrt{\frac{2q}{\nu}} + \cdots) \\
&\times \frac{3}{4}w^4 e^{-2}(1 - \frac{3}{2}w\sqrt{\frac{2q}{\nu}} + \cdots) + \frac{3}{8}w^4 e^{-2}(1 - 2w\sqrt{\frac{2q}{\nu}} + \cdots)] \\
&\approx Aa^2(-\frac{19}{8}w^4 e^{-2} + \frac{3}{8}w^4) + Aa^2[\frac{1}{2}w^4 e^{-2}(1 - \frac{1}{2}w\sqrt{\frac{2q}{\nu}}) + \frac{3}{4}w^4 e^{-2}(1 - w\sqrt{\frac{2q}{\nu}}) \\
&\times \frac{3}{4}w^4 e^{-2}(1 - \frac{3}{2}w\sqrt{\frac{2q}{\nu}}) + \frac{3}{8}w^4 e^{-2}(1 - 2w\sqrt{\frac{2q}{\nu}})] \\
&= 6Aa^2(\frac{w}{2})^4(1 - \frac{23}{3}e^{-2}w\sqrt{\frac{2q}{\nu}}).
\end{aligned} \tag{4.25}
$$

Comparing expressions (4.24) with (4.25), we see that (4.25) can be approximated by (4.24) as $(23/3)e^{-2} = 1.0376\cdots \approx 1.0$. So to a good approximation the solution for θ in $r > w$ can be extended to $r < w$. This result is valid in the nonlocal limit ν large, with the errors in (4.24) and (4.25) being $O(\nu^{-1})$. Without this approximation, the integrals cannot be evaluated due to the change in $\sin(2\psi_b)$ across $y = \mu_1 z + \mu_2$.

Using this approximation, the averaged Lagrangian $\mathcal{L}_\nu$ can be calculated. All the resulting integrals in $\mathcal{L}_0$ can be simply evaluated, except for the piecewise integration

$$
\begin{aligned}
&\int_{-\infty}^{+\infty}\int_{-\infty}^{+\infty} \Delta[x^2 + (y-\xi)^2] e^{-\frac{2}{w}\sqrt{x^2+(y-\xi)^2}}\, dxdy \\
&= \Delta_r \int_{-\infty}^{+\infty}\int_{-\infty}^{\mu_1 z+\mu_2} [x^2 + (y-\xi)^2] e^{-\frac{2}{w}\sqrt{x^2+(y-\xi)^2}}\, dydx \\
&+ \Delta_l \int_{-\infty}^{+\infty}\int_{\mu_1 z+\mu_2}^{+\infty} [x^2 + (y-\xi)^2] e^{-\frac{2}{w}\sqrt{x^2+(y-\xi)^2}}\, dydx.
\end{aligned}
$$

These two integrals cannot be evaluated exactly. So the equivalent Gaussian approximation of Chapter 2 and 3 is again used. The function $[x^2 + (y-\xi)^2] e^{-\frac{2}{w}\sqrt{x^2+(y-\xi)^2}}$ is then replaced by

the Gaussian $[x^2+(y-\xi)^2]e^{-\frac{1}{A_1 w}[x^2+(y-\xi)^2]}$, so that the piecewise integration becomes

$$
\begin{aligned}
&\Delta_r \int_{-\infty}^{+\infty}\int_{-\infty}^{\mu_1 z+\mu_2}[x^2+(y-\xi)^2]e^{-\frac{1}{A_1^2 w^2}[x^2+(y-\xi)^2]}\,dydx\\
&+\Delta_l \int_{-\infty}^{+\infty}\int_{\mu_1 z+\mu_2}^{+\infty}[x^2+(y-\xi)^2]e^{-\frac{1}{A_1^2 w^2}[x^2+(y-\xi)^2]}\,dydx\\
&=\Delta_r \int_{-\infty}^{+\infty} e^{-\frac{1}{A_1^2 w^2}x^2}\,dx\int_{-\infty}^{\mu_1 z+\mu_2}(y-\xi)^2 e^{-\frac{1}{A_1^2 w^2}(y-\xi)^2}\,dy\\
&+\Delta_r \int_{-\infty}^{+\infty} x^2 e^{-\frac{1}{A_1^2 w^2}x^2}\,dx\int_{-\infty}^{\mu_1 z+\mu_2} e^{-\frac{1}{A_1^2 w^2}(y-\xi)^2}\,dy\\
&+\Delta_l \int_{-\infty}^{+\infty} e^{-\frac{1}{A_1^2 w^2}x^2}\,dx\int_{\mu_1 z+\mu_2}^{+\infty}(y-\xi)^2 e^{-\frac{1}{A_1^2 w^2}(y-\xi)^2}\,dy\\
&+\Delta_l \int_{-\infty}^{+\infty} x^2 e^{-\frac{1}{A_1^2 w^2}x^2}\,dx\int_{\mu_1 z+\mu_2}^{+\infty} e^{-\frac{1}{A_1^2 w^2}(y-\xi)^2}\,dy\\
&=\Delta_r\cdot A_1 w\sqrt{\pi}\cdot[\frac{A_1^3 w^3\sqrt{\pi}}{4}(\mathrm{erf}(\frac{\mu_1 z+\mu_2-\xi}{A_1 w})+1)-\frac{A_1^2 w^2}{2}(\mu_1 z+\mu_2-\xi)e^{-\frac{(\mu_1 z+\mu_2-\xi)^2}{A_1^2 w^2}}]\\
&+\Delta_r\cdot\frac{A_1^3 w^3\sqrt{\pi}}{2}\cdot\frac{A_1 w\sqrt{\pi}}{2}[\mathrm{erf}(\frac{\mu_1 z+\mu_2-\xi}{A_1 w})+1]\\
&+\Delta_l\cdot A_1 w\sqrt{\pi}\cdot[\frac{A_1^3 w^3\sqrt{\pi}}{4}(1-\mathrm{erf}(\frac{\mu_1 z+\mu_2-\xi}{A_1 w}))+\frac{A_1^2 w^2}{2}(\mu_1 z+\mu_2-\xi)e^{-\frac{(\mu_1 z+\mu_2-\xi)^2}{A_1^2 w^2}}]\\
&+\Delta_l\cdot\frac{A_1^3 w^3\sqrt{\pi}}{2}\cdot\frac{A_1 w\sqrt{\pi}}{2}[1-\mathrm{erf}(\frac{\mu_1 z+\mu_2-\xi}{A_1 w})]\\
&=\Delta_r\frac{\pi A_1^4 w^4}{2}\,\mathrm{erfc}(-\frac{\mu_1 z+\mu_2-\xi}{A_1 w})-\Delta_r\frac{A_1^3 w^3\sqrt{\pi}}{2}(\mu_1 z+\mu_2-\xi)e^{-\frac{(\mu_1 z+\mu_2-\xi)^2}{A_1^2 w^2}}\\
&+\Delta_l\frac{\pi A_1^4 w^4}{2}\,\mathrm{erfc}(\frac{\mu_1 z+\mu_2-\xi}{A_1 w})+\Delta_l\frac{A_1^3 w^3\sqrt{\pi}}{2}(\mu_1 z+\mu_2-\xi)e^{-\frac{(\mu_1 z+\mu_2-\xi)^2}{A_1^2 w^2}}
\end{aligned}
$$

The constants A, B and D are as in Section 2.1.2 and 3.2.1. Only the constant A_1 needs to be determined. For a uniform medium, the integral is

$$
\begin{aligned}
&\int_{-\infty}^{+\infty}\int_{-\infty}^{+\infty}[x^2+(y-\xi)^2]e^{-\frac{2}{w}\sqrt{x^2+(y-\xi)^2}}\,dxdy\\
&=\int_0^{2\pi}\int_0^{\infty} r^2 e^{-\frac{2}{w}r}r\,dr\,d\theta\\
&=\frac{12\pi}{(\frac{2}{w})^4}.
\end{aligned}
\tag{4.26}
$$

The integral for the equivalent Gaussian is

$$
\begin{aligned}
&\int_{-\infty}^{+\infty}\int_{-\infty}^{+\infty}[x^2+(y-\xi)^2]e^{-\frac{1}{A_1^2}[x^2+(y-\xi)^2]}\,dxdy\\
&=\int_{-\infty}^{+\infty} e^{-\frac{1}{A_1^2}x^2}\,dx\int_{-\infty}^{+\infty}(y-\xi)^2 e^{-\frac{1}{A_1^2}(y-\xi)^2}\,dy\\
&+\int_{-\infty}^{+\infty} x^2 e^{-\frac{1}{A_1^2}x^2}\,dx\int_{-\infty}^{+\infty} e^{-\frac{1}{A_1^2}(y-\xi)^2}\,dy\\
&=\pi A_1^4 w^4
\end{aligned}
\tag{4.27}
$$

Equating these integrals gives

$$A_1=(\frac{3}{4})^{\frac{1}{4}}.$$

The other piecewise integral term in $\mathcal{L}_\nu$, which is

$$\int_{-\infty}^{+\infty}\int_{-\infty}^{+\infty}\Delta[x^2+(y-\xi)^2]e^{-(\frac{2}{w}+\sqrt{\frac{2q}{\nu}})\sqrt{x^2+(y-\xi)^2}}\,dxdy$$
$$=\Delta_r\int_{-\infty}^{+\infty}\int_{-\infty}^{\mu_1 z+\mu_2}[x^2+(y-\xi)^2]e^{-(\frac{2}{w}+\sqrt{\frac{2q}{\nu}})\sqrt{x^2+(y-\xi)^2}}\,dydx \tag{4.28}$$
$$+\Delta_l\int_{-\infty}^{+\infty}\int_{\mu_1 z+\mu_2}^{+\infty}[x^2+(y-\xi)^2]e^{-(\frac{2}{w}+\sqrt{\frac{2q}{\nu}})\sqrt{x^2+(y-\xi)^2}}\,dydx \tag{4.29}$$

can also be evaluated by replacing the function $[x^2+(y-\xi)^2]e^{-(\frac{2}{w}+\sqrt{\frac{2q}{\nu}})\sqrt{x^2+(y-\xi)^2}}$ by the equivalent Gaussian $[x^2+(y-\xi)^2]e^{-A_2^2(\frac{2}{w}+\sqrt{\frac{2q}{\nu}})^2[x^2+(y-\xi)^2]}$. Repeating the same process gives $A_2=12^{-\frac{1}{4}}$.

Finally, the whole averaged Lagrangian from (4.7) [1] is

$$\mathcal{L}=-4\left(\frac{3}{8}a^2w^4+\Lambda_1 g^2\right)\left(\sigma'-V\xi'+\frac{1}{2}V^2\right)-8aw^3g'+8w^3ga'+24aw^2gw'-\frac{3}{4}a^2w^2$$
$$-2\Lambda_2 g^2+A_1^4Va^2w^4\left[\Delta_l\,\mathrm{erfc}(\lambda_1)+\Delta_r\,\mathrm{erfc}(-\lambda_1)+\frac{\lambda_1}{\sqrt{\pi}}(\Delta_l-\Delta_r)e^{-\lambda_1^2}\right] \tag{4.30}$$
$$+\sin^2(2\psi_{bl})\frac{3a^4w^3e^{\beta_l w}}{2\sqrt{2q_l\nu}}\left(\beta_l+\frac{2}{w}\right)^{-4}\times\left[\mathrm{erfc}(\lambda_l)+\frac{\lambda_l}{\sqrt{\pi}}e^{-\lambda_l^2}\right]$$
$$+\sin^2(2\psi_{br})\frac{3a^4w^3e^{\beta_r w}}{2\sqrt{2q_r\nu}}\left(\beta_r+\frac{2}{w}\right)^{-4}\times\left[\mathrm{erfc}(-\lambda_r)-\frac{\lambda_r}{\sqrt{\pi}}e^{-\lambda_r^2}\right].$$

Taking variations of this averaged Lagrangian with respect to the vortex parameters yields the variational, or modulation equations, for the evolution of the vortex

$$\frac{d}{dz}\left[\frac{3}{8}a^2w^4+\Lambda_1 g^2\right]=0, \tag{4.31}$$
$$4\frac{d}{dz}\left(aw^3\right)=2\Lambda_1 g\left[\sigma'-V\xi'+\frac{1}{2}V^2\right]+\Lambda_2 g, \tag{4.32}$$
$$\frac{d\xi}{dz}=V-\frac{1}{2}\left[\Delta_l\,\mathrm{erfc}(\lambda_1)+\Delta_r\,\mathrm{erfc}(-\lambda_1)\;+\frac{\lambda_1}{\sqrt{\pi}}\left(\Delta_l-\Delta_r\right)e^{-\lambda_1^2}\right], \tag{4.33}$$
$$4\frac{d}{dz}\left[\frac{3}{8}a^2w^4+\Lambda_1 g^2\right]V=\frac{A_1^3}{\sqrt{\pi}}a^2w^3V\left(\Delta_l-\Delta_r\right)\left(1+2\lambda_1^2\right)e^{-\lambda_1^2}$$
$$-\sin(2\psi_{bl})\frac{a^4w^3e^{\beta_l w-\lambda_l^2}}{4A_2^3\sqrt{2\pi q_l\nu}}\left(\beta_l+\frac{2}{w}\right)^{-3}\times\left(\frac{1}{2}+\lambda_l^2\right)$$
$$+\sin(2\psi_{br})\frac{a^4w^3e^{\beta_r w-\lambda_r^2}}{4A_2^3\sqrt{2\pi q_r\nu}}\left(\beta_r+\frac{2}{w}\right)^{-3}\times\left(\frac{1}{2}+\lambda_r^2\right), \tag{4.34}$$

$$\frac{dg}{dz} = \frac{3}{32}\frac{a}{w} + \frac{3Vaw}{64\sqrt{\pi}}\left(\Delta_l - \Delta_r\right)\lambda_1(1+2\lambda_1^2)\,e^{-\lambda_1^2}$$
$$+\sin(2\psi_{bl})\frac{3a^3e^{\beta_l w}}{32w\sqrt{2q_l\nu}}\left(\beta_l+\frac{2}{w}\right)^{-5}\times$$
$$\left[\frac{1}{\sqrt{\pi}}\left(\beta_l^2w^2-3\beta_l w+4\lambda_l^2\right)\lambda_l e^{-\lambda_l^2}\;-\left(2+3\beta_l w-\beta_l^2w^2\right)\mathrm{erfc}(\lambda_l)\right]$$
$$-\sin(2\psi_{br})\frac{3a^3e^{\beta_r w}}{32w\sqrt{2q_r\nu}}\left(\beta_r+\frac{2}{w}\right)^{-5}\times$$
$$\left[\frac{1}{\sqrt{\pi}}\left(\beta_r^2w^2-3\beta_r w+4\lambda_r^2\right)\lambda_r e^{-\lambda_r^2}+\left(2+3\beta_r w-\beta_r^2w^2\right)\mathrm{erfc}(-\lambda_r)\right], \qquad (4.35)$$

$$\frac{d\sigma}{dz} - V\frac{d\xi}{dz} + \frac{1}{2}V^2 = -w^{-2}$$
$$+\frac{1}{4}V\left[2\Delta_l\,\mathrm{erfc}(\lambda_1)+2\Delta_r\,\mathrm{erfc}(-\lambda_1)\;+\frac{1}{\sqrt{\pi}}\left(\Delta_l-\Delta_r\right)\left(1-2\lambda_1^2\right)\lambda_1 e^{-\lambda_1^2}\right]$$
$$+\sin(2\psi_{bl})\frac{a^2e^{\beta_l w}}{2w^2\sqrt{2q_l\nu}}\left(\beta_l+\frac{2}{w}\right)^{-5}\times$$
$$\left[\frac{1}{\sqrt{\pi}}\left(8+7\beta_l w-\beta_l^2w^2-4\lambda_l^2\right)\lambda_l e^{-\lambda_l^2}\;+\left(10+7\beta_l w-\beta_l^2w^2\right)\mathrm{erfc}(\lambda_l)\right]$$
$$-\sin(2\psi_{br})\frac{a^2e^{\beta_r w}}{2w^2\sqrt{2q_r\nu}}\left(\beta_r+\frac{2}{w}\right)^{-5}\times$$
$$\left[\frac{1}{\sqrt{\pi}}\left(8+7\beta_r w-\beta_r^2w^2-4\lambda_r^2\right)\lambda_r e^{-\lambda_r^2}\;-\left(10+7\beta_r w-\beta_r^2w^2\right)\mathrm{erfc}(-\lambda_r)\right]. \qquad (4.36)$$

Here

$$\Lambda_1 = w^2, \quad \Lambda_2 = \ln 3, \quad \beta_l = \sqrt{\frac{2q_l}{\nu}}, \quad \beta_r = \sqrt{\frac{2q_r}{\nu}},$$
$$\lambda_1 = \frac{\mu_1 z+\mu_2-\xi}{A_1 w}, \lambda_l = A_2\left(\beta_l+\frac{2}{w}\right)\left(\mu_1 z+\mu_2-\xi\right), \lambda_r = A_2\left(\beta_r+\frac{2}{w}\right)\left(\mu_1 z+\mu_2-\xi\right),$$
$$A_1 = \left(\frac{3}{4}\right)^{1/4}, \quad A_2 = 12^{-1/4}. \qquad (4.37)$$

The modulation equation (4.31) is the equation for conservation of optical power and (4.34) is that for conservation of y momentum [199]. As the vortex evolves it will shed diffractive radiation [104]. However, as for the refraction of a nematicon, this shed radiation is not significant over the z distances considered here.

4.2.2 Adjustments to Numerical Code

The governing equation (4.10) was solved using a pseudo-spectral method, as explained in Chapter 2. The director equation (4.11) was solved as a two-point boundary value problem using Picard iteration in Fourier space, again as explained in Chapter 2. These methods are described in more detail in Section 2.2.2 where they were applied to a $(2+1)$-D single nematicon problem. The modulation equations are solved in an identical manner to that described in Section 2.2.1. It is noted that the discontinuities in ψ_b and q across $x = \mu_1 z + \mu_2$ were smoothed using tanh to link the two levels, as for the refraction of a nematicon in Chapter 3. If this smoothing were not used, nonphysical oscillations in the vortex position and possible vortex break-up can occur.

4.3 Results

In this section, the results from the developed modulation theory will be compared with full numerical solutions of the nematicon equations governing the vortex. In accord with the previous Section 3.3, in the following analysis numerical solutions of the full governing equations (4.10) and (4.11) are referred to as "full numerical solutions" and numerical solutions of the modulation equations (4.31)-(4.36) are termed "modulation solutions." Specifically, the numerical y position of the vortex is calculated as its centre of mass position

$$\xi = \frac{\int_{-\infty}^{\infty}\int_{-\infty}^{\infty} y|E|^2\,dxdy}{\int_{-\infty}^{\infty}\int_{-\infty}^{\infty} |E|^2\,dxdy}. \tag{4.38}$$

As shown in Figure 3.3, the angle of incidence will still be measured by $V - \Delta_l$.

Let us first consider an optical vortex which travels from a less to a more optically dense medium. As an example, Figure 4.1 shows two examples of comparisons of the positions as given by the full numerical and modulation solutions, for the different initial values $V_0 = 0.5$ in Figure 4.1(a) and $V_0 = 1.0$ in Figure 4.1(b), respectively. Similar to the nematicon of the last chapter, the position comparison is excellent. Also, both the full numerical solution and the modulation solution show clear refraction in Figure 4.1.

The angle of refraction versus the angle of incidence as given by the full numerical and modulation solutions is shown in Figure 4.2. This figure shows comparisons between the final propagation constant after the vortex is well past the interface as a function of the initial propagation constant, as given by the full numerical and modulation solutions. The same as for nematicon, the refracted angles and the input angles are all measured by their tangents from their z axis using formula (3.26). As in Chapter 3, V_0 refers to the input value of V and V_f refers to the steady value after passing the interface. Excellent agreement can be seen. To further analyse the comparison, Figure 4.3 shows the absolute error e and percentage errors e_p between the full numerical solution and the modulation solution. It can be seen that there is excellent agreement between the numerical and modulation solutions, with the percentage error generally being less than 5%. It is noted that the percentage error e_p becomes large above $V_0 - \Delta_l = 0$ to $V_0 - \Delta_l = 0.1$ as the angle of refraction $V_f - \Delta_r$ is close to 0 and thus these errors are being calculated with a small divisor. In Figure 4.2 there is no abrupt change in the comparison between the full numerical solution and the modulation solution in the region above $V_0 - \Delta_l = 0$ to $V_0 - \Delta_l = 0.1$. Also, as seen in Figure 4.3(a), there is no abrupt change in the absolute error e. The change in the angle of propagation across the interface is $O(5^o)$, which is the same order as for the refraction of a nematicon, as discussed in the last Chapter [127, 196]. The change in the angle of propagation depends on the jump in the values of ψ and q as these parameters depend on the size of the two pre-tilting electric fields [101, 127]. Basically, it can be seen that these results for the refraction of a vortex to a more optically dense medium are quite similar to those for the refraction of a nematicon (solitary wave) [127].

Let us now consider the refraction of a vortex from a more to a less optically dense medium. Similar to the less-to-more case, two examples of position comparisons between the full numerical solution and the modulation solution are shown in Figure 4.4. For the same reasons as the previous cases (Figure 4.1), the position comparison is excellent. Figure 4.4 clearly shows the refraction of the vortex at the interface.

As discussed in the last chapter, the refraction of a nematicon displays a complicated range

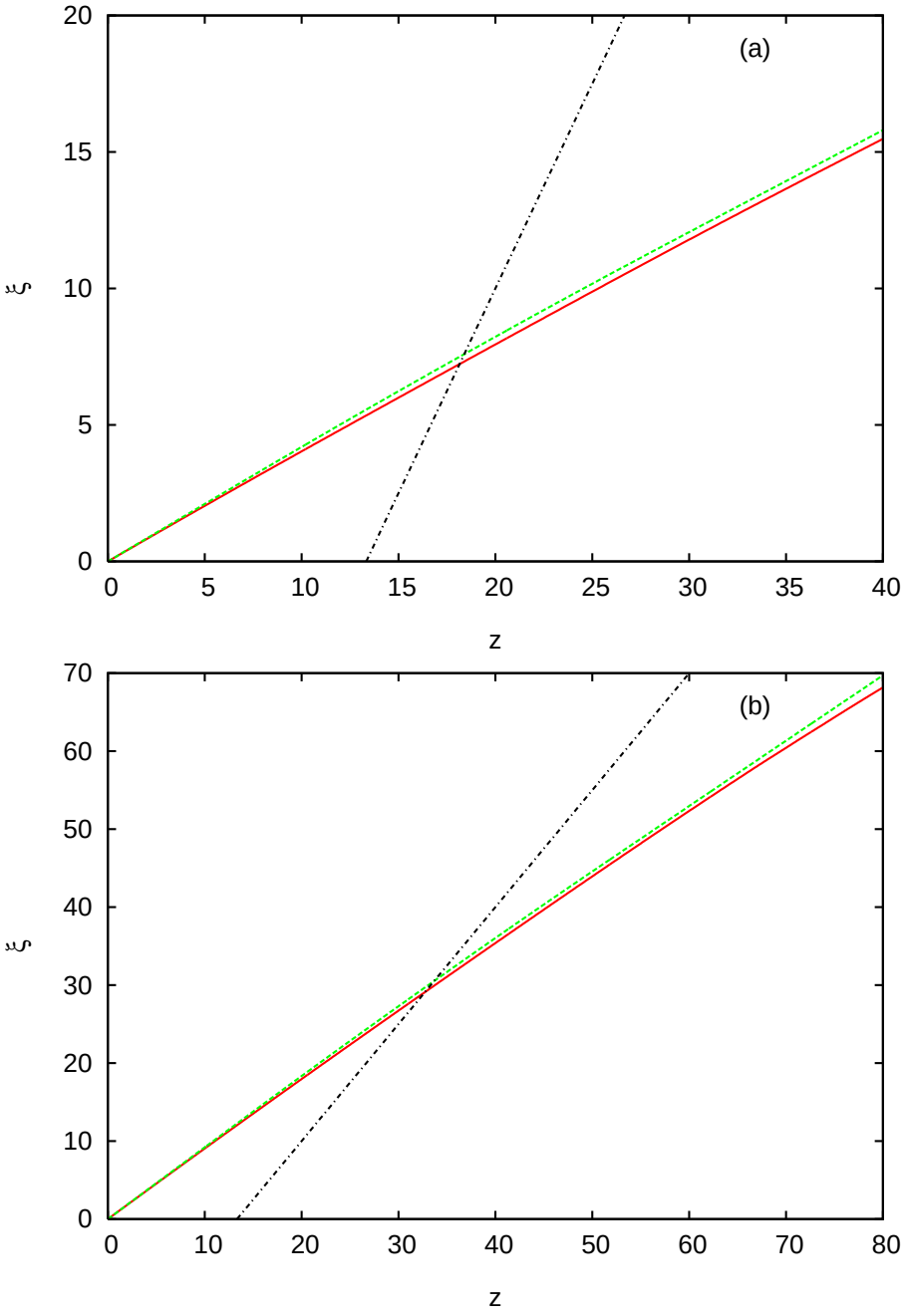

Figure 4.1: Comparison between vortex trajectories as given by the full numerical and modulation solutions for the initial values $a = 0.15$ and $w = 8.0$, with $\nu = 200$, $\psi_{bl} = 0.4$, $\psi_{br} = 0.9$, $q_l = 1.0$, $q_r = 1.3$, $\mu_1 = 2$ and $\mu_2 = -80$. Full numerical solution: — (red solid line); modulation solution: – – – (green, dashed line); interface: - · - · (black, dash dot line). (a) $V_0 = 0.5$, (b) $V_0 = 1.0$. (*The most parts of full numerical solution and modulation solution overlap to a high extent. Especially when printed in black and white, the superposition makes a solid line look like a dashed line.)

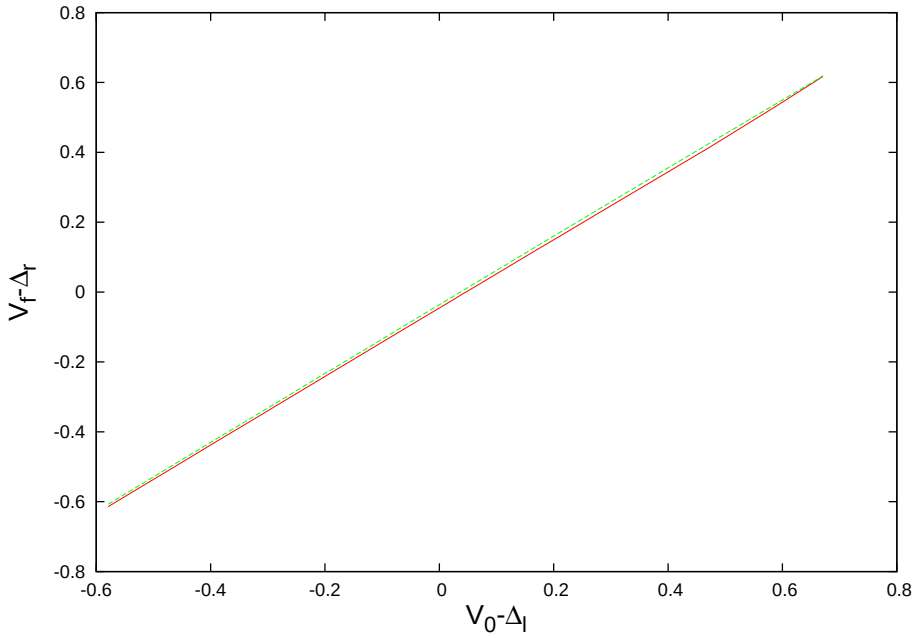

Figure 4.2: Comparison of refracted propagation constant $V_f - \Delta_r$ versus incident propagation constant $V_0 - \Delta_l$ as given by the full numerical and modulation solutions. The initial values are $a = 0.15$, $w = 8.0$, $\xi = 0$, with the parameter values $\nu = 200$, $\psi_{bl} = 0.4$, $\psi_{br} = 0.9$, $q_l = 1.0$, $q_r = 1.3$, $\mu_1 = 2$ and $\mu_2 = -80$. Full numerical solution: — (red, solid line); modulation solution: – – – (green, dashed line). (*The most parts of full numerical solution and modulation solution overlap to a high extent. Especially when printed in black and white, the superposition makes a solid line look like a dashed line.)

of behaviours depending on the initial propagation angle relative to the interface [127, 196, 202, 203], including the usual refraction to the second medium, the total internal reflection of ray theory, Goos-Hänchen reflection [208], whereby its centre refracts into the less dense medium before re-entering the original medium, and total internal reflection without its centre actually touching the interface. The latter two behaviours are due to a nematicon not being a point particle, but an extended object, so that when it is close to the interface it can respond to the refractive indices on both sides of it. However, there is a fundamental difference between a nematicon and an optical vortex. The director response to a vortex is more complicated than that for a nematicon due to the director response to the vortex core [160, 163, 164].

Therefore, an optical vortex shows different behaviour to a nematicon when $V_0 - \Delta_l$ is larger than a critical value, which will be discussed later. Figure 4.5 displays the same propagation constant comparison between the full numerical solution and the modulation solution as Figure 4.2. It can be seen that up to around $V_0 - \Delta_l = 0.9$ the agreement between the numerical and modulation solutions is similar to that of Figure 4.2. Figure 4.6 further shows the absolute and percentage errors for the modulation results compared with the numerical data. Again, for $V_0 - \Delta_l$ between -0.1 and -0.02 the percentage error e_p becomes large due to the angle of refraction $V_f - \Delta_r$ being near 0. Figure 4.5 and Figure 4.6(a) show no abrupt change in this range. In a similar manner as refraction to a more optically dense medium, the change in propagation angle is $O(5^o)$, up to about 10^o, similar to that for the equivalent refraction of a nematicon [127, 196]. Above around $V_0 - \Delta_l = 0.9$, the reasons for this increasing difference between the numerical and modulation results is more complicated than the simple distortion for the refraction of a nematicon and will be discussed in detail below.

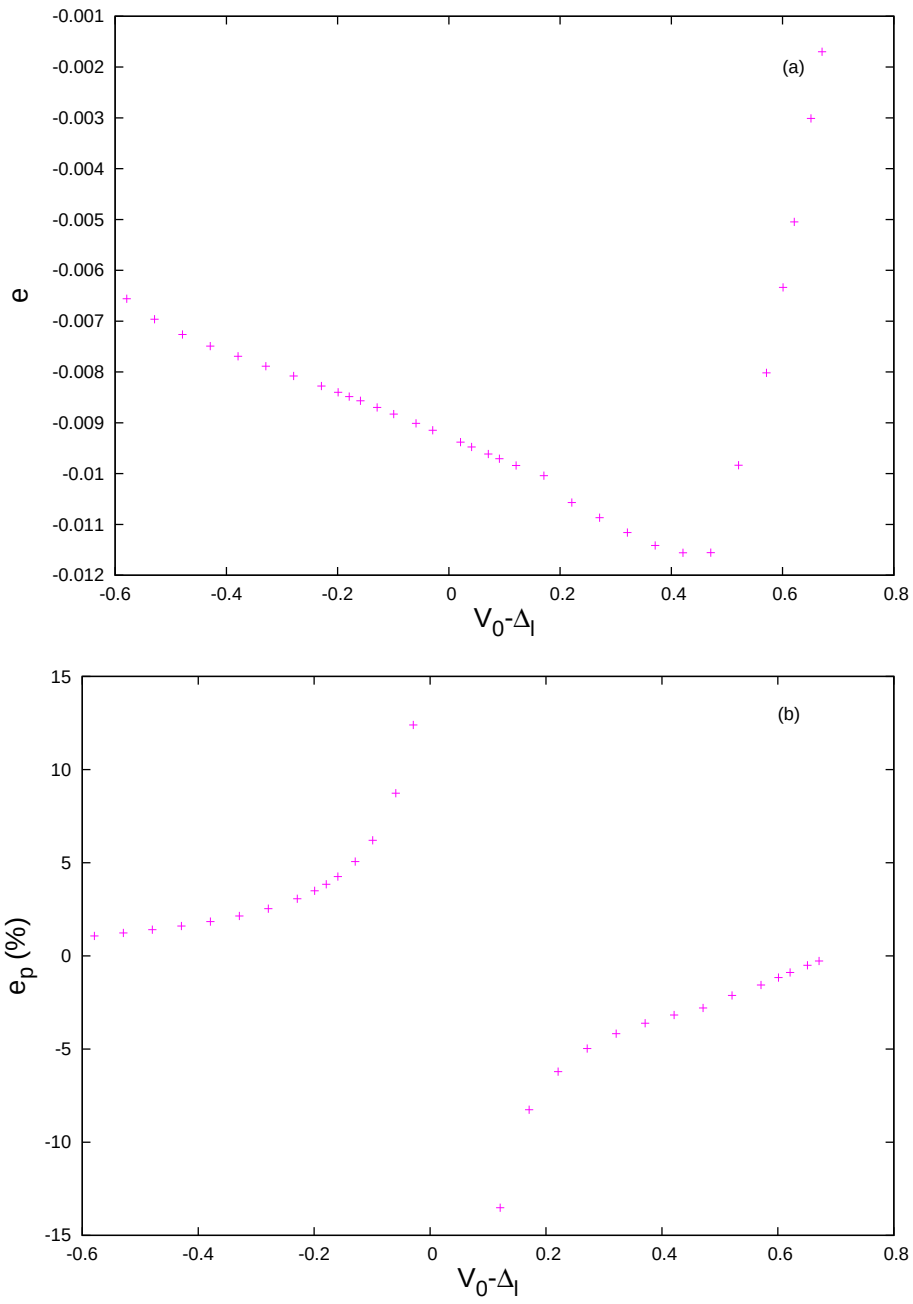

Figure 4.3: The error in the refracted propagation constant $V_f - \Delta_r$ as given by the modulation theory compared with the numerical solution as a function of incident propagation constant $V_0 - \Delta_l$. The initial values are $a = 0.15$, $w = 8.0$, $\xi = 0$, with the parameter values $\nu = 200$, $\psi_{bl} = 0.4$, $\psi_{br} = 0.9$, $q_l = 1.0$, $q_r = 1.3$, $\mu_1 = 2$ and $\mu_2 = -80$. (a) error e, (b) percentage error e_p.

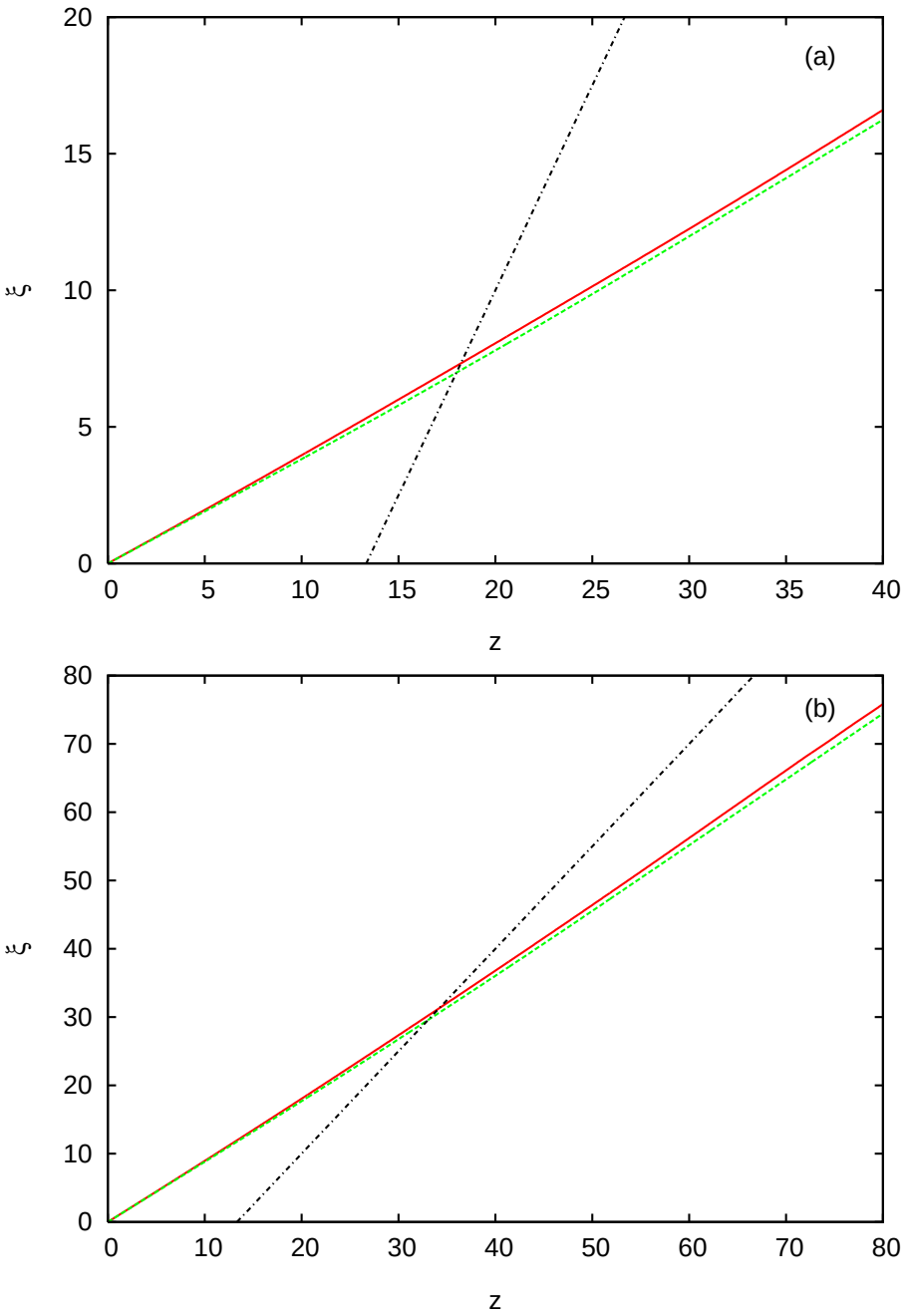

Figure 4.4: Comparison between vortex trajectories as given by the full numerical and modulation solutions for the initial values $a = 0.15$ and $w = 8.0$, with $\nu = 200$, $\psi_{bl} = 0.8$, $\psi_{br} = 0.4$, $q_l = 1.3$, $q_r = 1.0$, $\mu_1 = 1.5$ and $\mu_2 = -20$. Full numerical solution: — (red, solid line); modulation solution: – – – (green, dashed line); interface: - · - · (black, dash dot line). (a) $V_0 = 0.5$, (b) $V_0 = 1.0$. (*The most parts of full numerical solution and modulation solution overlap to a high extent. Especially when printed in black and white, the superposition makes a solid line look like a dashed line.)

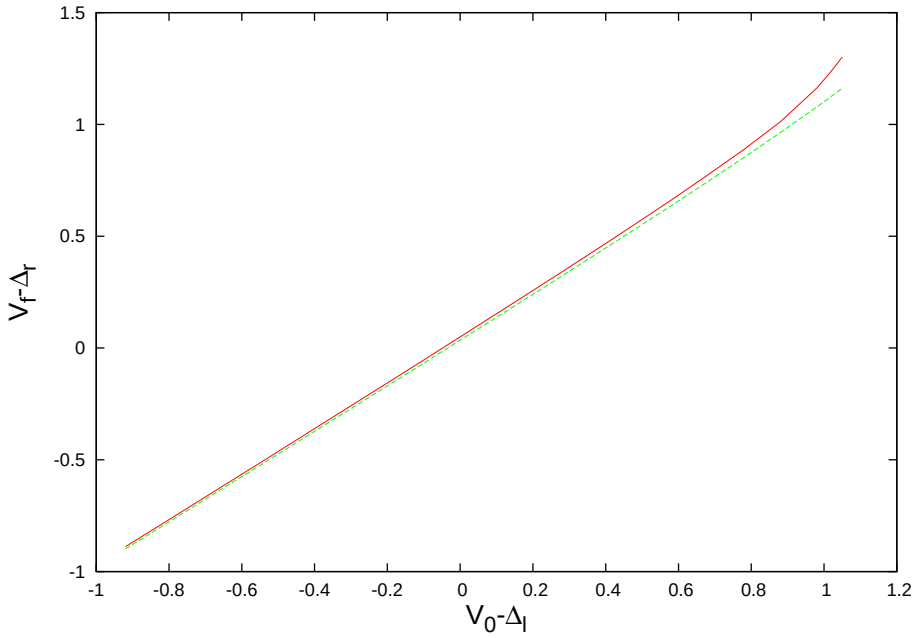

Figure 4.5: Comparison of refracted propagation constant $V_f - \Delta_r$ versus incident propagation constant $V_0 - \Delta_l$ as given by the full numerical and modulation solutions. The initial values are $a = 0.15$, $w = 8.0$, $\xi = 0$, with the parameter values $\nu = 200$, $\psi_{bl} = 0.8$, $\psi_{br} = 0.4$, $q_l = 1.3$, $q_r = 1.0$, $\mu_1 = 1.5$ and $\mu_2 = -20$. Full numerical solution: — (red, solid line); modulation solution: – – – (green, dashed line). (*The most parts of full numerical solution and modulation solution overlap to a high extent. Especially when printed in black and white, the superposition makes a solid line look like a dashed line.)

It should be noted that in Figure 4.4(b) the vortex is close to total internal reflection. While from the previous discussion it would appear that the vortex is undergoing less distortion than a nematicon, this is not the case, however, due to fundamental differences between the stability of a nematicon and an optical vortex. Unlike a nematicon, an optical vortex has an azimuthal structure, as seen in the trial function (4.15). If the nonlocality ν is not large enough, the charge 1 vortex can then have a mode two azimuthal instability which results in its breaking up into two nematicons [146, 160], as recently reported in experiments [77]. For the parameter values used here, in particular the nonlocality $\nu = 200$, the optical vortices are stable in the uniform media on either side of the interface. However, the interaction with the interface triggers the mode 2 azimuthal instability. Figure 4.7 shows numerical vortex solutions well after the vortex has crossed the interface for refraction to both more and less optically dense media. The mode 2 azimuthal distortion can be clearly seen, with the azimuthal perturbation being larger for refraction to the less dense medium. In addition to the vortices, the diffractive radiation shed by them as they evolve can be clearly seen. By shedding radiation, the vortices can evolve to a steady state of a circumferentially uniform vortex.

Figure 4.8 shows full numerical solutions for $|E|$ for $V_0 = 1.3$, which gives $V_0 - \Delta_l = 1.1803$, at $z = 0$, $z = 20$ when the vortex reaches the interface at $y = 1.5 * 20 - 20 = 10$, $z = 120$ when the beam is still in the vicinity of the interface, which is at $y = 1.5 * 120 - 20 = 160$, at $z = 150$, when the interface is at $y = 1.5 * 150 - 20 = 205$, at $z = 180$, when the interface is at $y = 1.5 * 180 - 20 = 250$, and at $z = 200$, when the interface is at $y = 1.5 * 200 - 20 = 280$. It can be seen from the vortex at $z = 20$ in Figure 4.8(b) that the interface perturbs the vortex profile. Figure 4.8(c), with the vortex at $z = 120$ shows that the vortex initially breaks up into two

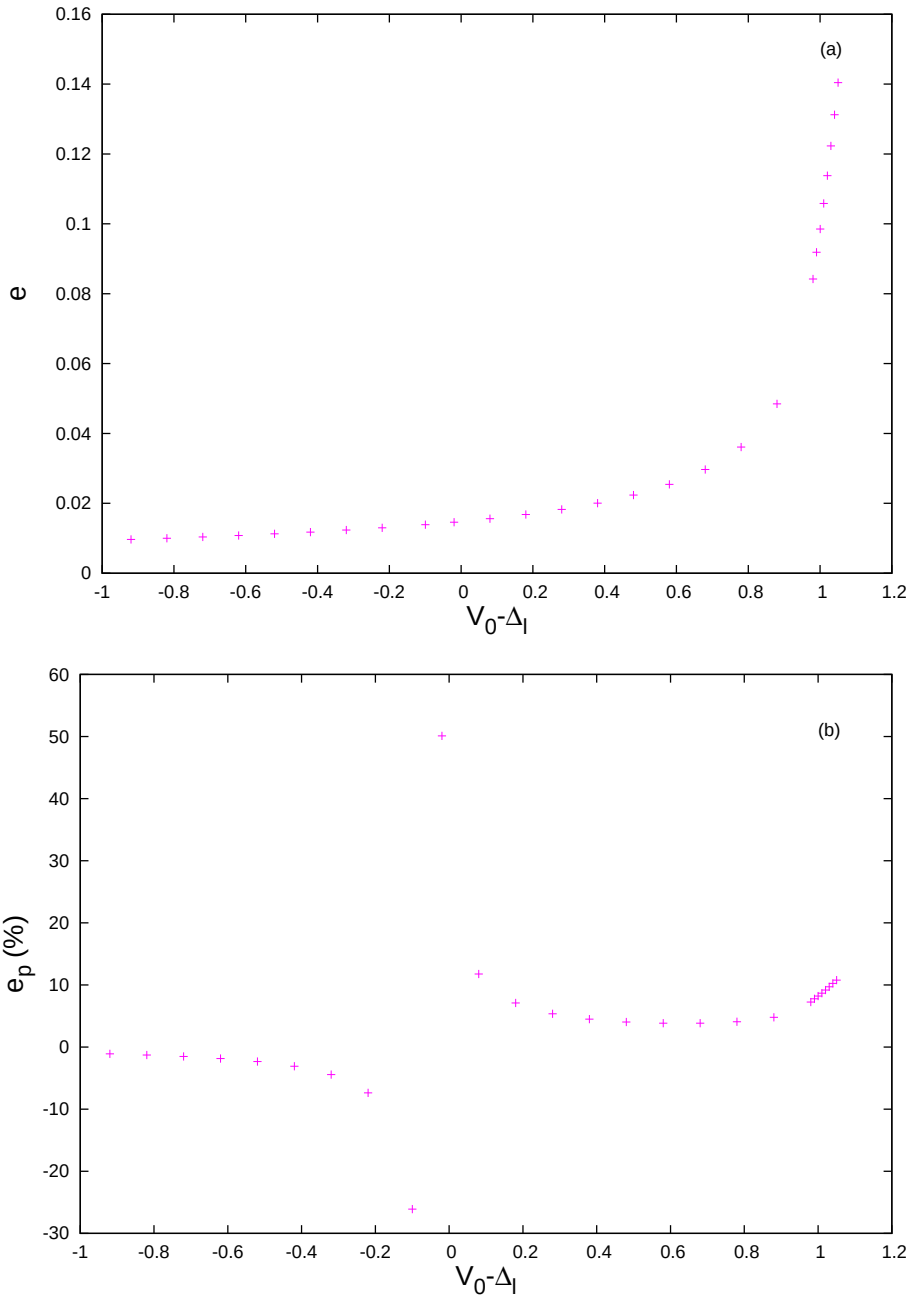

Figure 4.6: The error in the refracted propagation constant $V_f - \Delta_r$ as given by the modulation theory compared with the numerical solution as a function of incident propagation constant $V_0 - \Delta_l$. The initial values are $a = 0.15$, $w = 8.0$, $\xi = 0$, with the parameter values $\nu = 200$, $\psi_{bl} = 0.8$, $\psi_{br} = 0.4$, $q_l = 1.3$, $q_r = 1.0$, $\mu_1 = 1.5$ and $\mu_2 = -20$. (a) error e, (b) percentage error e_p.

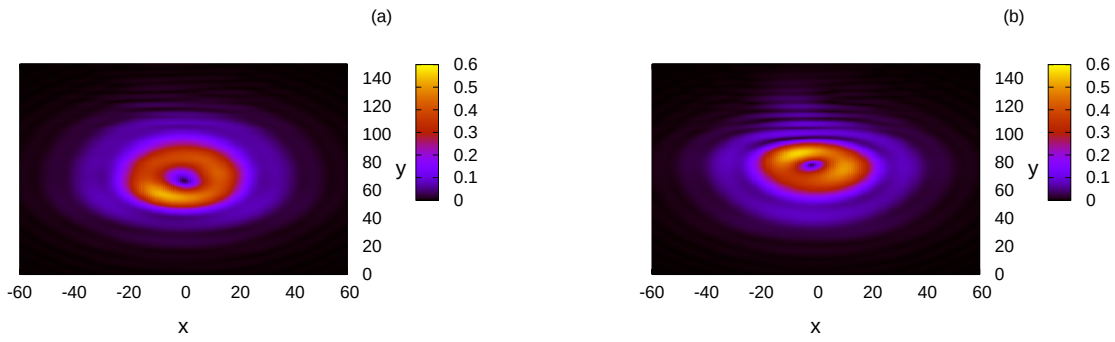

Figure 4.7: Numerical solution $|E|$ for vortex at $z = 120$ for initial values $a = 0.15$, $w = 8.0$ and $V_0 = 1.0$, with $\nu = 200$. (a) $\psi_{bl} = 0.4$, $\psi_{br} = 0.9$, $q_l = 1.0$, $q_r = 1.3$, $\mu_1 = 2$ and $\mu_2 = -80$, (b) $\psi_{bl} = 0.8$, $\psi_{br} = 0.4$, $q_l = 1.3$, $q_r = 1.0$, $\mu_1 = 1.5$ and $\mu_2 = -20$.

nematicons, with one nematicon on either side of the interface, due to the forcing of the mode 2 instability. Figure 4.8(d), with the vortex at $z = 150$ shows that the remnants of the vortex linking these two nematicons initially form into a third nematicon. And finally three nematicon form, with two of them on the incident side of the interface and another one on the other side of the interface, as seen in Figure 4.8(e) and they are further confirmed in Figure 4.8(f). The equivalent refraction of a nematicon shows no such instability [127, 196]. As discussed in section 1.4, a charge 1 optical vortex has a mode 2 azimuthal instability if the nonlocality ν is not large enough [146, 160]. This instability pinches off the vortex width in a symmetrical fashion, so that it breaks up into two solitary waves. For a vortex in a uniform medium, if the nonlocality $\nu > 100$, then the vortex is stable against this azimuthal mode [146, 160]. So in a uniform nematic, the vortex of Figure 4.8 is stable. The destabilising effect of the interface can be seen in Figure 4.8(b). The interface has perturbed the vortex in a manner broadly similar to a mode 2 azimuthal perturbation. For $V_0 < 1.1$ the vortex refracts through the interface and does not stay close to it for a long range of z. However, for $V_0 > 1.1$ the vortex is close to total internal reflection and propagates close to the interface for an extended range of z. This close proximity to the interface for an extended range of z forces the unstable azimuthal mode long enough to cause the vortex to become unstable and split into two nematicons, as in Figure 4.8(c). A contrary example for $V_0 = 0.5$ of a vortex refracting through the interface and remaining stable is shown in Figure 4.9, which shows the vortex well after it has passed through the interface which is at $y = 40$. The vortex has returned to a uniform state and resembles the initial vortex shown in Figure 4.8(a). Numerical solutions show that the vortex becomes unstable at $V_0 = 1.1$, in good agreement with the modulation prediction of $V_0 = 1.18$. The modulation equations show that the longer the vortex propagates near the interface, the larger the amplitude oscillation. It eventually becomes so large that when the amplitude comes down again, it goes to zero. This ties in with the numerical vortex splitting for $V_0 > 1.1$. The modulation equations can show that the vortex is becoming unstable, but it cannot split in the modulation equations as there is no angle dependence in the trial function. So the modulation theory gives the instability as far as it can. Once the amplitude goes to 0, the modulation equations are invalid.

The refraction of an optical vortex to a less optically dense medium then does not show

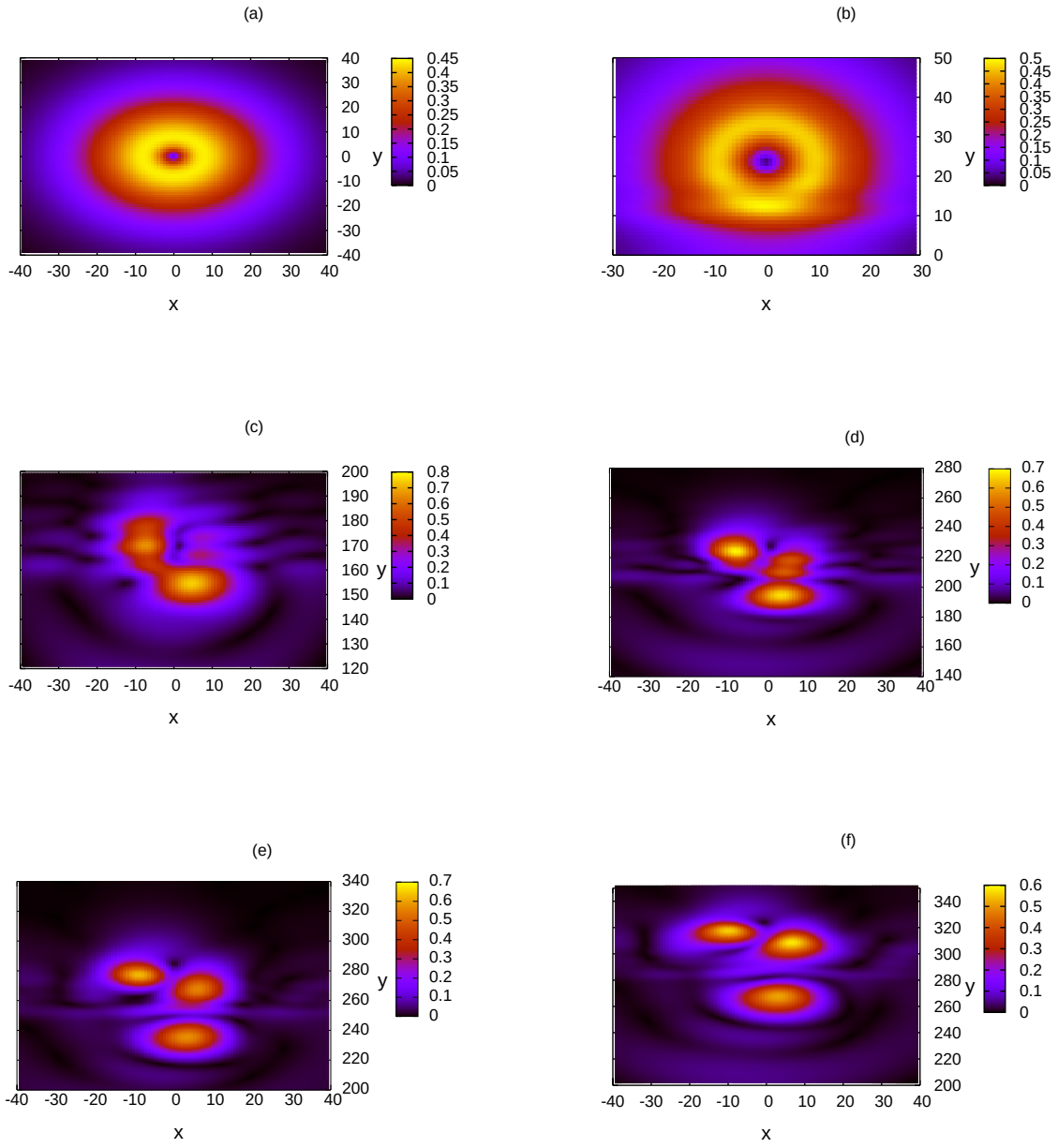

Figure 4.8: Numerical solution for $|u|$ for the parameter values $a = 0.15$, $w = 8.0$ and $V = 1.3$ at $z = 0$, with $\nu = 200$, $\psi_{bl} = 0.8$, $\psi_{br} = 0.4$, $q_l = 1.3$, $q_r = 1.0$, $\mu_1 = 1.5$ and $\mu_2 = -20$. (a) $z = 0$, (b) $z = 20$, (c) $z = 120$, (d) $z = 150$, (e) $z = 180$, (f) $z = 200$

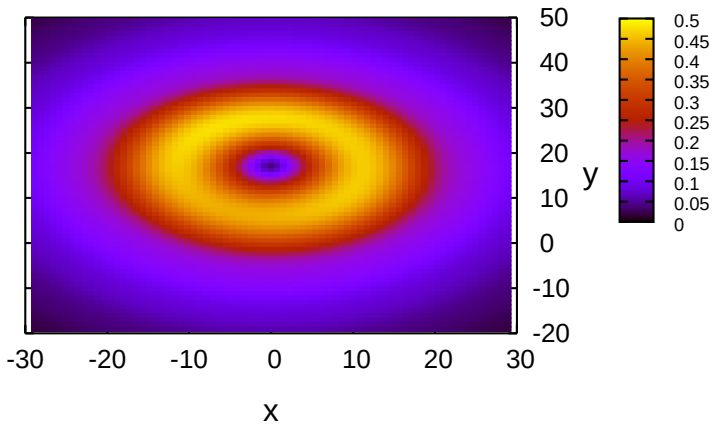

Figure 4.9: Numerical solution for $|u|$ at $z = 40$ for the parameter values $a = 0.15$, $w = 8.0$ and $V = 0.5$, with $\nu = 200$, $\psi_{bl} = 0.8$, $\psi_{br} = 0.4$, $q_l = 1.3$, $q_r = 1.0$, $\mu_1 = 1.5$ and $\mu_2 = -20$.

Goos-Hänchen reflection and standard total internal reflection as the instability is triggered before these can occur. The instability of the vortex for $V_0 > 1.1$, or $V_0 - \Delta_l > 0.9803$, explains the increasing difference visible in the comparison of Figure 4.5 for $V_0 - \Delta_l > 0.9$.

Due to this inherent instability of a vortex, Goos-Hänchen reflection and total internal reflection, as seen in the refraction of a nematicon [127, 196], will not occur. Remarkably, Figures 4.6(a) and 4.6(b) show that even when the vortex splits into two nematicons, the modulation theory position is still in good agreement with the numerical centre of mass position (4.38), with the percentage difference e_p only going up to $\sim 10\%$. This is due to overall momentum conservation and shows that when the vortex splits, it does not shed much mass and momentum into diffractive radiation. Experiments with nematicons obtained changes in angles of propagation of up to 22^o for propagation into a less optically dense nematic [196], greater than the 10^o obtained here. However, these larger angles were for the case of total internal reflection, for which the vortex is unstable. Furthermore, as for refraction to a more optically dense medium, the change in angle depends on the voltage difference of the pre-tilting electric fields, and so on the changes in the values of ψ and q. Finally, in principle, increasing the nonlocality should stabilise the vortex. However, even an unrealistically large value $\nu = 1000$ did not stop the vortex breaking up into nematicons.

4.4 Discussion

The refraction of an optical vortex at an interface between two regions of different refractive index in a nematic liquid crystal has been investigated using both modulation theory and full numerical solutions of the governing equations. A nematic liquid crystal is a specific example of a nonlinear, nonlocal optical medium and the results obtained here would transfer over to other such media [197, 198]. The refraction of a vortex displays distinct behaviour, depending

on whether it propagates into a more or less optically dense medium. Refraction to a more optically dense medium is similar to the equivalent refraction of a nematicon [127, 196]. As for the refraction of a nematicon, excellent agreement was found between modulation theory results and numerical solutions, with the change in propagation angle of the vortex being similar to that for a nematicon.

The refraction of a vortex to a less optically dense medium shows major differences to the equivalent refraction of a nematicon [127, 196]. Unlike a nematicon (solitary wave), an optical vortex has an unstable azimuthal mode, which can be triggered if the vortex propagates for too far too close to the interface. In a related context, it has been found that if an optical vortex in a nematic liquid crystal cell propagates too close to the cell walls it can become unstable, even if the nonlocality is large enough so that it is stable away from the boundary [165, 166]. However, this effect is different to that investigated here in that as it is the non-zero value of the optical axis perturbation under the vortex which stabilises it, the cell walls destabilise the vortex as, due to the anchoring conditions, the optical axis is fixed there. In the present context, the vortex is an extended structure and can have portions on both sides of the interface. The resulting shape perturbation can then trigger its azimuthal instability.

Optical vortices are inherently less stable structures than optical solitary waves, nematicons. It is then of interest to study the behaviour and stability of optical vortices in nematic cells with varying properties and refractive index [111, 118, 101, 103, 188, 190, 191, 192, 193, 194, 195]. Such variations in refractive index in a cell are the basis for proposed applications of nonlinear optical beams in liquid crystals as they allow the trajectory of the beam to be controlled.

Chapter 5

Conclusions

5.1 Summary of Research

Both nonlinear waves and liquid crystals are blooming fields with vast scientific and technological applications. The research in this thesis is at the junction between these two areas. The NLC nonlinear response to a light beam can be highly nonlocal due to molecular reorientation. The exceptional controllability of this response leads to the self-trapping of the beam by balancing diffraction and self-focusing. This allows the creation of optical solitary waves, including solitons and vortices. Optical solitons and vortices have a number of applications in scientific fields. In the work of this thesis, the research focused on the interaction of optical solitons and vortices with a dielectric interface between two regions of NLCs. Accurate numerical solutions of the full governing equations revealed the detailed evolution of optical solitary waves, while solutions from modulation theory provided far more insight into the mechanics of the evolution of the optical solitary waves. Full numerical solutions of the governing equations were used to analyse the accuracy of the approximate solutions obtained from modulation theory. The approximate method was based on the method of Kath and Smyth [96] and is an extended variational approximation which can include the effect of shed diffractive radiation. An appropriate trial function to be subsitituted into the Lagrangian has to be chosen to accurately balance beam dynamics and returning simple modulation equations on which a meaningful analysis can be conducted. In order to accurately portray the parameter oscillations displayed in full numerical solutions, the amplitude and width oscillations in the trial functions need to vary independently. The agreement between full numerical and modulation solutions proves the quality of the trial function(s) chosen in the variational method. When computing the averaged Lagrangian for trial functions, certain integrals could not be evaluated exactly. To tackle it, equivalent Gaussians were used to replace the hyperbolic secant terms in these integrals. Adjustable parameters in equivalent Gaussians then allowed the integrals to have the same asymptotic value in the nonlocal limit. This was applied in both Chapter 3 and Chapter 4. Radiation loss was shown to be the essential mechanism allowing beams to evolve to steady optical solitary waves [96]. However, due to the short propagation distances considered, the inclusion of this radiation was not necessary. Once the final modulation equations representing variations of the beam parameters were found, they were solved numerically using the standard fourth order Runge-Kutta scheme. To make comparisons, the full governing equations were solved numerically using a pseudospectral method, with z stepping performed using the fourth

order Runge-Kutta scheme once again, however this time in Fourier space.

The results sections of Chapter 3 and Chapter 4 showed that combining an accurate numerical portrayal with an approximate modulation solution allows a detailed mechanical description and understanding of the evolution of optical solitary waves in NLCs. Agreement between full numerical solutions and modulation solutions was excellent in general.

5.2 Future Research

5.2.1 Extension of the present methods

Since Kath and Smyth extended modulation theory to include radiation loss in order to approximate the evolution of a pulse in an optical fibre [96], modulation theory has been applied to develop approximate solutions for varied soliton problems where their evolution is governed by NLS-like equations, coupled nonlinear Schrödinger equations (CNLS)-like equations and the Sine-Gordon equation [218, 219]. So there is no reason why modulation theory could not be applied to approximate other nonlinear PDEs. Modulation theory may be generalised to approximate other PDEs, assuming a proper trial function can be found, for instance by guessing an appropriate form from full numerical solutions of the PDE.

This thesis has concentrated on nematicons, but there are close relationships between the nematicon governing equations and equations governing solitons in different media. A diverse range of governing equations is suitable for the application of the modulation theory. For example, the equations governing a thermoelastic waveguide are the same as the nematicon governing equations [220]. Other similar equations are also found governing solitons in colloidal suspensions [214, 221], media with an optical thermal nonlinearity [220, 222] and photorefractive crystals [223, 224].

5.2.2 Improvement of the present methods

The inclusion of time could be made to the present approach to tackle the nematicon problems. Some previous research used a NLS-like equation for the beam envelope similar to the ones used in this thesis, but the molecular director was described by a time dependent equation. This allowed the evolution of beams to be described in both time and space. For example, Beeckman *et al* investigated how nematicons form in planar NLC cells [225] and Strinić *et al* studied spatiotemporal optical instabilities of nematicons [226, 227]. However, the spatiotemporal governing equations cannot be easily approximated, meaning that all of the benefits associated with approximating soliton evolution are lost, which makes that the advantage of this approach with time included is limited. The improvement of the present methods is then a big challenge, but still being expected.

5.2.3 Soliton and Vortex

In physics, waves and particles are two fundamental models. In the earlier centuries classical physics made a fundamental distinction between them. However, in the microcosmic world, wave-particle duality arises. A soliton is macroscopic wave, but it shows some particle properties, such as after two interacting, solitons emerge unchanged in the form. Solitons on protein and DNA chains, magnetic fields and Bose-Einstein condensates are also interesting fields.

Back to the research in this thesis, it dealt with one soliton beam travelling in a NLC cell with two distinct regions formed by applying different electric fields. It could be extended to allow two soliton beams propagate in a NLC with an interface. The research could be based on two parallel beams, or nonparallel beams and how their interaction would affect the refraction. Also, two beams inputted from two opposite sides of the NLC cell could be studied. Similar extended research can also be applied to vortices in NLCs. Further research could be on the interaction between a soliton and a vortex in NLCs. Furthermore, the research on refraction could be extended from the present refraction of bright nematicons to dark nematicons and dark vortices.

As introduced in Chapter 1, research on the interaction of nematicons has been done [37, 47, 105, 106, 108, 109, 110], which could be extended to optical vortices.

5.2.4 Liquid crystal and Conductive polymer

NLCs are an excellent material platform to exhibit and investigate nonlinear optical phenomena, particularly solitons, and also vortices. A number of nonlinear phenomena related to light induced director rotation and localization in NLCs still await proper study [66], from instabilities and dynamical effects, to spontaneous or stimulated polarization conversion and scattering [228, 229], to multi-wave mixing and slow light [230], to bistability, turbulence [231] and the excited state response of resonant systems [91]. The variety of NLCs available and the infinite set of doping possibilities could bring a growing number of improvements and applications of nematicons [66]. Whilst nonlocality is one of the most important factors controlling soliton stability and long-range interactions in NLCs, the response time of liquid crystal is relatively slow for some applications [66]. Hence, a good deal of future work will have to focus on material, as well as geometrical optimisation, aiming at reducing both the electro-optic and the all-optical response time [66]. The combination of NLCs with polymers and/or nanoparticles, and their use in hybrid structures exploiting properties of other organic/inorganic materials might further enhance the properties and uses of nonlinear beams in liquid crystals [66]. Nonlinear phenomena in nonlinear optical materials, such as conductive polymers may need attention as well. Solitons have been found in conductive polymers [232]. Research on nonlinear phenomena in conductive polymers may also be interesting and inspiring.

Appendix A

Publication

- Published

  1) G. Assanto, N. F. Smyth and W. Xia, "Modulation analysis of nonlinear beam refraction at an interface in liquid crystals", *Phys. Rev. A,* **84**, 033818 (2011).

  2) N. F. Smyth and W. Xia, "Refraction and Instability of Optical Vortices at an Interface in a Liquid Crystal", *J. Phys. B: At. Mol. Opt. Phys.,* **45**, 165403 (2012).

- Accepted

  3) G. Assanto, N. F. Smyth and W. Xia, "Refraction of Nonlinear Light Beams in Nematic Liquid Crystals", *JNOPM.,* **21**, 3 (2012).

- Submitted

  4) Xia, W., McKinnon, K. and Simmonds, P., "Modeling mutational and selection pressures on dinucleotides in eukaryotic phyla identification of separate and additional selection pressures against CpG and UpA in cytoplasmically expressed RNA sequences and in RNA viruses", *Molecular Biology and Evolution,* (2012).

Bibliography

[1] G. B. Whitham, *Linear and Nonlinear Waves,* (Wiley, New York, 1974).

[2] R. D. Knight, *Physics for Scientists and Engineers: A Strategic Approach,* (Addison Wesley, San Francisco, 2004).

[3] W. M. Telford, L. P. Geldart, E. S. Robert, *Applied Geophysics,* (Cambridge University Press, 2011).

[4] Y. S. Kivshar and G. P. Agrawal, *Optical Solitons: From Fibers to Photonics,* (Academic Press, San Diego, 2003).

[5] G. G. Stokes, "On the theory of oscillatory waves," *Transactions of the Cambridge Philosophical Society,* **8**, 441-455 (1847).

[6] J. S. Russell, "Report on waves," *Fourteenth meeting of the British Association for the Advancement of Science,* (1844).

[7] J. Boussinesq, "Théorie de l'intumescence liquide, applelé onde solitaire ou de translation, se propageant dans un canal rectangulaire," *Comptes Rendus de l'Academie des Sciences,* **72**, 755-759 (1871).

[8] L. Rayleigh, "On waves," *Philosophical Magazine, ser. 5, vol. 1,* **4**, 257-279 (1876).

[9] Korteweg, D. J. and de Vries, G., "On the change of form of long waves advancing in a rectangular canal and on a new type of long stationary waves," *Philosophical Magazine,* **39**, 422-443 (1895).

[10] N. J. Zabusky and M. D. Kruskal, "Interaction of 'solitons' in a collisionless plasma and the recurrence of intial states," *Phys. Rev. Lett.,* **15**, 240 (1965).

[11] C. Gardner, J. Greene, M. Kruskal and R. Miura, "Method for solving the Korteweg-deVires equation," *Phys. Rev. Lett.,* **19**, 1095-1097 (1967).

[12] P. G. Drazin and R. S. Johnson, *Solitons: an introduction,* (Cambridge University Press, 2nd ed.,) (1989).

[13] Hasegawa, A., Tappert, F, "Transmission of stationary nonlinear optical pulses in dispersive dielectric fibers. I. Anomalous dispersion," *Appl. Phys. Lett.,* **23**, 142-144 (1973).

[14] Emplit, P., Hamaide, J. P., Reynaud, F., Froehly, C., Barthelemy, A., "Picosecond steps and dark pulses through nonlinear single mode fibers," *Optics. Comm.,* **62**, 374-379 (1987).

[15] Mollenauer, Linn F., Gordon, James P., *Solitons in optical fibers,* (Elsevier Academic Press,) (2006).

[16] A. S. Davydov, *Solitons in molecular systems, Mathematics and its applications,* (Kluwer Academic Publishers, 1991).

[17] L. V. Yakushevich, *Nonlinear physics of DNA,* (Wiley-VCH, 2004).

[18] Z. Sinkala, "Soliton/exciton transport in proteins," *J. Theor. Biol.,* **241**, 91927 (2006).

[19] A. M. Kosevich, V. V. Gann, A. I. Zhukov and V. P. Voronov, "Magnetic soliton motion in a nonuniform magnetic field," *Journal of Experimental and Theoretical Physics,* **87**, 401407 (1998).

[20] G. W. Gibbons, "BornInfeld particles and Dirichlet p-branes," *Nuclear Physics B,* **514**, 603639 (1998).

[21] Devin Powell, "Rogue Waves Captured," *Science News,* **179**, 12 (2011).

[22] Chiao, R.Y., Garmire, E., Townes, C.H., "Self-trapping of optical beams," *Phys. Rev. Lett.,* **13**, 479-482 (1964).

[23] Talanov, V.I., "On self-focusing of electromagnetic waves in nonlinear media," *Izvest. Vuz Radiofiz.,* **7**, 564 (1964).

[24] Bjorkholm, J.E., Ashkin, A.A., "Cw self-focusing and self-trapping of light in sodium vapor," *Phys. Rev. Lett.,* **32**, 129-132 (1974).

[25] Aitchison, J.S., Weiner, A.M., Silberberg, Y., Oliver, M.K., Jackel, J.L., Leaird, D.E., Vogel, E.M., Smith, P.W.E., "Observation of spatial optical soliton in nonlinear waveguide," *Opt. Lett.,* **15**, 471-473 (1990).

[26] Duree, G.C., Shultz, J.L., Salamo, G.J., Segev, M., Yariv, A., "Observation of self-trapping of an optical beam due to the photorefractive effect," *Phys. Rev. Lett.,* **71**, 533-536 (1993).

[27] Valley, G.C., Segev, M., Crosignani, B., Yariv, A., Fejer, M.M., Bashav, M.C., "Dark and bright photovoltaic spatial solitons," *Phys. Rev. A,* **50**, R4457-R4460 (1994).

[28] Torruellas, W.E., Wang, Z., Hagan, D.J., VanStryland, E.W., Stegeman, G.I., Torner, L., Menyuk, C.R., "Observation of two-dimensional spatial solitary waves in a quadratic medium," *Phys. Rev. Lett.,* **74**, 5036-5039 (1995).

[29] Kang, J.U., Stegeman, G.I., Aitchison, J.S., Akhmediev, N., "Observation of Manakov spatial solitons in AlGaAs planar waveguides," *Phys. Rev. Lett.,* **76**, 3699-3702 (1996).

[30] Leo, G., Assanto, G., Torruellas, W.E., "Bidimensional spatial solitary waves in quadratically nonlinear bulk media," *J. Opt. Soc. Am.,* **14**, 3134 (1997).

[31] Friedrich, L., Stegeman, G.I., Millar, P., Hamilton, C.J., Aitchison, J.S., "Dynamic, electronically controlled angle steering of spatial solitons in AlGaAs slab waveguides," *Opt. Lett.,* **23**, 1438-1440 (1998).

[32] Segev, M., "Spatial solitons," *Opt. Quantum Electron,* **30**, 503-533 (1998).

[33] Trillo, S., Torruellas, W.E., *Spatial Solitons,* (Springer-Verlag, Berlin, 1998).

[34] Stegeman, G.I., Segev, M., "Optical spatial solitons and their interactions: universality and diversity," *Science,* **286**, 1518-1523 (1999).

[35] Stegeman, G.I., Christodoulides, D.N., Segev, M., "Optical spatial solitons: historical perspectives," *IEEE J. Sel. Top. Quantum Electron.,* **6**, 1419-1427 (2000).

[36] Leo, G., Colace, L., Amoroso, A., Di Falco, A., Assanto, G., "Spatial optical simultons in nonlinearly-coupled planar waveguides," *Opt. Lett.,* **28**, 1031-1033 (2003).

[37] Kivshar, Y.S., Agrawal, G.P., *Optical Solitons: From Fibers to Photonic Crystals,* (Academic Press, San Diego, 2003).

[38] Conti, C., Assanto, G., "Nonlinear optics applications: bright spatial solitons," *Encyclopedia Modern Opt.,* **5**, 43 (2004).

[39] Leo, G., Amoroso, A., Colace, L., Assanto, G., Roussev, R.V., Fejer, M.M., "Low-threshold spatial solitons in Reverse Proton Exchanged PPLN waveguides," *Opt. Lett.,* **29**, 1778 (2004).

[40] P. Weinberger, "John Kerr and his Effects Found in 1877 and 1878," *Philosophical Magazine Letters,* **88**, 897907 (2008).

[41] Pasquazi, A., Stivala, S., Assanto, G., Gonzalo, J., Solis, J., Afonso, C.N., "Near-infrared spatial solitons in heavy metal oxide glasses," *Opt. Lett.,* **32**, 2103-2105 (2007).

[42] Assanto, G., Karpierz, M., "Nematicons: self-localized beams in nematic liquid crystals," *Liq. Cryst.,* **36**, 1161 (2009).

[43] Zakharov, V.E., Shabat, A.B., "Exact theory of two-dimensional self-focusing and one-dimensional self-modulation of waves in nonlinear media," *Soviet Physics JETP,* **34**, 62 (1972).

[44] Snyder, A.W., Mitchell, D.J., Poladian, L., Ladoucer, F., "Self-induced optical fibers - spatial solitary waves," *Opt. Lett.,* **16**, 21-23 (1991).

[45] Kelley, P.L., "Self-focusing of optical beams," *Phys. Rev. Lett.,* **15**, 1005-1008 (1965).

[46] Maneuf, S., Desailly, R., Froehly, C., "Stable self-trapping of laser beams: observation in a nonlinear planar waveguide," *Opt. Commun.,* **65**, 193-198 (1988).

[47] Maneuf, S., Reynaud, F., "Quasi-steady state self-trapping of first, second and third order subnanosecond soliton beams," *Opt. Commun.,* **66**, 325-328 (1988).

[48] De Martini, F., Townes, C.H., Gustafson, T.K., Kelley, P.L., "Self-steepening of light pulses," *Phys. Rev.,* **164**, 312-323 (1967).

[49] Dawes, E.L., Marburger, J.H., "Computer studies in self-focusing," *Phys. Rev.,* **179**, 862-868 (1969).

[50] Skarka, V., Berezhiani, V.I., Miklaszewski, R., "Spatiotemporal dynamics of electromagnetic pulses in saturating nonlinear optical media with normal group velocity dispersion," *Phys. Rev. E,* **60**, 7622-7625 (1999).

[51] Dyshko, A.L., Lugovi, V.N., Prokhorov, A.M., "Multifocus structure of a beam in a nonlinear medium," *Sov. Physics JETP,* **34**, 1235 (1972).

[52] Silberberg, Y., "Solitons and two-photon absorption," *Opt. Lett.,* **15**, 1005-1007 (1990).

[53] Blair, S., Wagner, K., McLeod, R., "Material figures of merit for spatial soliton interactions in the presence of absorption," *J. Opt. Soc. Amer. B,* **13**, 2141-2153 (1996).

[54] Lawrence, B.L., Stegeman, G.I., "Two-dimensional bright spatial solitons stable over limited intensities and ring formation in polydiacetylene paratoluene sulfonate," *Opt. Lett.,* **23**, 591-593 (1998).

[55] Mlejnek, M., Wright, E.M., Moloney, J.V., "Moving-focus versus self-waveguiding model for long-distance propagation of femtosecond pulses in air," *IEEE J. Quantum Electron.,* **35**, 1771-1776 (1999).

[56] Aközbek, N., Scalora, M., Bowden, C.M., Chin, S.L., "White-light continuum generation and filamentation during the propagation of ultra-short laser pulses in air," *Opt. Commun.,* **191**, 353-362 (2001).

[57] Fibich, G., Papanicolaou, G.C., "Self-focusing in the presence of small time dispersion and nonparaxiality," *Opt. Lett.,* **22**, 1379-1381 (1997).

[58] A. Barthelemy, S. Maneuf and C. Froehly, "Propagation soliton et auto-confinement de faisceaux laser par non linearité optique de kerr," *Opt. Comm.* **55**, (3): 201 (1985).

[59] J. Beeckman, K. Neyts, X. Hutsebaut, C. Cambournac, M. Haelterman, "Simulations and Experiments on Self-focusing Conditions in Nematic Liquid-crystal Planar Cells," *Opt. Express* **12**, (6): 1011-1018 (2004).

[60] Reinitzer, F., "Beitrge zur kenntniss des cholesterins," *Monatshefte fr Chemie (Wien)* **9**, 421-441 (1888).

[61] Collings, P., Hird, M., *Introduction to Liquid Crystals Chemistry and Physics*, (CRC, London, 1997).

[62] de Gennes, P., Prost, J., *The Physics of Liquid Crystals, 2nd edition*, (Oxford University Press, USA, London, 1995).

[63] I. C. Khoo, *Liquid Crystals: Physical Properties and Nonlinear Optical Phenomena*, J. Wiley and Sons (1995).

[64] Khoo, I.C., "Theory of optically induced molecular reorientations and quantitative experiments on wave mixing and the self-focusing of light," *Phys. Rev. A* **25**, 1637 (1982).

[65] Tabiryan, N.V., Sukhov, A., Zeldovich, B.Y., "The orientational optical nonlinearity of liquid crystals," *Mol. Cryst. Liq. Cryst.* **136**, 1 (1986).

[66] M. Peccianti and G. Assanto, "Nematicons," *Physics Reports* **516**, 147208 (2012).

[67] Khoo, I.C., Yan, P.Y., H, L.T., "Nonlocal radial dependence of optically induced director axis reorientation of a nematic liquid crystal filmtheory and experiment," *J. Opt. Soc. Am. B* **4**, 115-120 (1987).

[68] M. Peccianti, A. De Rossi, G. Assanto, A. De Luca, C. Umeton and I. Khoo, "Electrically assisted self-confinement and waveguiding in planar nematic liquid crystal cells," *Appl. Phys. Lett.***77**, 7-9 (2000).

[69] Geary, J.M., Goodby, J.W., Kmetz, A.R., Patel, J.S., "The mechanism of polymer alignment of liquid-crystal materials," *J. Appl. Phys.***62**, 4100-4108 (1987).

[70] Seo, D.S., Muroi, K.I., Kobayashi, S., "Generation of pretilt angles in nematic liquid-crystal, 5CB, media aligned on polyimide films prepared by spincoating and LB techniques - effect of the rubbing," *Mol. Cryst. Liq. Cryst.***213**, 223-228 (1992).

[71] G. Assanto, M. Peccianti, and C. Conti, "Nematicons: optical spatial solitons in nematic liquid crystals," *Opt. Photonics News Feb.*, 44-48 (2003).

[72] A. Piccardi, A. Alberucci, U. Bortolozzo, S. Residori and G. Assanto, "Soliton gating and switching in liquid crystal light valve," *Appl. Phys. Lett. 96*, 071104 (2010).

[73] Assanto, G., Stegeman, G.I., "Simple physics of quadratic spatial solitons," *Optics Exp.***10**, 388-396 (2002).

[74] Conti, C., Assanto, G., "Nonlinear optics applications: bright spatial solitons," *Encyclopedia Modern Opt.***5**, 43 (2004).

[75] Peccianti, M., Assanto, G., "Signal readdressing by steering of spatial solitons in bulk nematic liquid crystals," *Opt. Lett.***26**, 1690-1692 (2001).

[76] Beeckman, J., Neyts, K., Vanbrabant, P.J.M., James, R., Fernandez, F.A., "Finding exact spatial soliton profiles in nematic liquid crystals," *Opt. Exp.***18**, 3311-3321 (2010).

[77] Izdebskaya, Y.V., Desyatnikov, A.S., Assanto, G., Kivshar, Y.S., "Multimode nematicon waveguides," *Opt. Lett.***36**, 184 (2011).

[78] C. Conti, M. Peccianti and G. Assanto, "Route to nonlocality and observation of accessible solitons," *Phys. Rev. Lett.,* **91**, 073901 (2003).

[79] C. Conti, M. Peccianti and G. Assanto, "Observation of optical spatial solitons in a highly nonlocal medium," *Phys. Rev. Lett.,* **92**, 113902 (2004).

[80] Mitchell, M., Chen, Z.G., Shih, M.F., Segev, M., "Self-trapping of partially spatially incoherent light," *Phys. Rev. Lett.***77**, 490-493 (1996).

[81] Mitchell, M., Segev, M., "Self-trapping of incoherent white light," *Nature***387**, 880-883 (1997).

[82] Christodoulides, D.N., Coskun, T.H., Mitchell, M., Segev, M., "Theory of incoherent self-focusing in biased photorefractive media," *Phys. Rev. Lett.***78**, 646-649 (1997).

[83] Christodoulides, D.N., Coskun, T.H., Mitchell, M., Segev, M., "Multimode incoherent spatial solitons in logarithmically saturable nonlinear media," *Phys. Rev. Lett.***80**, 2310-2313. (1998).

[84] Shen, M., Shi, J., Wang, Q., "Incoherent accessible white-light solitons in strongly nonlocal Kerr media," *Phys. Rev. E.***74**, 27601. (2006).

[85] Kong, Q., Shen, M., Shi, J., Wang, Q., "Incoherent solitons in strongly nonlocal media: The coherent density theory," *Phys. Rev. A.***372**, 244-251. (2008).

[86] Anderson, D., Helczynski-Wolf, L., Lisak, M., Semenov, V.E., "Interaction between two partially incoherent soliton stripes," *Opt. Commun.***281**, 3919-3923. (2008).

[87] Peccianti, M., Assanto, G., "Incoherent spatial solitary waves in nematic liquid crystals," *Opt. Lett.***26**, 1791-1793 (2001).

[88] Peccianti, M., Assanto, G., "Nematic liquid crystals: A suitable medium for self-confinement of coherent and incoherent light," *Phys. Rev. E.***65**, 35603 (2002).

[89] Born, M., Wolf, E., *Principles of Optics: Electromagnetic Theory of Propagation, Interference and Diffraction of Light,* (Pergamon Press, London, 1959).

[90] Alberucci, A., Assanto, G., "On beam propagation in anisotropic media: one-dimensional analysis," *Opt. Lett.***36**, 334-336 (2011).

[91] Janossy, I., Lloyd, A., Wherrett, B., "Anomalous optical Freedericksz transition in an absorbing liquid crystal," *Mol. Cryst. Liq. Cryst.***179**, 1-12 (1990).

[92] Janossy, I., Kosa, T., "Influence of Anthraquinone dyes on optical reorientation of nematic liquid crystals," *Opt. Lett.***17**, 1183-1185 (1992).

[93] Piccardi, A., Alberucci, A., Assanto, G., "Self-turning self-confined light beams in guesthost media," *Phys. Rev. Lett.***104**, 213904 (2010).

[94] Alberucci, A., Assanto, G., "Non-paraxial (1 + 1)D spatial solitons in uniaxial media," *Opt. Lett.***36**, 193-195 (2011).

[95] Alberucci, A., Assanto, G., "Non paraxial solitary waves in anisotropic dielectrics," *Phys. Rev. A.***83**, 033822 (2011).

[96] W.L. Kath and N.F. Smyth, "Soliton evolution and radiation loss for the nonlinear Schrödinger equation," *Phys. Rev. E,* **51**, 1484-1492 (1995).

[97] C. García-Reimbert, A.A. Minzoni, and N.F. Smyth, "Spatial soliton evolution in nematic liquid crystals in the nonlinear local regime," *J. Opt. Soc. Am. B,* **23**, 2 (2006).

[98] C. García-Reimbert, A.A. Minzoni, N.F. Smyth and A.L. Worthy, "Large-amplitude nematicon propagation in a liquid crystal with local response," *J. Opt. Soc. Amer. B,* **23**, 2551-2558 (2006).

[99] García-Reimbert, C., Minzoni, A.A., Marchant, T.R., Smyth, N.F. and Worthy, A.L., "Dipole soliton formation in a nematic liquid crystal in the nonlocal limit," *Physica D,* **237**, 1088-1102 (2008).

[100] Assanto, G., Marchant, T.R., and Smyth, N.F., "Collisionless shock resolution in nematic liquid crystals," *Phys. Rev. A,* **78**, 063808 (2008).

[101] G. Assanto, A.A. Minzoni, M. Peccianti and N.F. Smyth, "Optical solitary waves escaping a wide trapping potential in nematic liquid crystals: modulation theory," *Phys. Rev. A,* **79**, 033837 (2009).

[102] Alberucci, A., Assanto, G., Buccoliero, D., Desyatnikov, A., Marchant, T.R., and Smyth, N.F., "Modulation analysis of boundary induced motion of nematicons," *Phys. Rev. A,* **79**, 043816 (2009).

[103] G. Assanto, B.D. Skuse and N.F. Smyth, "Optical path control of spatial optical solitary waves in dye-doped nematic liquid crystals," *Photon. Lett. Poland,* **1**, 154-156 (2009).

[104] A.A. Minzoni, N.F. Smyth and A.L. Worthy, "Modulation solutions for nematicon propagation in non-local liquid crystals," *J. Opt. Soc. Amer. B,* **24**, 1549-1556 (2007).

[105] Mitchell, D.J., Snyder, A.W., Poladian, L., "Interacting self-guided beams viewed as particles: Lorentz force derivation," *Phys. Rev. Lett.,* **77**, 271-273 (1996).

[106] Snyder, A.W., Mitchell, D.J., "Accessible solitons," *Science,* **276**, 1538-1541 (1997).

[107] Peccianti, M., Conti, C., Assanto, G., "Nonlocal optical propagation in nonlinear nematic liquid crystals," *J. Nonlinear Opt. Phys. Mater.,* **12**, 525-538 (2003).

[108] Shih, M.F., Segev, M., Salamo, G., "Three-dimensional spiraling of interacting spatial solitons," *Phys. Rev. Lett.,* **78**, 2551-2554 (1997).

[109] Pasquazi, A., Alberucci, A., Peccianti, M., Assanto, G., "Signal processing by opto-optical interactions between self-localized and free propagating beams in liquid crystals," *Appl. Phys. Lett.,* **87**, 261104 (2005).

[110] Serak, S.V., Tabiryan, N.V., Peccianti, M., Assanto, G., "Spatial soliton all-optical logic gates," *IEEE Photon. Tech. Lett.,* **18**, 1287-1289 (2006).

[111] G. Assanto, B.D. Skuse and N.F. Smyth, "Solitary wave propagation and steering through light-induced refractive potentials," *Phys. Rev. A,* **81**, 063811 (2010).

[112] Canva, M.T.G., Fuerst, R.A., Baboiu, S., Stegeman, G.I., Assanto, G., "Quadratic spatial soliton generation by seeded down conversion of a strong harmonic pump beam," *Opt. Lett.,* **22**, 1683-1685 (1997).

[113] A.A. Minzoni, N.F. Smyth, A.L. Worthy and Y.S. Kivshar, "Stabilization of vortex solitons in nonlocal nonlinear media," *Phys. Rev. A,* **76**, 063803 (2007).

[114] Alberucci, A., Peccianti, M., Assanto, G., Dyadyusha, A., Kaczmarek, M., "Two-color vector solitons in nonlocal media," *Phys. Rev. Lett.,* **97**, 153903 (2006).

[115] Skuse, B.D., and Smyth, N.F., "Two-colour vector soliton interactions in nematic liquid crystals in the local response regime," *Phys. Rev. A,* **77**, 013817 (2008).

[116] Assanto, G., Smyth, N.F., and Worthy, A.L., "Two colour, nonlocal vector solitary waves with angular momentum in nematic liquid crystals," *Phys. Rev. A,* **78**, 013832 (2008).

[117] Barboza, R., Alberucci, A., Assanto, G., "Large electro-optic beam steering with Nematicons," *Opt. Lett.,* **36**, 2611-2613 (2011).

[118] G. Assanto, A.A. Minzoni, N.F. Smyth and A.L. Worthy, "Refraction of nonlinear beams by localised refractive index changes in nematic liquid crystals," *Phys. Rev. A,* **82**, 053843 (2010).

[119] Emile, O., Galstyan, T., Le Floch, A., Bretenaker, F., "Measurement of the nonlinear Goos-Hnchen effect for Gaussian optical beams," *Phys. Rev. Lett.,* **75**, 1511-1513 (1995).

[120] Ostrovskii, L.A., "Propagation of wave packets and spacetime self-focusing in a nonlinear medium," *Sov. Phys. JETP,* **24**, 797 (1969).

[121] Bespalov, V.I., Talanov, V.I., "On filamentary structure of light beams in liquids," *Sov. Phys. JETP,* **3**, 307 (1966).

[122] Peccianti, M., Conti, C., Assanto, G., "Optical modulational instability in a nonlocal medium," *Phys. Rev. E,* **68**, 25602 (2003).

[123] Beeckman, J., Hutsebaut, X., Haelterman, M., Neyts, K., "Induced modulation instability and recurrence in nematic liquid crystals," *Opt. Exp.,* **15**, 11185-11195 (2007).

[124] Piccardi, A., Alberucci, A., Tabiryan, N., Assanto, G., "Dark nematicons," *Opt. Lett.,* **36**, 1456-1458 (2011).

[125] Assanto, G., Marchant, T., Minzoni, A.A., Smyth, N.F., "Reorientational versus Kerr dark and grey solitary waves using modulation theory," *Phys. Rev. E,* **84**, 066602 (2011).

[126] Assanto, G., García-Reimbert, C., Minzoni, A.A., Smyth, N.F., and Worthy, A.L., "Lagrange solution for three wavelength solitary wave clusters in nematic liquid crystals," *Physica D,* **240**, 1213-1219 (2011).

[127] G. Assanto, N.F. Smyth and W. Xia, "Modulation analysis of nonlinear beam refraction at an interface in liquid crystals," *Phys. Rev. A,* **84**, 033818 (2011).

[128] Minzoni, A.A., Sciberras, L.W., Smyth, N.F., and Worthy, A.L., "Propagation of optical spatial solitary waves in bias-free nematic liquid crystal cells," *Phys. Rev. A,* **84**, 043823 (2011).

[129] Assanto, G., Marchant, T.R., Minzoni, A.A., and Smyth, N.F., "Reorientational versus Kerr dark and grey solitary waves using modulation theory," *Phys. Rev. E,* **84**, 066602 (2011).

[130] Alberucci, A., Assanto, G., Minzoni, A.A., and Smyth, N.F., "Scattering of reorientational optical solitary waves at dielectric perturbations," *Phys. Rev. A,* **85**, 013804 (2012).

[131] Yu. S. Kivshar and E. A. Ostrovskaya, "Optical vortices: Folding and twisting waves of light," *Opt. Photon. News***12**, 24-28 (2001).

[132] M. Berry, "Making waves in physics," *Nature (London)* **403**, 21 (2000).

[133] J.F.Nye and M.V. Berry, "Dislocations in wave trains," *Proc. R. Soc. London Sect.A* **336**, 165-90 (1974).

[134] M. Soskin and M.Vasnetsov, "Singular optics as a new chapter of modern photonics," *Photonics Sci. News* **4**, 22-42 (1999).

[135] Y.S. Kivshar and B. Luther-Davies, "Optical dark solitons: physics and applications," *Phys. Rep.* **298**, 81-197 (1998).

[136] Jeanna Bryner, "Twisted Physics: Scientists Create Light Knots," *LiveScience*, 17 January 2010.

[137] D. J. Thouless, *Topological quantum numbers in nonrelativistic physics,* (World Scientific., ISBN 9810229003, 1998).

[138] Mikio Nakahara, *Geometry, topology, and physics,* (Taylor & Francis., ISBN 0750306068, 2003).

[139] A. S. Desyatnikov, Yu. S. Kivshar, and L. Torner, "Optical vortices and vortex solitons," *Progress in Optics Vol.* **47**, (2005).

[140] D. Mihalache, D. Mazilu, I. Towers, B. A. Malomed, and F. Lederer, "Stable spatiotemporal spinning solitons in a bimodal cubic-quintic medium," *Phys. Rev. E* **67**, 056608 (2003).

[141] A. V. Gorbach, D. V. Skryabin, and C. N. Harvey, "Vortex solitons in an off-resonant Raman medium," *Phys. Rev. A* **77**, 063810 (2008).

[142] Geoffrey New, *Introduction to Nonlinear Optics,* (Cambridge University Press, New York, 2011).

[143] E.G.Sauter, *Nonlinear Optics,* (John Wiley & Sons, Inc., Canada, 1996).

[144] J. Kerr, "A new relation between electricity and light: dielectrified media birefringent," *Phil. Mag. (4th Series)***50**, 337 (1875).

[145] R. W. Boyd , *Nonlinear Optics(3rd ed.),* (Academic Press, ISBN 978-0123694706, 2008).

[146] A.I. Yakimenko, Yu.A. Zaliznyak and Yu.S. Kivshar, "Stable vortex solitons in nonlocal self-focusing nonlinear media," *Phys. Rev. E,* **71**, 065603(R) (2005).

[147] C. Conti, M. Peccianti, and G. Assanto, "Route to Nonlocality and Observation of Accessible Solitons," *Phys. Rev. Lett.* **91**, 073901 (2003).

[148] V. I. Petviashvili and V. V. Yankov, "Solitons and turbulence," *Review in Plasma Physics, edited by B. B. Kadomtsev Vol.* **14**, 1-62 (1989).

[149] V.Tikhonenko, J. Christou, B. Luther-Davies, and Y. S. Kivshar, "Observation of vortex solitons created by the instability of dark soliton stripes," *Opt. Lett.* **21**, 1129-31 (1996).

[150] Y. S. Kivshar,A.Nepomnyashehy,V.Tikhonenko, J. Christou, and B. Luther-Davies, "Vortex-stripe soliton interaction," *Opt. Lett.* **25**, 123-5 (2000).

[151] G.A. Swartzlander and C.T. Law, "Optical vortex solitons observed in Kerr nonlinear media," *Phys. Rev. Lett.***69**, 2503-6 (1992).

[152] A.V.Mamaev, M. Saffman, and A.A. Zozulya, "Vortex evolution and bound pair formation in anisotropic nonlinear optical media," *Phys. Rev. Lett.***77**, 4544-7 (1996).

[153] Z. Chen, M. Segev, D.W.Wilson, R. E. Muller, and P.D. Maker, "Self-trapping of an optical vortex by use of the bulk photovoltaic effect," *Phys. Rev. Lett.***78**, 2948-51 (1995).

[154] Vladimir Tikhonenko, Yuri S. Kivshar, Victoria V. Steblina, and Alex A. Zozulya, "Vortex solitons in a saturable optical medium," *J. Opt. Soc. Am. B***15**, 79-86 (1998).

[155] Dmitri V. Petrov, Lluis Torner, Jordi Martorell, Ramon Vilaseca, Juan P. Torres, and Crina Cojocaru, "Observation of azimuthal modulational instability and formation of patterns of optical solitons in a quadratic nonlinear crystal," *Opt. Lett.***23**, 1444-1446 (1998).

[156] D. Voloschenko and O. D. Lavrentovich, "Optical vortices generated by dislocations in a cholesteric liquid crystal," *Opt. Lett.***25**, 317-319 (2000).

[157] D. Mihalache, D. Mazilu, I. Towers, B. A. Malomed, and F. Lederer, "Stable spatiotemporal spinning solitons in a bimodal cubic-quintic medium," *Phys. Rev. E***67**, 056608(2003).

[158] Alexander I. Yakimenko, Yuri A. Zaliznyak, and Yuri Kivshar, "Stable vortex solitons in nonlocal self-focusing nonlinear media," *Phys. Rev. E***71**, 065603(R)(2005).

[159] M.P. MacDonald, P. Prentice and K. Dholakia, "Optical vortices produced by diffraction from dislocations in two-dimensional colloidal crystals," *New J. Phys.,* **8**, 257 (2006).

[160] A.A. Minzoni, N.F. Smyth, A.L. Worthy and Y.S. Kivshar, "Stabilization of vortex solitons in nonlocal nonlinear media," *Phys. Rev. A,***76**, 063803 (2007).

[161] Alexander Dreischuh, Dragomir N. Neshev, Vesselin Z. Kolev, Solomon Saltiel, Marek Samoc, Wieslaw Krolikowski, and Yuri S. Kivshar, "Nonlinear dynamics of two-color optical vortices in lithium niobate crystals," *Optics Express,* **16**, 5406-5420 (2008).

[162] Etienne Brasselet, Naoki Murazawa, Hiroaki Misawa, and Saulius Juodkazis, "Optical Vortices from Liquid Crystal Droplets," *Phys. Rev. Lett.,***103**, 103903 (2009).

[163] Z. Xu, N.F. Smyth, A.A. Minzoni and Y.S. Kivshar, "Vector vortex solitons in nematic liquid crystals," *Opt. Lett.,* **34**, 1414-1416 (2009).

[164] A.A. Minzoni, N.F. Smyth, Z. Xu and Y.S. Kivshar, "Stabilization of vortex-soliton beams in nematic liquid crystals," *Phys. Rev. A,* **79**, 063808 (2009).

[165] A.A. Minzoni, N.F. Smyth and Z. Xu, "Stability of an optical vortex in a circular nematic cell," *Phys. Rev. A,* **81**, 033816 (2010).

[166] Y.V. Izdebskaya, A.S. Desyatnikov, G. Assanto and Y.S. Kivshar, "Dipole azimuthons and vortex charge flipping in nematic liquid crystals," *Opt. Expr.,* **19**, 21457-21466 (2011).

[167] D.L. Andrews, *Structured Light and Its Applications: An Introduction to Phase-Structured Beams and Nanoscale Optical Forces,* (Academic Press-Elsevier, Burlington, 2008).

[168] M. Peccianti, C. Conti, G. Assanto, A. De Luca and C. Umeton, "Routing of anisotropic spatial solitons and modulational instability in liquid crystals," *Nature,* **432**, 733-737 (2004).

[169] G. Assanto, M. Peccianti, K. A. Brzdkiewicz, A. De Luca and C. Umeton, "Nonlinear wave propagation and spatial solitons in nematic liquid crystals," *J. Nonl. Opt. Phys. Mat.* **12**, 123-134 (2003).

[170] B. A. Malomed, "Variational methods in nonlinear fiber optics and related fields," *Progress in Optics* **43**, E. Wolf, Elsevier Science, 71-193 (2002).

[171] D. Anderson, "Variational approach to nonlinear pulse propagation in optical fibers," *Phys. Rev. A* **27**, 3135-3145 (1983).

[172] M. Quiroga-Teixeiro and H. Michinel, "Stable azimuthal stationary state in quintic nonlinear optical media," *J. Opt. Soc. Am. B* **14**, 2004-2009 (1997).

[173] Anton Desyatnikov, Andrey Maimistov, and Boris Malomed, "Three-dimensional spinning solitons in dispersive media with the cubic-quintic nonlinearity," *Phys. Rev. E* **61**, 3107 (2000).

[174] M Syafwan, H Susanto, S M Cox and B A Malomed, "Variational approximations for traveling solitons in a discrete nonlinear Schr dinger equation," *J. Phys. A: Math. Theor.* **45**, 075207 (2012).

[175] G. Assanto, *Nematicons: Spatial Optical Solitons in Nematic Liquid Crystals,* (Wiley-Blackwell, 2012).

[176] E. Nöther, "Invariante Variationsprobleme," *Math-phys. Klasse* , 235-257 (1918).

[177] N. F. Smyth and W. L. Kath, "Radiative losses due to pulse interactions in birefringent nonlinear optical fibers," *Phys. Rev. E,* **63**, 036614 (2001).

[178] J. Yang, "Vector solitons and their internal oscillations in birefringent nonlinear optical fibers," *Stud. Appl. Math.,* **98**, 61-97 (1997)..

[179] C. Conti, M. Peccianti and G. Assanto, "Route to nonlocality and observation of accessible solitons," *Phys. Rev. Lett.,* **91**, 073901 (2003).

[180] T. R. Taha and M. J. Ablowitz, "Analytical and Numerical Aspects of Certain Nonlinear Evolution Equations. II. Numerical, Nonlinear Schrödinger Equation", *Journal of Computational Physics,* **2**, 55 (1984).

[181] I. M. Gelfand, S. V. Fomin, *Calculus of Variations,* (Courier Dover Publications, 2000).

[182] B. Fornberg and G. B. Whitham, A Numerical and Theoretical Study of Certain Nonlinear Wave Phenomena, *Phil. Trans. R. Soc. Lond. A,* **289**, 373-403 (1978).

[183] B. D. Skuse, "The Interaction and Steering of Nematicons," Ph.D. Thesis, University of Edinburgh (2010).

[184] F. If, P. Berg, P. L. Christiansen and O. Skovgaard, Split-step spectral method for nonlinear Schrodinger equation with absorbing boundaries, *J. Comp. Phys.,* **72**, 501-503 (1987).

[185] W. H. Press, S. A. Teukolsky, W. T. Vetterling and B. P. Flannery, *Numerical Recipes in Fortran: The Art of Scientific Computing*, Cambridge University Press, UK (1992).

[186] W. H. Press, B. P. Flannery, S. A. Teukolsky, W. T. Vetterling, *Numerical Recipes in Fortran 77 - The Art of Scientific Computing*, Cambridge University Press (1986, 1992).

[187] L. Atkinson, P. J. Harley and J. D. Hudson, *Numerical methods with Fortran 77: A practical introduction*, Longman Group, UK (1989).

[188] M. Peccianti, C. Conti, G. Assanto, A. de Luca and C. Umeton, "All-optical switching and logic gating with spatial solitons in liquid crystals," *Appl. Phys. Lett.,* **81**, 3335-3337 (2002).

[189] M. Peccianti, C. Conti, G. Assanto, A. de Luca and C. Umeton, "Routing of anisotropic spatial solitons and modulational instability in liquid crystals," *Nature,* **432**, 733-737 (2004).

[190] S.V. Serak, N.V. Tabiryan, M. Peccianti and G. Assanto, "Spatial soliton all-optical logic gates" *IEEE Photon. Tech. Lett.,* **18**, 1287-1289 (2006).

[191] M. Peccianti, A. Dyadyusha, M. Kaczmarek and G. Assanto, "Escaping solitons from a trapping potential," *Phys. Rev. Lett.,* **101**, 153902 (2008).

[192] A. Piccardi, G. Assanto, L. Lucchetti and F. Simoni, "All-optical steering of soliton waveguides in dye-doped liquid crystals," *Appl. Phys. Lett.* **93**, 171104 (2008).

[193] G. Assanto, A. Piccardi, A. Alberucci, S. Residori and U. Bortolozzo, "Liquid crystal light valves: a versatile platform for nematicons," *Photonics Letters of Poland,* **1**, 151-153 (2009).

[194] A. Alberucci, A. Picardi, U. Bortolozzo, S. Residori and g. Assanto, "Nematicon all-optical control in liquid crystal light valves," *Opt. Lett.,* **35**, 390-392 (2010).

[195] A. Piccardi, A. Alberucci, U. Bortolozzo, S. Residori and G. Assanto, "Soliton gating and switching in liquid crystal light valve," *Appl. Phys. Lett.,* **96**, 071104 (2010).

[196] M. Peccianti, A. Dyadyusha, M. Kaczmarek and G. Assanto, "Tunable refraction and reflection of self-confined light beams," *Nature Phys.,* **2**, 737-742 (2006).

[197] A.B. Aceves, J.V. Moloney and A.C. Newell, "Theory of light-beam propagation at nonlinear interfaces. I Equivalent-particle theory for a single interface," *Phys. Rev. A,* **39**, 1809-1827 (1989).

[198] A.B. Aceves, P. Varatharajah, A.C. Newell, E.M. Wright, G.I. Stegeman, D.R. Heatley, J.V. Moloney and H. Adachihara, "Particle aspects of collimated light channel propagation at nonlinear interfaces and in waveguides," *J. Opt. Soc. Amer. B,* **7**, 963-974 (1990).

[199] D.J. Kaup and A.C. Newell, "Solitons as particles, oscillators, and in slowly changing media: a singular perturbation theory," *Proc. Roy. Soc. Lond. A,* **361**, 413-446 (1978).

[200] J. Sánchez-Curto, P. Chamorro-Posada and G.S. McDonald, "Black and gray Helmholtz-Kerr soliton refraction," *Phys. Rev. A,* **83**, 013828 (2011).

[201] A. Piccardi, A. Alberucci, N. Tabiryan, and G. Assanto, "Dark nematicons," *Opt. Lett.,* **36**, 1356-1358 (2011).

[202] M. Peccianti, G. Assanto, A. Dyadyusha and M. Kaczmarek, "Nonspecular total internal reflection of spatial soliton at the interface between highly birefringent media," *Phys. Rev. Lett.,* **98**, 113902 (2007).

[203] M. Peccianti, G. Assanto, A. Dyadyusha and M. Kuczmarek, "Nonlinear shift of spatial solitons at a graded dielectric interface," *Opt. Lett.,* **32**, 271-273 (2007).

[204] M. Peccianti, A. Fratalocchi and G. Assanto, "Transverse dynamics of nematicons," *Opt. Express,* **12**, 6524-6529 (2004).

[205] M. Peccianti, A. De Rossi, G. Assanto, A. De Luca, C. Umeton, and I.C. Khoo, "Electrically assisted self-confinement and waveguiding in planar nematic liquid crystal cells," *Appl. Phys. Lett.,* **77**, 7-9 (2000).

[206] M.J. Ablowitz, S.D. Dixon, T.P. Horikis and D.J. Frantzeskakis, "Perturbations of dark solitons," *Proc. R. Soc. Lond. A,* **467**, 2597-2621 (2011).

[207] M. Abramowitz and I.A. Stegun, *Handbook of Mathematical Functions with Formulas, Graphs and Mathematical Tables,* Dover Publications, Inc., New York (1972).

[208] F. Goos and H. Hänchen, "Ein neuer und fundamentaler Versuch zur Totalreflexion," *Ann. Phys.,* **436**, 333-346 (1947).

[209] E. Brasselet, N. Murazawa, H. Misawa and S. Juodkazis, "Optical vortices from liquid crystal droplets," *Phys. Rev. Lett.,* **103**, 103903 (2009).

[210] E. Brasselet and C. Loussert, "Electrically controlled topological defects in liquid crystals as tunable spin-orbit encoders for photons," *Opt. Lett.,* **36**, 719-721 (2011).

[211] Y.V. Izdebskaya, J. Rebling, A.S. Desyatnikov and Y.S. Kivshar, "Observation of vector solitons with hidden vorticity," *Opt. Lett.,* **37**, 767-769 (2012).

[212] E. Brasselet, "Tunable optical vortex arrays from a single nematic topological defect," *Phys. Rev. Lett.,* **108**, 087801 (2012).

[213] D. Voloschenko and O.D. Lavrentovich, "Optical vortices generated by dislocations in a cholesteric liquid crystal," *Opt. Lett.,* **25**, 317-319 (2000).

[214] M. Matuszewski, W. Krolikowski and Y. S. Kivshar, "Spatial solitons and light-induced instabilities in colloidal media," *Opt. Exp.,* **16**, 1371-1376 (2008).

[215] M. Matuszewski, W. Krolikowski and Y. S. Kivshar, "Soliton interactions and transformations in colloidal media," *Phy. Rev. A,* **79**, 023814 (2009).

[216] *CRC Handbook of Laser Science and Technology: Optical Materials*, Suppl. 2, ed. M.J. Weber, CRC Press, New York (1995).

[217] J. Sánchez-Curto, P. Chamarro-Posada and G.S. McDonald, "Helmholtz bright and dark soliton splitting at nonlinear interfaces," *Phys. Rev. A,* **85**, 013836 (2012).

[218] Kath, W.L. and Smyth, N.F., Soliton evolution and radiation loss for the Korteweg-de Vries equation, *Phy. Rev. E,* **51**, 661-670 (1995).

[219] N. F. Smyth and A. L. Worthy, Soliton evolution and radiation loss for the sine-Gordon equation, *Phy. Rev. E,* **60**, 2330-2336 (1999).

[220] E. A. Kuznetsov, A. M. Rubenchick and V. E. Zakharov, Soliton stability in plasmas and hydrodynamics, *Phy. Rep.,* **142**, 103-165 (1986).

[221] N. Ghofraniha, C. Conti, C. and G. Ruocco, Aging of the nonlinear optical susceptibility in doped colloidal suspensions, *Phy. Rev. B,* **75**, 224203 (2007).

[222] C. Rotschild, B. Alfassi, O. Cohen and M. Segev, Long-range interactions between optical solitons, *Nature Physics,* **2**, 769-774 (2006).

[223] A. V. Mamaev, A. A. Zozulya, V. K. Mezentsev, D. Z. Anderson and M. Saffman, Bound dipole solitary solutions in anisotropic nonlocal self-focusing media, *Phy. Rev. A,* **56**, R1110-R1113 (1997).

[224] M. Segev, G. C. Valley, B. Crosignani, P. DiPorto and A. Yariv, Steady-state spatial screening solitons in photorefractive materials with external applied field, *Phy. Rev. Lett.,* **73**, 3211-3214 (1994).

[225] J. Beeckman, K. Neyts, X. Hutsebaut, C. Cambournac and M. Haelterman, Time Dependence of Soliton Formation in Planar Cells of Nematic Liquid Crystals, *IEEE J. Quantum Electron.,* **41**, 735-740 (2005).

[226] A. Strinić, D. Timotijević, D. Arsenović, M. Petrović, and M. Belić, Spatiotemporal optical instabilities in nematic solitons, *Opt. Express,* **13**, 493-504 (2005).

[227] A. I. Strinić, D. M. Jović, M. S. Petrović, D. V. Timotijević, N. B. Aleksić, and M. R. Belić, Counterpropagating beams in nematic liquid crystals, *Opt. Express,* **14**, 12310-12315 (2006).

[228] Khoo, I.C., Liang, Y., "Stimulated orientational and thermal scatterings and self-starting optical phase conjugation with nematic liquid crystals," *Phy. Rev. E,* **62**, 6722-6733 (2000).

[229] Khoo, I.C., Ding, J., All-optical cw laser polarization conversion at 1.55 micron by two beam coupling in nematic liquid crystal film, *Appl. Phys. Lett.,* **81**, 2496-2498 (2002).

[230] Residori, S., Bortolozzo, U., Huignard, J.P., Slow and fast light in liquid crystal light valves, *Appl. Phys. Lett.,* **100**, 203603 (2008).

[231] Bortolozzo, U., Laurie, J., Nazarenko, S., Residori, S., Optical wave turbulence and the condensation of light, *J. Opt. Soc. Amer. B,* **26**, 2280-2284 (2009).

[232] A. J. Heeger, S. Kivelson, J. R. Schrieffer and W. -P. Su, Solitons in conducting polymers, *Rev. Mod. Phys.,* **60**, 781-850 (1988).